

Optical trapping and Feshbach spectroscopy of an ultracold Rb-Cs mixture

Dissertation

zur Erlangung des akademischen Grades
Doktor der Naturwissenschaften

eingereicht an der
Fakultät für Mathematik, Informatik und Physik
der Universität Innsbruck

von

Karl Pilch

Betreuer der Dissertation:
Univ.Prof. Dr. Rudolf Grimm

Jänner 2009

Abstract

We investigate quantum-mechanical interactions between ultracold rubidium and cesium in an optical trap at temperatures of a few microkelvin. Our results provide, on the one hand, an experimental key to understand the collisional properties and, on the other hand, a tool to control the interspecies interactions. By performing loss measurements we locate several Feshbach resonances, which provide insight into the energy structure of weakly bound RbCs molecules near the dissociation threshold and allow for the production of such heteronuclear Feshbach molecules. In the future we will transfer these loosely-bound molecules into the absolute internal ground state. The availability of ultracold heteronuclear ground state molecules will open the door to investigate phenomena associated with ultracold polar quantum gases.

In our new experimental set-up we are able to trap and cool rubidium and cesium atoms in their lowest internal states. First we load both species into a two-color magneto-optical trap, having full control over the single-species atom number. We extend the technique of degenerate Raman-sideband cooling to a two-color version, which is able to simultaneously cool and polarize both rubidium and cesium. Thereafter we load the atoms into a levitated crossed optical dipole trap. Because of the presence of the gradient magnetic field the trap is highly state selective and consequently provides perfect spin-polarization of the sample. Furthermore, a coincidence of the magnetic-moment-to-mass ratios of the two species allows for simultaneous levitation of both, which assures an almost perfect spatial overlap between the species.

We perform Feshbach spectroscopy in two different spin channels of the mixture within a magnetic field ranging from 20 to 300G. In the lowest spin combination of the species we locate 23 interspecies Feshbach resonances, while in a higher spin mixture we find 2 resonances. The high number of resonances found within this range of magnetic field is unusual for alkali mixtures. The presence of many resonances points to scattering properties of the mixture, which include higher-order coupling mechanisms. The obtained data on the Feshbach spectroscopy provide, on one hand, fundamental experimental input to characterize the Rb-Cs scattering properties and, on the other hand, identification of possible starting points for the association of ultracold heteronuclear RbCs molecules.

In addition we show preliminary results on spectroscopy of the binding energy of RbCs dimers, based on a modulation of the magnetic field. The recently obtained Bose-Einstein condensate of Cs atoms, which represents a benchmark for the performance of the present apparatus, will be discussed as well as the potential pathways towards a double-degenerate mixture. We follow two main goals, first the production of a double Bose-Einstein condensate and, second, the transfer of shallow bound Feshbach molecules to the absolute internal ground state. The production of heteronuclear ground state molecules allows to enter the world of ultracold polar quantum systems.

Zusammenfassung

Wir untersuchen die quantenmechanischen Streueigenschaften eines ultrakalten Gases bestehend aus Cäsium und Rubidium Atomen in einer optischen Dipolfalle bei einer Temperatur von wenigen Mikrokkelvin. Unsere Resultate liefern einerseits einen experimentellen Zugang zum Verständnis der Streueigenschaften und andererseits ein Werkzeug die Wechselwirkungen zwischen den Spezies zu kontrollieren. Mit Hilfe von Verlustmessungen entdecken wir mehrere Feshbach Resonanzen, die einen Einblick in die energetische Struktur von schwach gebundenen heteronuklearen Molekülen nahe der Dissoziationsgrenze gewähren und es erlauben heteronukleare Feshbach Moleküle zu erzeugen. Für die Zukunft planen wir diese in ihren absoluten Grundzustand zu transferieren. Heteronukleare Grundzustandsmoleküle legen den Grundstein zur Untersuchung ultrakalter polarer Quantengase.

Mit unserem neuen Experiment können wir Rubidium und Cäsium Atome in ihrem absoluten Grundzustand fangen und kühlen. Zuerst laden wir beide Spezies in eine kombinierte magneto-optische Falle, wobei wir volle Kontrolle über die Atomzahlen der einzelnen Spezies haben. Wir erweitern die Technologie des Raman Seitenband Kühlens, um beide Spezies gleichzeitig zu kühlen und zu polarisieren. In einem nächsten Schritt werden die Atome in eine levitierte gekreuzte optische Dipolfalle geladen. Auf Grund des magnetischen Gradientenfeldes ist diese zustandsselektiv und stellt somit ein perfekt spinpolarisiertes Gemisch zur Verfügung. Wegen des ähnlichen magnetischen Moment zu Masse Verhältnisses der beiden Spezies ist ein nahezu perfekter räumlicher Überlapp zwischen den Atomsorten gegeben.

Wir vermessen das Feshbach Spektrum für zwei verschiedene Spin Kombinationen in einem Magnetfeldbereich zwischen 20 and 300G. In der energetisch tiefsten Spinkombination finden wir 23 heteronukleare Feshbach Resonanzen, in einer anderen finden wir 2 Resonanzen. Die hohe Anzahl von Feshbach Resonanzen in diesem Magnetfeldbereich ist ungewöhnlich für Alkalimischungen. Dies deutet auf Streueigenschaften der Mischung, die Kopplungen höherer Ordnung beinhalten. Die experimentellen Daten der Feshbach Spektroskopie ermöglichen einerseits fundamentale Einsichten zur Charakterisierung der Streueigenschaften, andererseits stellen sie mögliche Ausgangspunkte für die Produktion von heteronuklearen Molekülen dar.

Zudem zeigen wir vorläufige Daten zur Messung der Bindungsenergie von schwach gebundenen RbCs Dimeren, die auf einer Modulation des Magnetfeldes basieren. Das in unserem Experiment kürzlich produzierte Bose Einstein Kondensat, was die Leistungsfähigkeit der gegenwärtigen Apparatur zeigt, sowie mögliche Wege ein Doppelkondensat zu erreichen werden diskutiert. Wir verfolgen zwei Hauptziele, einerseits die Produktion eines Doppelkondensats und andererseits den Transfer von schwach gebundenen Feshbach Molekülen in den absoluten Grundzustand. Heteronukleare Grundzustandsmoleküle ermöglichen die Untersuchung von ultrakalten polaren Quantensystemen.

Contents

1	Introduction	1
1.1	Ultracold atomic quantum gases	1
1.2	Towards ultracold mixtures and heteronuclear molecules	2
1.3	Mixture of Rb and Cs	4
2	Two-body interactions and Feshbach resonances	6
2.1	Ultracold collisions and atomic interactions	6
2.1.1	Elastic and inelastic collisions	6
2.1.2	Atomic interactions - unperturbed Hamiltonian	9
2.1.3	Van-der-Waals interaction and exchange term	10
2.1.4	Dipolar interactions	10
2.2	Selection rules and molecular channel formalism	12
2.2.1	Selection rules	12
2.2.2	The separated atom picture	13
2.2.3	Alternative basis	14
2.3	Feshbach resonances	15
2.3.1	Feshbach resonances - basic understanding	15
2.3.2	Feshbach resonances in alkali atoms and applications	18
3	Rb-Cs mixture: Apparatus and experimental procedure	21
3.1	Apparatus and magnetic fields setup	22
3.1.1	Double-species oven and Zeeman slower	23
3.1.2	Glass cell and magnetic fields	25
3.2	Two-color magneto-optical trap	28
3.2.1	Rb and Cs laser setup	29
3.2.2	Two-color magneto-optical trap setup	31
3.2.3	Experimental procedure and results	33
3.3	Two-color degenerate Raman-sideband cooling	37
3.3.1	Degenerate Raman-sideband cooling - basic concepts	37
3.3.2	Technical setup	38
3.3.3	Experimental procedure and results	41
3.4	Levitated optical dipole traps	44
3.4.1	The reservoir and the dimple	45

Contents

3.4.2	Aspects and problems of the current dipole trap setup	48
3.4.3	Experimental procedure and results	50
4	Heteronuclear Feshbach resonances in an ultracold mixture of Cs and Rb	53
4.1	Sample preparation	54
4.1.1	Experimental procedure	54
4.1.2	^{87}Rb state transfer	56
4.2	Feshbach resonances in the lowest spin channel	58
4.3	Feshbach resonances in a higher spin channel	60
4.4	General considerations and interpretation	61
4.5	Status of theoretical assignment	66
5	Towards molecules and double-degenerate mixtures	69
5.1	Magnetic field association	69
5.1.1	The wiggle technique - basic concepts	69
5.1.2	Preliminary results and discussion	71
5.2	Towards a double-degenerate atomic mixture	76
5.2.1	Production of a Cs BEC	77
5.2.2	Ways to obtain a double BEC	81
5.3	Towards heteronuclear ground state molecules	85
6	Conclusions	89
A	Microwave spectroscopy and magnetic field calibration	91
A.1	Microwave spectroscopy	92
A.2	Magnetic field calibration	93
B	Extended level scheme of Cs	96
C	Publications	97
	References	98

1 Introduction

“ An unavoidable consequence of quantum mechanics is that, for sufficiently short length scales, all objects appear to be “ wavy ” . We do not notice this effect in our everyday lives because, for objects larger than an electron, the length scale over which the waviness occurs is fantastically short, far too small to be observed by the unaided eye. Nature makes an exception to this rule, however, in the case of extreme cold. ” [Fal00]

1.1 Ultracold atomic quantum gases

The realization of laser cooling and trapping [Met99] of atoms has paved the way towards ultracold quantum gases. Subsequent evaporative cooling made the achievement of Bose-Einstein condensation (BEC) possible. The realization of laser cooling as well as the achievement of BEC of ^{87}Rb and ^{23}Na [Cor02, Ket02] were honored by Nobel prizes in 1997 and 2001. Thereafter, other alkali atoms including bosonic as well as fermionic isotopes of lithium and potassium have been cooled to quantum degeneracy [Bra95, DeM99, Roa02, Mod02a]. A condensate of Cs atoms was achieved in 2002 [Web03a]. Apart from alkali atoms degeneracy has also been obtained for other atomic species like ytterbium [Tak03, Fuk07], hydrogen [Fri98], metastable helium [San01, Rob01] and chromium [Gri05]. Bose-Einstein condensation in dilute gases typically requires temperatures in the nK range at typical atom number densities around 10^{13}cm^{-3} . Already at temperatures of around $1\mu\text{K}$ quantum properties start to appear, as the de-Broglie wave packets of the particles start to overlap [Ket99]. In the ultracold regime the behavior of the quantum system is governed by quantum statistics.

Pioneering work has been done investigating basic properties of quantum degenerate systems. Prominent examples are the observation of interference between two Bose-condensed clouds [And97], the realization of an atom laser [Blo99] or the creation of vortices in superfluid quantum gases [Mad00], just to name a few examples [Ket99].

The use of optical lattices, which produce an array of optical micro-potentials, is a way to connect ultracold atoms to the world of condensed-matter physics. Atoms which are located in an optical lattice, which is formed by standing-wave light fields [Gri00, Gre03, Blo01], experience a trapping potential. This induces a band structure, which is comparable to the band structure of the energy spectrum in solid state physics [Blo08]. Because of excellent experimental control of variable parameters ultracold

1 Introduction

atoms in periodic optical potentials exhibit a new playground to study quantum phase transitions [Gre02].

Particularly important in the field of ultracold quantum gases is the full control over the interactions. For ultracold atoms the interaction between the particles can be described by a single parameter, the s -wave scattering length. In a Bose-Einstein condensate the sign and strength of the scattering length determine the mean field interaction [Dal99]. In this context so-called Feshbach resonances [Ino98] represent the essential tool to control and manipulate ultracold atoms.

Feshbach resonances feature the way to form and manipulate molecules starting from free atomic samples [Köh06]. The availability of molecules offer many new possibilities, since they have much richer energy structure than atoms. Especially dipolar molecules are of substantial interest. The anisotropic nature of the long-range dipolar interaction exhibits novel quantum phases like checker-board phase and different types of supersolid phases [Gór02, Yi07].

1.2 Towards ultracold mixtures and heteronuclear molecules

In recent years attention has turned to mixtures of quantum gases. Ultracold mixtures exhibit a wide range of fascinating phenomena not present in single-species experiments. One of the early experiments regarding ultracold mixtures uses two different isotopes of the same species [Blo05]. Further progress has been made towards mixtures of different species. Sympathetic cooling between ^{133}Cs and ^7Li has been investigated [Mud02], while degenerate Bose-Fermi mixtures have been produced on ^{23}Na plus ^6Li [Had02] and ^{40}K plus ^{87}Rb [Roa02]. The first double-BEC on a bosonic mixture of ^{41}K and ^{87}Rb has been produced in Florence [Mod01, Mod02a, Mod02b]. The interactions between a double-BEC of ^{85}Rb and ^{87}Rb have been investigated and can be controlled via the use of a single-component Feshbach resonance [Pap08].

Optical lattices have also been applied to mixtures of different species [Lew04, Gün06, Osp06]. The character of the system can be changed by tuning the interactions or the depths of the periodic optical potential. Bose-Bose and Bose-Fermi mixtures loaded into optical lattices have been investigated, showing the loss of phase coherence of one species in the presence of the respective other [Cat08].

Even quantum systems with more than two different atomic species are currently under investigation [Wil08, Wil09, Tag08]. Different masses and different responses to external fields, as well as the use of different isotopes of the species lead to a large variety of new experiments and phenomena.

Sympathetic cooling is one of the major topics for mixed atomic samples. For species where standard evaporative cooling techniques are insufficient (because of unfavorable collisional properties, like forbidden s -wave collisions for identical

1.2 Towards ultracold mixtures and heteronuclear molecules

fermions) the addition of a cooling agent can overcome these limitations [Mud02]. Besides the use of different internal states of fermions of the same species [DeM99], degenerate Fermi gases have been achieved in Bose-Fermi mixtures by forced evaporation of the bosonic component [Roa02].

Intra- and interspecies interactions play a crucial role in ultracold mixtures. Sympathetic cooling relies on the elastic interspecies collision cross section. The rate of interspecies elastic collisions can hardly be predicted by theory and has thus often to be determined by experimental investigation. The collisional dynamics of a mixed species quantum gas crucially rely on both the single- and interspecies collisional properties. For example in a mixture of ^{40}K and ^{87}Rb the collapse of a degenerate Fermi gas was observed, caused by the presence of large interspecies attraction [Mod02b]. If Feshbach resonances are accessible, either homo- or heteronuclear resonances, the dynamics of the two quantum gases can be controlled, providing the ability to change the miscibility of the two-component gas [Pap08, Roa07].

Ultracold molecules can be associated by the use of a Feshbach resonance. Feshbach molecules have been produced for homonuclear species like ^{40}K , ^{133}Cs , ^6Li , ^{23}Na [Reg03a, Her03, Str03, Cub03, Xu03]. The use of a magnetic field ramp across a Feshbach resonance to associate dimers [Chi08, Köh06] can also be applied to mixed species experiments. The production of heteronuclear dimers allows to enter the world of polar molecules. Heteronuclear molecules associated directly via a Feshbach resonance, thus being loosely bound, and homonuclear molecules in general show very small permanent electric dipole moments. In contrast, ground state heteronuclear molecules can exhibit a large permanent electric dipole moment. The long-range and anisotropic dipole-dipole interaction can dominate over the simple contact interaction [Bar08]. Dipolar quantum gases are predicted to be applicable for novel experiments in the field of quantum computation, measurement of time-dependent constants, the electric dipole moment of the electron and others [DeM02, Büc07, Bar08].

Basically there are three different ways to obtain an ultracold ensemble of ground state molecules. One concept uses photoassociation of ground state molecules by shining light of different wavelengths in a defined sequence of pulses onto the atomic sample. In reference [Sag05] they used a scheme of five different laser pulses for production and detection of ground state RbCs molecules, with the drawback, that this method of transferring the atoms to the ground state is very inefficient. Alternative approaches, relying on buffer gas cooling or Stark deceleration [JD04], are not yet capable of reaching the ultracold regime. Another concept starts with loosely bound Feshbach molecules, which are subsequently pumped to the ground state of the molecular potential by two-photon stimulated rapid-adiabatic-passage (STIRAP) [Stw04, Win07]. Recently the production of both homo- and heteronuclear ground state molecules at ultralow temperatures has been achieved [Dan08, Ni08, Lan08a, Dei08].

1.3 Mixture of Rb and Cs

The present thesis describes the development of a new experimental setup to produce an optically-trapped ultracold mixture of ^{133}Cs and ^{87}Rb . First results on the observation of heteronuclear Feshbach resonances of the two species are obtained with the new setup [Pil08]. Up to the starting point of this new mixture experiment in Innsbruck, very little was known on a mixture of Rb and Cs. Rubidium and cesium, the two heaviest stable alkali species, are both well established in Bose-Einstein condensation experiments. While Rb represents the first atomic species ever condensed [And95], cesium BEC had to await the development of efficient optical trapping methods [Web03a, Kra04]. The individual two-body interaction properties of Rb and Cs are very well understood as a result of extensive studies by Feshbach spectroscopy [Chi08, Chi00, Mar02]. Cesium shows a quite unique scattering behavior because of a very large background scattering length in combination with many Feshbach resonances and pronounced high-order Feshbach coupling. A few experiments on Rb-Cs mixtures have been performed in magnetic traps [And05, Har08, Haa07]. The observation of rapid thermalization between the two different species points to a large interspecies background scattering length [Tie06]. Feshbach resonances in the Rb-Cs system have not been observed so far. Knowledge on such resonances is desired both as spectroscopic input to precisely determine the scattering properties of the mixture and to enable experimental control species interaction.

A special motivation for combining Rb and Cs is the production of a quantum gas of polar molecules, as recently demonstrated for a Bose-Fermi mixture of bosonic Rb and fermionic K atoms [Ni08]. As the Rb-Cs mixture is a Bose-Bose system, the molecules would be bosons and could eventually form a condensate of polar molecules. For studying dipolar phenomena in such a system, RbCs molecules in the rovibrational ground state are expected to carry a comparatively large electric dipole moment of 1.25 debye [Kot06]. For this application, Feshbach resonances have proven an efficient tool to associate molecules and thus to serve as a gateway from the atomic into the molecular world [Chi08, Fer08]. The Feshbach molecules are then transferred by optical Raman processes into the rovibrational ground state.

This thesis is organized as follows:

- Chapter 2 gives an overview of two-body interactions including the basic contributions to the Hamiltonian describing the collision between two neutral atoms. Additional information is given on so-called Feshbach resonances.
- Chapter 3 describes the major experimental techniques and setups we use to produce an ultracold mixture of Rb and Cs in an optical trap.
- Chapter 4 presents and discusses the results on Feshbach spectroscopy, where we identify 23 interspecies Feshbach resonances in the lowest spin channel of both species and another 2 resonances in a higher channel.
- Chapter 5 shows preliminary results on the spectroscopy of the binding energy of RbCs molecules close to a Feshbach resonance. We discuss potential ways towards a double-degenerate mixture and towards RbCs ground state molecules.

2 Two-body interactions and Feshbach resonances

This chapter gives an overview of the interactions between cold atoms. Collisions between atoms play a crucial role in the field of ultracold atoms. An intense study of collisions will enable the development of a tool to control the collisional properties [Chi08, Köh06].

Section 2.1 describes the different contributions to the Hamiltonian modeling binary collisions. The followed section 2.2 is focused on the different basis used to describe molecular bound states. The final section 2.3 provides a simple model of a so-called Feshbach resonance. Feshbach resonances open unprecedented ways to control the interatomic interactions and lead to experiments like the production of molecules from atomic samples or the investigation of the BCS crossover in fermionic systems.

2.1 Ultracold collisions and atomic interactions

2.1.1 Elastic and inelastic collisions

Two colliding atoms can scatter elastically or inelastically. Elastic collisions are important for thermalisation and efficient evaporative cooling of the atomic samples. Inelastic collisions usually result in trap loss.

Elastic collisions

In an elastic collision the relative kinetic energy of two colliding particles does not change, while the kinetic energy of the individual atoms can change. Elastic collisions provide thermal equilibrium of the sample and make forced evaporation possible. The Schrödinger equation describing the relative motion of the atoms in the presence of an interaction potential can be written as

$$H\psi_k(r) = E_k\psi_k(r). \quad (2.1)$$

The Hamiltonian is written as the sum of the relative kinetic energy and the interaction potential as

$$H = E_{\text{kin}} + V(r). \quad (2.2)$$

2.1 Ultracold collisions and atomic interactions

E_{kin} denotes the relative kinetic energy of the atoms. $V(r)$ is associated with the interaction potential, where r is the distance between the particles. $\psi_k(r)$ is the two-particle wavefunction, where k denotes the wavenumber. The scattering potential $V(r)$ is spherically symmetric, hence the Hamiltonian can be decoupled into a radial part and a part depending on the angular momentum l [Pet02], hence

$$H = -\frac{\hbar^2}{2\mu} \left[\frac{1}{r^2} \frac{d}{dr} \left(r^2 \frac{d}{dr} \right) - \frac{l(l+1)}{r^2} \right] + V(r), \quad (2.3)$$

where μ is the reduced mass and l denotes the quantum number of the angular orbital momentum. For $l \neq 0$ the interaction potential will be modified, since a centrifugal barrier is added to the long-range attractive part of the potential.

In the limit of $r \rightarrow \infty$ the wavefunction is expanded into an incoming plane wave and an outgoing spherical wave

$$\psi_k(r) = e^{ikr} + f(\vartheta, k) \frac{e^{ikr}}{r}, \quad (2.4)$$

where k is the wavenumber of the atoms and $f(\vartheta, k)$ is associated with the scattering amplitude depending on the angle ϑ between the direction of incidence \mathbf{k}/k and the direction of observation \mathbf{r}/r .

The second part of equation 2.4 can be written in terms of a partial-wave expansion. We use the symmetry of the scattering problem and the eigenfunctions of the angular momentum as the basis to write the outgoing spherical part of the wavefunction $\psi_k(r)^{\text{out}}$ as

$$\psi_k(r)^{\text{out}} = \sum e^{i(\frac{\pi}{2}l + \delta_l)} \frac{\sqrt{4\pi(2l+1)}}{kr} \sin(kr - \frac{\pi}{2}l + \delta_l) Y_{lm}(\vartheta), \quad (2.5)$$

where l is the quantum number of the angular momentum, Y_{lm} are spherical harmonics functions and δ_l is defined as an additional phase relative to the incoming wave, which is added by the scattering process. In the limit of low collision energies partial waves with $l \neq 0$ are neglected. Usually in literature partial waves $l = 1, 2, 3, 4, \dots$ are labeled by s, p, d, f, \dots waves. For experiments working in the ultracold regime a description of the elastic collision process is reduced to pure s -wave collisions. These collisions are described by the elastic s -wave cross section

$$\sigma(k) = \frac{4\pi}{k^2} \sin^2 \delta_0(k) \quad (2.6)$$

and the s -wave scattering length

$$a = -\lim_{k \rightarrow 0} \frac{\tan \delta_0(k)}{k}, \quad (2.7)$$

which is in the zero-energy limit a universal parameter describing the collision. With the use of the s -wave scattering length a the elastic cross section can be written in the form¹

¹regardless corrections for the effective range

2 Two-body interactions and Feshbach resonances

$$\sigma(k) = \frac{4\pi a^2}{1 + k^2 a^2}. \quad (2.8)$$

The scattering length a strongly depends on the shape of the scattering potential. An overview of the contributions to the Hamiltonian describing the details of the collision is given in the next sections.

Inelastic collisions

Atoms which undergo an inelastic collision change their internal state during the scattering process. Because of energy and momentum conservation a loss of internal energy goes together with a rise of the kinetic energy of the particles. Usually the gain of kinetic energy is larger than the trap depth. Therefore inelastic collisions lead to losses.

We distinguish between three different contributions: the single particle loss, the two-body loss and the three-body loss. Single particle loss is the removal of atoms from the trapped sample by background-gas collisions. For inelastic two-body collisions the atoms undergo a change of the internal state. The gain of kinetic energy in such spin- or hyperfine-changing collisions is typically orders of magnitude larger than the trap depth, hence leading to losses. If the atoms are prepared in the lowest internal state, two-body decay is forbidden. Nonetheless three-body loss can limit the achievable densities in cold atomic samples. A collision between three atoms can result in a deeply bound molecule and a single atom. Due to energy and momentum conservation the molecule and the remaining atom will carry away 1/3 and 2/3 of the binding energy. Usually the gain of kinetic energy will lead to the loss of all three particles involved in the collision. The following equation combines all these inelastic processes in a time-dependent differential equation

$$\dot{N} = -\alpha N - L_2 \int n^2 d^3r - L_3 \int n^3 d^3r, \quad (2.9)$$

where α is the single-particle loss rate, L_2 and L_3 are the two- and the three-body loss coefficients. N and n are the particle number and the atom number density, respectively.

The different loss-rate coefficients are different for various species. Typically the dipolar relaxation rate L_2 is on the order of $10^{-15} \text{cm}^3/\text{s}$ for Rb in the ($F = 2, m_F = 2$) state [Boe96], where three body loss coefficient L_3 for Rb in the same state is about $10^{-29} \text{cm}^6/\text{s}$ [Bur97]. As it will be explained in more detail in section 4.4 cesium shows pretty high inelastic two-body loss rates [GO98a, GO98b, Hop00]. The three-body loss coefficient for Cs is on the order of a few $10^{-26} \text{cm}^6/\text{s}$, hence three orders of magnitude higher than for Rb². Enhanced losses from magnetic traps have been observed at high densities, preventing the gases from condensation [Söd98, Arl98]. Even for the absolute ground state of Cs, where no two-body losses are possible, three-body loss can be

²calculated for a scattering length of $a = 500a_0$

2.1 Ultracold collisions and atomic interactions

detrimentally high [Web03b]. Rubidium on the other side is a very convenient species to work with, as both the two- and three-body losses are moderately low. Therefore condensates in different sub-states and trapping configurations (optical dipole traps, magnetic traps) have been realized so far.

2.1.2 Atomic interactions - unperturbed Hamiltonian

We will restrict our discussion to alkali atoms, i.e. to atoms with one valence electron. This subsection is based on references [Chi01, Köh06]. Each of the two alkali atoms has an unpaired electron spin \mathbf{s}_1 and \mathbf{s}_2 , which can be coupled to a total spin $\mathbf{S} = \mathbf{s}_1 + \mathbf{s}_2$ with the quantum numbers $S = 1$ or $S = 0$. The states associated with the quantum numbers $S = 1$ and $S = 0$ are called triplet and singlet states, respectively.

For a single atom the spin \mathbf{s} and the electronic orbital angular momentum \mathbf{l} are coupled to the total electronic angular momentum $\mathbf{j} = \mathbf{s} + \mathbf{l}$. The nuclear spin \mathbf{i} and the total electronic angular momentum are coupled to the total angular momentum $\mathbf{f} = \mathbf{j} + \mathbf{i}$, producing hyperfine levels. Under the influence of an external magnetic field the hyperfine levels will split into Zeeman components. The quantum number m_f denotes the projection of the total angular momentum on the magnetic field axis.

To get insight into the collisional properties of scattering particles one has to look at the interactions on a microscopic level. Basically the Hamiltonian for the interatomic interactions can be written as the sum

$$H = H_0 + H_{\text{int}} \quad (2.10)$$

of the unperturbed single particle Hamiltonian H_0 and the Hamiltonian taking account for inter-particle interactions H_{int} . At very large interatomic distances ($r \rightarrow \infty$) the energy of the two-body system is given by the sum of the single particle contributions

$$H_0 = E_{\text{kin}} + H_{\text{hfs}} + H_{\text{zee}}. \quad (2.11)$$

The first term in equation 2.11 denotes the kinetic energy $E_{\text{kin}} = \hbar^2 k^2 / 2\mu$, where μ is the reduced mass. H_{hfs} and H_{zee} represent the hyperfine interaction $\propto \mathbf{s}_1 \mathbf{i}_1 + \mathbf{s}_2 \mathbf{i}_2$ and the Zeeman energy $-\mu_B (g_j (\mathbf{s}_1 + \mathbf{s}_2) + g_I (\mathbf{i}_1 + \mathbf{i}_2)) \mathbf{B}$, respectively. The Bohr magneton is denoted by μ_B , g_j and g_I are the g factors for the electron and the core respectively.

The Hamiltonian taking account for interactions between the atoms is written as the sum of the van-der-Waals interaction, the exchange term and the Hamiltonian taking account for dipole-dipole interactions,

$$H_{\text{int}} = H_{\text{vdW}} + H_{\text{ex}} + H_{\text{dd}}. \quad (2.12)$$

2.1.3 Van-der-Waals interaction and exchange term

The van-der-Waals interaction

The van-der-Waals interaction originates from the induced dipole-dipole interaction between the unpaired electrons of the colliding atoms. As one immediately realizes, the van-der-Waals interaction does not depend on the spins and can therefore not induce transitions between internal states. The Hamiltonian for the long-range interaction can be written as

$$H_{\text{vdW}}(r) = -C_6 r^{-6} - C_8 r^{-8} - C_{10} r^{-10} + \dots, \quad (2.13)$$

where C_6 is the van-der-Waals coefficient.

The exchange term

The exchange term has its origin in the antisymmetry of the electronic wavefunction. The exchange interaction gets stronger, when the atoms come close together, since their electronic wavefunctions start to overlap. The exchange term

$$H_{\text{ex}}(r) = V_{\text{ex}}(r) \left(\frac{1}{2} + 2\mathbf{s}_1 \mathbf{s}_2 \right) \quad (2.14)$$

ouples states conserving the total quantum number $m_{\text{tot}} = m_{f_1} + m_{f_2}$. At large interatomic separation the overlap between the electronic wavefunctions drops exponentially and hence

$$V_{\text{ex}}(r) = C_{\text{ex}} e^{-r/r_{\text{ex}}}, \quad (2.15)$$

where C_{ex} and r_{ex} characterize the strength and the range of the interaction, respectively. The spin dependence of H_{ex} in contrary to H_{vdW} couples the singlet and the triplet parts of the wave function. Figure 2.1 shows the singlet and triplet potentials for cesium atoms. Under the constraint of the conservation of the m_{tot} quantum number transitions between levels with different m_f quantum numbers are allowed. As a consequence the so-called stretched states are immune against transitions caused by the exchange interaction. This means that the states $(f, m_f = \pm f)$ do not suffer from spin exchange in zero order, but nevertheless the lifetime of these states can be limited by higher order effects like the dipolar interactions.

2.1.4 Dipolar interactions

Dipolar interactions are responsible for limited lifetimes of samples, even if they are fully polarized in a stretched state. We distinguish between the spin-spin interaction (also called magnetic dipole-dipole interaction) and the second order spin-orbit interaction.

2.1 Ultracold collisions and atomic interactions

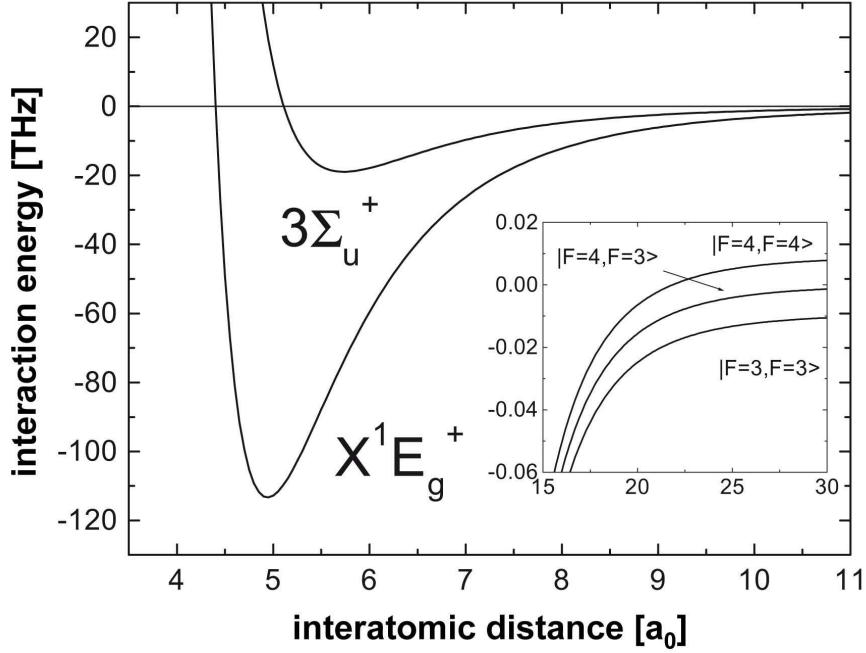


Figure 2.1: Singlet and triplet potential of cold Cs atoms are shown. The interaction is dominated by the van-der-Waals interaction and the exchange term. Because of the spin dependence of the exchange term singlet and triplet parts of the wave function are coupled. The inset shows a zoom of the long range part of the potential, which is dominated by the hyperfine interaction. Figure from [Chi01].

The spin-spin interaction

The spin-spin interaction is a direct magnetic dipole-dipole interaction and is of the following form

$$H_{ss} = V_1(r)V_s(\mathbf{s}_1\mathbf{s}_2). \quad (2.16)$$

The second order spin-orbit interaction

The spin-orbit interaction gains importance for very heavy alkali atoms like ^{133}Cs , as they can show big relativistic spin-orbit effects,

$$H_{so} = V_2(r)V_s(\mathbf{s}_1\mathbf{s}_2). \quad (2.17)$$

Both the spin-spin and the second order spin-orbit interaction have the same dependence on the spin but different behavior regarding the internuclear separation. While the spin-spin interaction scales as r^{-3} , V_2 drops exponentially with the distance between the atoms. The sum of the two dipole-dipole interactions can be written with the Hamiltonian

2 Two-body interactions and Feshbach resonances

$$H_{\text{dd}} = H_{\text{ss}} + H_{\text{so}} \quad (2.18)$$

$$= (V_1 r + V_2 r) V_s(\mathbf{s}_1 \mathbf{s}_2) \quad (2.19)$$

$$\propto \left(\frac{a}{r^3} - e^{r/b} \right) (\mathbf{s}_1 (3\mathbf{r}\mathbf{r} - 1) \mathbf{s}_2), \quad (2.20)$$

where a and b are constants. In contrast to the exchange term (see 2.1.3) dipolar interactions enable transitions between states, which have a difference of four orders in angular momentum. Therefore we have to extend the accessible states with the rule

$$0 < |\Delta m_{\text{tot}}| < 4. \quad (2.21)$$

2.2 Selection rules and molecular channel formalism

From the Hamiltonian describing the interactions between neutral atoms we are able to deduce selection rules. These selection rules are based on atomic and molecular symmetries, which allow to define accessible molecular states using quantum numbers. Those accessible molecular channels can be labeled in different basis using quantum numbers. To explain the labeling of the channels is the scope of subsections 2.2.2 and 2.2.3

2.2.1 Selection rules

In addition to the quantum numbers associated with single separated atoms we introduce two more quantum numbers l and m_l , which are associated with the angular momentum of the relative motion and its projection on the magnetic field axis, respectively. For non-identical atoms all values of $l = 0, 1, 2, 3, \dots$ are possible. Due to the symmetry properties of the wave function only even values of the l -quantum number are allowed for identical bosons, whereas for identical fermions it is vice versa.

Just one selection rule has to be followed, which is the conservation of the total quantum number associated with the projection of the total angular momentum onto the magnetic field axis

$$m_{\text{tot}}^i = m_{\text{tot}}^f \quad (2.22)$$

$$m_{f_1}^i + m_{f_2}^i + m_l^i = m_{f_1}^f + m_{f_2}^f + m_l^f. \quad (2.23)$$

2.2 Selection rules and molecular channel formalism

The indices i and f denote the quantum numbers before and after the scattering process, respectively. Apart from this selection rule, we implicitly follow:

- Two colliding identical bosons couple to molecular channels with even values of l , identical fermions couple to molecular channels with odd values of l
- for an incoming s wave identical bosons will in first order couple to a molecular s -wave channel, on second order coupling to higher partial waves (d or g waves) is possible due to the exchange term and the dipole-dipole interactions, see section 2.1. Consequently the difference between $m_{f_1}^i + m_{f_2}^i$ and $m_{f_1}^f + m_{f_2}^f$ can be either 0, 2 or 4 for identical bosons.
- For nonidentical particles all $l = 0, 1, 2, 3, \dots$ quantum numbers are allowed. One still has to fulfill symmetry arguments. Therefore incoming even partial waves will only couple to even partial waves, whereas odd incoming partial waves just couple to p or f states.

With the knowledge of a simple rule, which restricts the possible molecular channels accessible by an incoming channel, we can label the states as it is presented in the following subsection. There we will present two different ways of labeling the channels, each of which has its specific advantages.

2.2.2 The separated atom picture

For this and the following subsection we will use the way of labeling similar to the one described in reference [Köh06]. An intuitive way of describing the molecular states that can be populated by two colliding atoms in well defined states is the use of the separated atom picture. Every channel has its set of quantum numbers $\{f_1, f_2, m_{f_1}, m_{f_2}, m_l\}$. The separated atom bases is used to get a fast insight of the possible molecular channels, but leads to problems at short distances between the atoms because of off-diagonal elements in the Hamiltonian. To gain better understanding of the power of this assignment, we show an example of two ^{87}Rb atoms in the absolute internal ground state $f = 1, m_f = 1$. We restrict the case to coupling of incoming s -waves to molecular s and d states. Table 2.1 shows the relevant quantum numbers in the separated atom picture for pure s - to s -wave scattering. Table 2.2 displays the accessible d states. The tables are calculated according to the selection rule 2.23, consequently conserving $m_{\text{tot}} = 2$.

We distinguish between open and closed channels, depending on whether the accessible molecular state is energetically lower or higher lying than the incoming channel, respectively. The energies of the channels are calculated at zero magnetic field by evaluating the hyperfine splitting.

2 Two-body interactions and Feshbach resonances

Table 2.1: Separated atom picture for an incoming s wave of two ^{87}Rb atoms in the state $f = 1, m_f = 1$. The table of accessible states is restricted to s -wave molecular states. The comments open and closed clarify if the channel is energetically lower or higher than the incoming one.

f_1	f_2	m_{f_1}	m_{f_2}	m_l	comment
1	1	1	1	0	open
1	2	1	1	0	closed
1	2	0	2	0	closed
2	2	1	1	0	closed
2	2	0	2	0	closed

Table 2.2: Separated atom picture for an incoming s wave of two ^{87}Rb atoms in the state $f = 1, m_f = 1$. The table of accessible states is restricted to d -wave molecular states.

f_1	f_2	m_{f_1}	m_{f_2}	m_l	comment
1	1	1	1	0	open
1	1	1	0	1	closed
1	1	0	0	2	closed
1	1	1	-1	2	closed
1	2	1	1	0	closed
1	2	1	0	1	closed
1	2	0	0	2	closed
1	2	1	-1	2	closed
1	2	0	2	0	closed
1	2	-1	2	1	closed
2	2	1	1	0	closed
2	2	1	0	1	closed
2	2	0	0	2	closed
2	2	1	-1	2	closed
2	2	0	2	0	closed
2	2	-1	2	1	closed
2	2	-2	2	2	closed

2.2.3 Alternative basis

To circumvent the problem of off-diagonal elements in the Hamiltonian at short inter-atomic distances, we can introduce the molecular basis. We couple the electronic and the nuclear spins of the atoms to resulting \mathbf{S} and \mathbf{I} . After coupling \mathbf{S} and \mathbf{I} to a resultant \mathbf{F} , the coupling to \mathbf{I} will result in a total angular momentum \mathbf{F}_{tot} . The quantum number associated with the projection of the total angular momentum onto the magnetic field axis is given by M . The full set of quantum numbers describing the channels is given by $\{S, I, F, l, F_{\text{tot}}, M\}$.

2.3 Feshbach resonances

Table 2.3: Alternative separated atom picture for an incoming s wave of two ^{87}Rb atoms. The table is restricted to the s - and d -wave molecular channels.

f_1	f_2	Fl (s wave)						Fl (d wave)			
2	2	0s		2s		4s	0d		2d		4d
1	2		1s	2s	3s			1d	2d	3d	
1	1	0s		2s			0d		2d		

More often used in literature is a basis with the quantum numbers $\{f_1, f_2, F, l, F_{\text{tot}}, M\}$, similar to the set of quantum numbers used for the description of the molecular channels in 2.2.2. Coupling \mathbf{F} and \mathbf{l} gives the total angular momentum \mathbf{F}_{tot} . M is the quantum number associated with the projection of \mathbf{F}_{tot} onto the magnetic field axis.

This basis is strictly speaking valid, as long as F may be viewed as a good quantum number. This basis is often used in literature, without displaying the full set of quantum numbers. For simplicity the quantum numbers are reduced to a minimum: $\{F, l\}$. To affiliate the precedent example of ^{87}Rb , table 2.3 shows the labeling of all possible channels regardless the selection rule of equation 2.23. To take account for the conservation of the projection of the total angular momentum on the magnetic field axis, we pick those states of the table, which allow for $M = 2$, hence $\{2, 2, 2s\}$, $\{2, 2, 4s\}$, $\{1, 2, 2s\}$, $\{1, 2, 3s\}$ and $\{1, 1, 2s\}$. The same holds for higher partial waves, being aware of having implicitly a manifold of channels with different m_f and m_l quantum numbers within a single channel label.

The exchange interaction couples states in between the same column, whereas the dipole-dipole interactions are responsible for coupling of different columns.

2.3 Feshbach resonances

Since the first observation of a Feshbach resonance in the field of ultracold gases [Ino98], the use of these scattering resonances opened the way for many breakthroughs. First we briefly discuss the basic physics of a Feshbach resonance, while later some examples are presented. This section is based on the review article [Chi08].

2.3.1 Feshbach resonances - basic understanding

The occurrence of a Feshbach resonance can be explained by a simple picture using two potential curves $V_{\text{bg}}(r)$ and $V_c(r)$, see figure 2.2. For large internuclear separation r , the background potential $V_{\text{bg}}(r)$ correlates asymptotically with two free atoms in an ultracold gas. In the limit of low collision energies this potential curve represents the energetically open channel, also called entrance channel. The other potential V_c , also

2 Two-body interactions and Feshbach resonances

called closed channel, supports molecular bound states near the threshold of the open channel. A Feshbach resonance occurs, when the scattering state of two free atoms associated with the entrance channel can couple to a molecular bound state supported by the closed channel.

If the open and the closed channel have different magnetic moments, the energy difference between the entrance channel and the bound molecular state can be tuned via an external magnetic field. If the energy of the molecular and the scattering state are brought to degeneracy, resonant Feshbach coupling between the states is achieved. If a molecular bound state happens to be closely above (below) the threshold of the entrance channel, the coupling between the channels will modify the s-wave scattering length a and therefore be largely negative (positive). In the case of resonant coupling the scattering length will show a singularity. Hence the scattering length and therefore the interaction between the atoms can be tuned via an external magnetic field between minus infinity, zero and plus infinity.

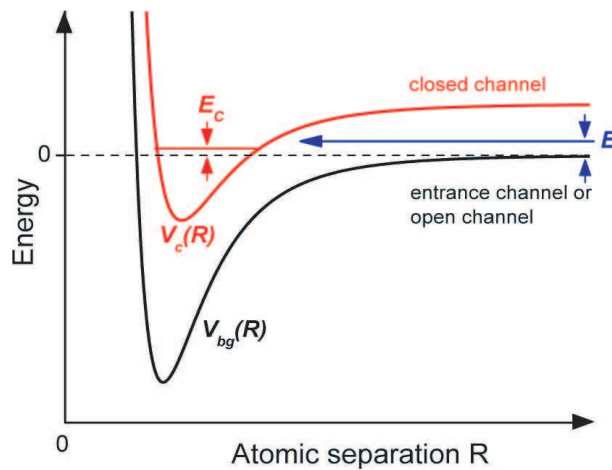


Figure 2.2: A Feshbach resonance occurs, when the scattering state associated with the entrance channel V_{bg} resonantly couples to a molecular bound state, which is supported by the closed channel V_c . Figure from [Chi08].

For a magnetically tunable Feshbach resonance³ the behavior of the scattering length close to a Feshbach resonance can be estimated by [Chi08, Köh06]:

$$a(B) = a_{bg} \left(1 - \frac{\Delta}{B - B_0} \right), \quad (2.24)$$

where B_0 identifies the magnetic field position of the resonance, Δ is the width of the resonance and a_{bg} is the background scattering length, which is related to the last

³Besides magnetically tunable Feshbach resonances optically tuned Feshbach resonances also have been investigated [The04, Tha05].

bound vibrational level of the incoming channel.

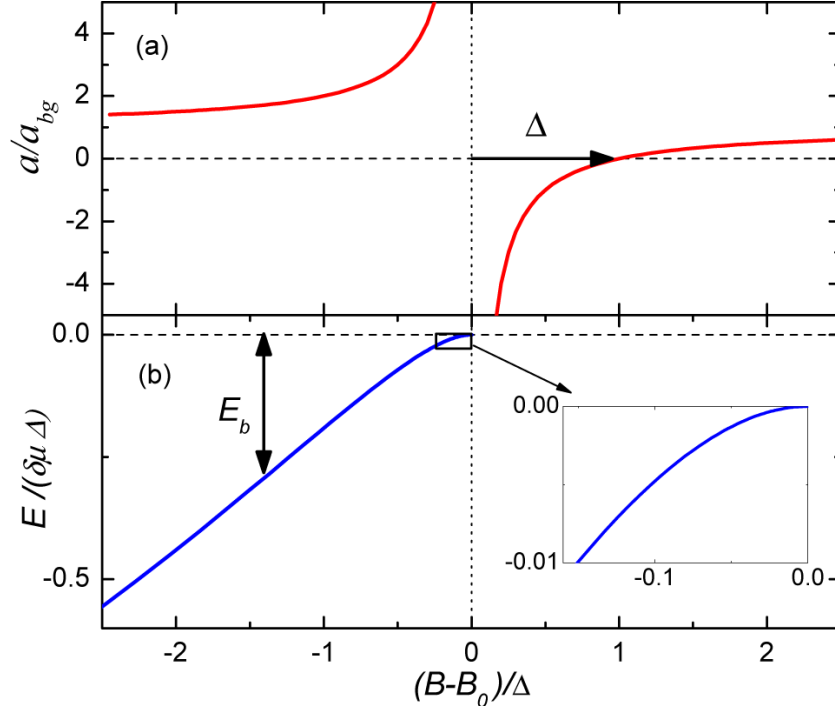


Figure 2.3: Panel (a) shows the behavior of the scattering length a depending on the magnetic field. When the magnetic field approaches the resonance position, the scattering length diverges. Panel (b) displays the binding energy E_b of the molecular bound state. E_b vanishes where the molecular state hits the threshold defined by the Zeeman energy of the entrance channel. The inset of panel (b) zooms into the region close to the resonance position, where the binding energy of the bound state quadratically depends on the scattering length. Figure from [Chi08].

Figure 2.3 shows the energy dependence of a molecular state with respect to the magnetic field. The upper plot in the figure displays the scattering length, which shows a divergence at the position where the bound state hits the threshold. The zero crossing of the scattering length occurs at a magnetic field $B = B_0 + \Delta$, where Δ is the width of the resonance. The binding energy of the molecular bound state scales linearly with the magnetic field strength, where the slope is given by the difference in magnetic moment $\delta\mu$ of the entrance and closed channels. Close to the resonance position, where the scattering length is large, the coupling between the channels strongly modifies the molecular state. The binding energy in the vicinity of the resonance position depends quadratically on the scattering length

$$E_b = \frac{\hbar^2}{2\mu a^2}, \quad (2.25)$$

2 Two-body interactions and Feshbach resonances

where μ is the reduced mass of the atom pair.

2.3.2 Feshbach resonances in alkali atoms and applications

Since the first observation of a Feshbach resonance in the field of ultracold atoms [Cou98, Abe98, Ino98], Feshbach resonances have been found in essentially all alkali atoms [Chi08] up to now. However different species show various scattering properties and Feshbach resonances of various character.

One common way to observe Feshbach resonances in an experiment is the observation of losses induced by resonantly enhanced two- and three-body processes, which can be quantified by equation 2.9. Apart from measurements of trap losses Feshbach resonances can be identified by quantifying the elastic scattering rate. As the s -wave elastic scattering cross section is depending on the scattering length (see equation 2.8) one e.g. is able to measure the thermalization rate by recording the remaining atom number after a forced evaporative ramp. At the position of a Feshbach resonance the scattering length a diverges that leads to an increase of the elastic scattering cross section. One can also track down the position of the Feshbach resonance by locating the zero crossing of the scattering length.

One important application of Feshbach resonances is the control of the so-called mean-field interaction in Bose-Einstein condensates, since the change of the scattering length leads to a modification of the mean-field interaction. Atomic Bose-Einstein condensates in a trap are commonly described by the time-dependent Gross-Pitaevskii equation [Dal99]

$$i\hbar\frac{\partial}{\partial t}\phi = \left(-\frac{\hbar^2\nabla^2}{2m} + V_{\text{ext}} + V_{\text{mf}}\right)\phi, \quad (2.26)$$

where ϕ is the condensate wave function, V_{ext} is regarding the external trapping potential and V_{mf} is known as the mean-field potential. The mean-field potential is taking account for the interactions between the particles and is written in the form

$$V_{\text{mf}} = \frac{4\pi\hbar^2 a}{m}|\phi|^2. \quad (2.27)$$

For a stable BEC the scattering length has to be positive. At negative a the interaction between the atoms is attractive and the condensate will undergo a collapse [Ryc04b, Web03a]. Interesting phenomena like the formation of bright matter-wave solitons [Cor06] or the so-called Bosenova [Don01] can be observed by tuning the scattering length around zero.

The crossing of a molecular bound state with the two-body threshold opens the way to actively produce dimers in a controlled way. Feshbach association of molecules by applying time-varying magnetic fields to atomic samples is a well established technique [Köh06]. The atomic gas is prepared away from the resonance, where no molecular bound state is available. A sweep of the magnetic field across the Feshbach

2.3 Feshbach resonances

resonance (to the side where a molecular bound state is energetically below the threshold) will allow for the association of dimers.

Cesium in its ground state features many narrow and broad resonances in a magnetic field range, which is easily accessible [Chi00]. A broad resonance located at negative magnetic field enables the experimentalist to control the scattering length precisely between $-2500a_0$ and $+1500a_0$ (a_0 is the Bohr radius), including the possibility to investigate the zero crossing of the scattering length at 17.1G [Gus08]. Furthermore Cs shows various Feshbach resonances related to higher molecular channels including s , d and g waves. Its relatively strong dipole-dipole interactions (see 2.1.4) enable coupling to higher partial waves. The rich structure of molecular channels for Cs allows for the production of dimers [Mar05] and the change in between Cs_2 molecules of different l -quantum number by cruising through the energy spectrum with the magnetic field [Kno08]. Furthermore with Cs it was first time possible to evidently show the existence of an Efimov resonance [Kra06].

Rubidium in its energetically lowest internal state has no Feshbach resonances up to a magnetic field of about 300G. Reference [Mar02] experimentally locates four s -wave Feshbach resonances up to a magnetic field of 1260G, of which the broadest with a width of about 170mG is located at 1007G. Other Feshbach resonances, which are associated with d -wave molecular states show widths which are typically below 1mG. In contrast to the Cs case the background scattering length of Rb is basically constant at a value of $100a_0$.

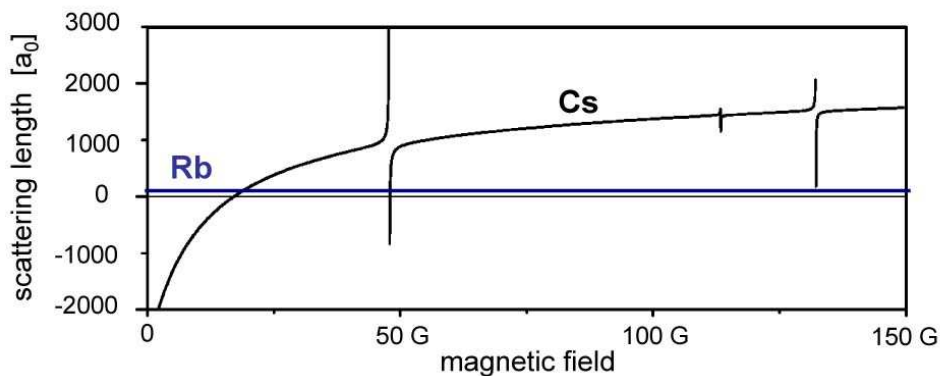


Figure 2.4: The dependence on the magnetic field of the single species scattering lengths of Rb and Cs in their energetically lowest internal states is shown. Cs has various Feshbach resonances, hence giving the opportunity to tune the interactions between the Cs atoms over a wide range. Rb on the other hand does not show any dependence of the scattering length on the magnetic field in the plotted region. Therefore interactions between Cs atoms can be adjusted while keeping the scattering length of Rb uninfluenced at a moderate value of $a_{bg} \approx 100a_0$.

2 Two-body interactions and Feshbach resonances

In figure 2.4 the magnetic field dependence of the scattering length of ^{133}Cs and ^{87}Rb is plotted. Cs has a very rich structure of Feshbach resonances (in contrary to Rb) and hence offers an easy way of tuning the scattering length. The behavior of the single-species scattering properties has important consequences for applications in mixed systems. In a mixture of Rb and Cs we can tune the scattering length and therefore the sign and the strength of the interaction between Cs atoms, while we keep the scattering properties of the Rb atoms uninfluenced. An open question remains the behavior of the interspecies scattering length, which can hardly be predicted by theory.

Up to the present work no interspecies Feshbach resonances have been observed in a mixture of Rb and Cs. On one hand side, the presence of interspecies Feshbach resonances allows for the control of the interspecies collisional properties. As it will be discussed in more detail in section 5.2, the relative strengths of inter- and intraspecies interactions define the stability and miscibility of a double-degenerate mixture. On the other hand, the availability of interspecies Feshbach resonances allows for the production of heteronuclear molecules. In general heteronuclear molecules in their ground state carry a permanent electric dipole moment on the order of 1D. The presence of a dipolar long-range anisotropic interaction opens the door to study polar quantum systems, which are expected to exhibit new phenomena [Bar08].

3 Rb-Cs mixture: Apparatus and experimental procedure

In this chapter we give an overview of the technical setup and the experimental procedures we use to produce an ultracold mixture of rubidium and cesium atoms. In the last years advanced techniques have been implemented to produce ultracold atomic samples by means of optical and magnetic fields. An overview of techniques used for single species preparation can be found in [Met99]. We focus on the presentation of special properties of the current experimental setup and cooling procedures, that are necessary to obtain an ultracold mixture of Rb and Cs. We make use of optical dipole traps [Gri00] to confine and cool both species. Cesium shows high inelastic two-body losses in excited states because of high rates for spin- and hyperfine-changing collisions [GO98a, GO98b, Hop00]. Therefore the use of magnetic traps to cool cesium below the microkelvin regime turns out to be limited by these inelastic losses in magnetically trappable states. The only state, which is stable against inelastic losses caused by two-body collisions, is the absolute ground state, which cannot be trapped with magnetic forces. The use of optical dipole traps is therefore indispensable on the way to submicrokelvin temperatures. The main experimental steps can be summarized as follows:

1. An effusive beam of Rb and Cs atoms is produced in the double-species oven section (see subsection 3.1.1). The atoms fly through a differential pumping section into the ultra-high vacuum region of the apparatus.
2. The effusive thermal beam of atoms from the oven is slowed down using the Zeeman-slowing technique (see 3.1.1).
3. Both species are captured by a combined two-color magneto-optical trap (MOT) in the main chamber (see 3.2 and 3.1.2).
4. The mixture is compressed by an increase of the magnetic gradient field, and a short phase of optical molasses is applied. About 5×10^8 atoms for each species are obtained at temperatures of approximately $40\mu\text{K}$.
5. We apply two-color degenerate Raman-sideband cooling on both species to further decrease the temperature (see section 3.3).

3 Rb-Cs mixture: Apparatus and experimental procedure

6. The atoms are released into a levitated crossed optical dipole trap (see section 3.4). After this stage the system is composed of 2.5×10^6 atoms for both species at temperatures of about $3\mu\text{K}$.

3.1 Apparatus and magnetic fields setup

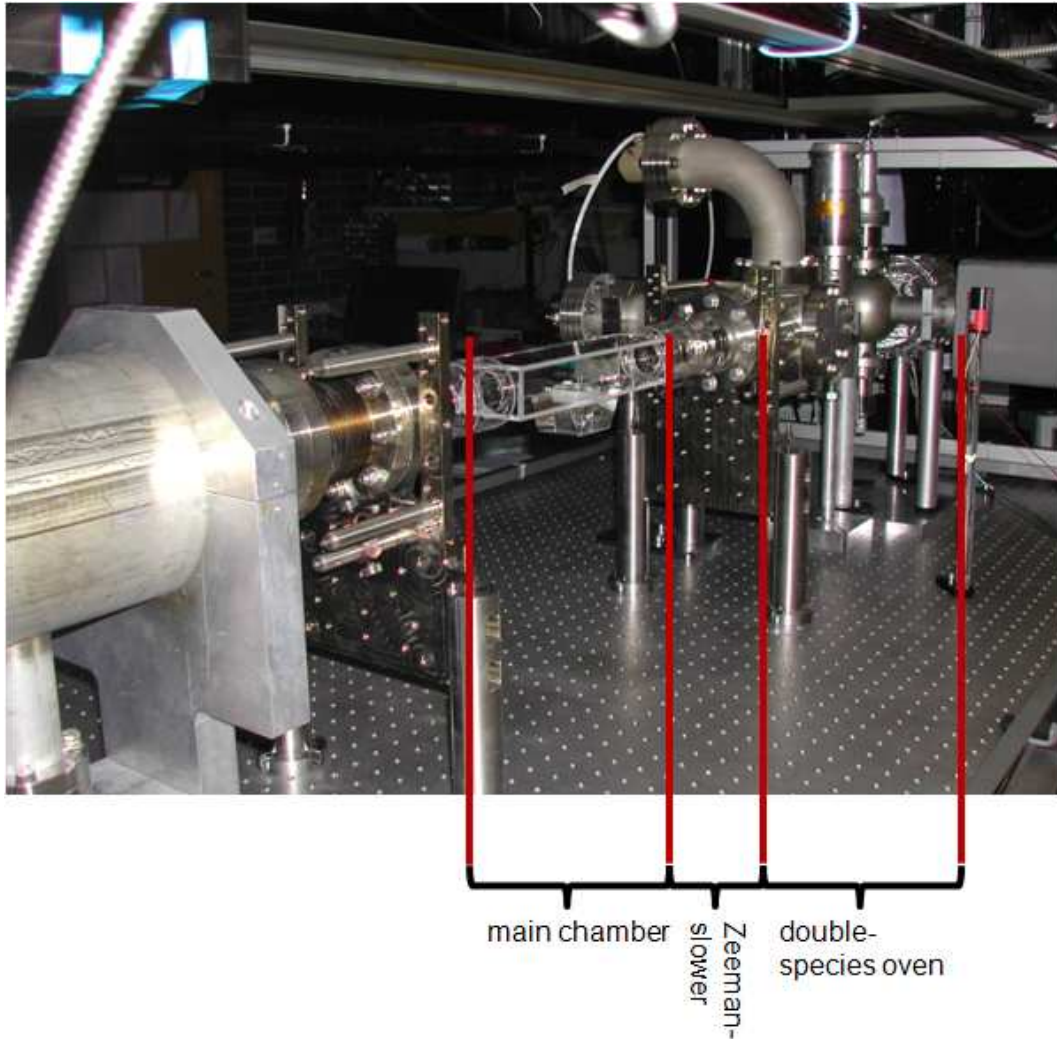


Figure 3.1: Vacuum chamber before installation of the optics. The apparatus can be divided into three different sections: The double-species oven including the differential pumping section, the Zeeman-deceleration path and the main experimental chamber.

Our current experimental setup has been upgraded from a previous apparatus operating only on Cs atoms. Detailed information on the previous experimental setup can be found in references [Ryc04b, Ham02b, Ham03, Ham02a, Ryc04a, Eng06]. The

3.1 Apparatus and magnetic fields setup

design of the apparatus has been substantially modified and implemented to include the Rb species. A picture of the vacuum apparatus without any optical components is shown in figure 3.1.

The addition of rubidium to the existing apparatus made the design of a new oven section necessary. Details on the double-species oven are given in subsection 3.1.1, where the use of a single Zeeman-slower setup for both species is discussed. Furthermore changes on the magnetic field setup and specialties of our main experimental chamber are given in subsection 3.1.2.

3.1.1 Double-species oven and Zeeman slower

The current double-species oven was originally designed for a three-species experiment, which is also located in Innsbruck [Wil09, Wil08]. The oven design was adopted for our purpose of having two species using bulk Cs and Rb as a starting point. The unique design of the oven meets several advantages:

- The reservoirs for cesium and rubidium are locally separated, hence preventing the atomic species from unwanted reactions already in the oven section.
- The different sections of the oven for different species allow to heat and temperature stabilize each section independently, hence having the control over single species atom flux.
- Each reservoir of the oven associated with a species is provided with its own valve separating the reservoir sections from the main oven section. Therefore the flux of different species through the differential pumping section can be controlled independently. Additionally there is no need to break the vacuum if a refill of the species is necessary, as each species-section can be connected separately to an external vacuum pump.
- For a nozzle we use micro-tubes with an inner diameter of $200\mu\text{m}$. The use of micro-tubes has two main advantages: First, the micro-tubes serve as an additional differential pumping line. Second, the micro-tubes collimate the atomic beam, therefore increasing the flux of atoms to the region of interest.

Figure 3.2 shows a photograph of the double-species oven. Each section of the oven is temperature controlled and heated to different temperatures. The reservoir for Cs atoms is heated to about 80°C , while the Rb side is stabilized to approximately 100°C . The region of the micro-tubes is set to a slightly higher temperature to prevent the atoms from sticking to the walls of the tubes and hence blocking them. The entire hot part of the oven is surrounded by a metal box including a fan, that guides the hot air away from the vacuum apparatus and prevents unwanted heating and temperature fluctuations of the remaining experimental setup.

3 Rb-Cs mixture: Apparatus and experimental procedure



Figure 3.2: Photograph of the double-species oven. The different sections associated with the different species can be independently temperature controlled.

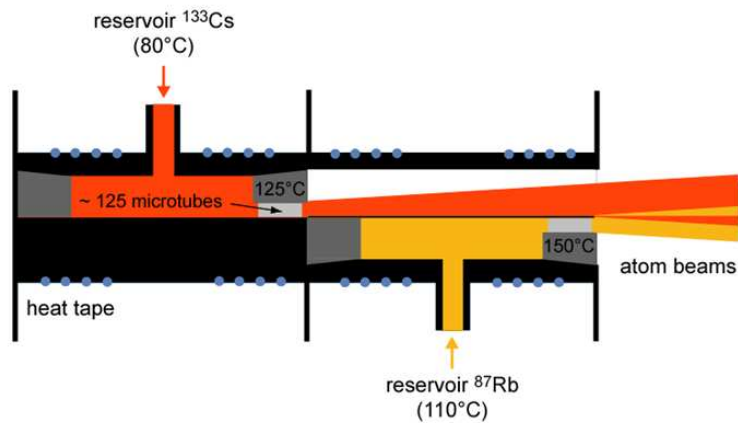


Figure 3.3: Cut through the double-species oven. Different sections of the oven are stabilized independently to different temperatures.

Figure 3.3 shows a cut through the double species oven including the micro-tubes¹. Two evacuated glass ampullae with 1 gram of Rb and Cs each is put into the reservoir sections of the oven. After pumping down to operating vacuum conditions, the ampullae are broken in vacuum by imposing an external force to the steel housing. We do not observe a reduced flux of atoms yet, which indicates that there is up to now no necessity to refill.

¹about 125 micro-tubes with a diameter of 200nm are used for each species

3.1 Apparatus and magnetic fields setup

The atoms leave the oven with a most probable speed of around 200m/s and pass the differential pumping section (details can be found in [Eng06]) to enter the ultra-high vacuum part of the chamber. The speed of the atoms has to be reduced to at least the capture velocity of the double-species magneto-optical trap [Met99]. To do so, we use the Zeeman-slowing technique. The force and therefore the deceleration of the atoms is imposed by space dependent resonant light scattering controlled by a clever design of the magnetic field, compensating for the Doppler-shift along the deceleration path. The use of a single Zeeman slower for two species can be challenging. We calculate the optimum design of the Zeeman-slower magnetic field for both species. A simulation of the efficiency of the Zeeman slower shows, that we can operate the Zeeman slower magnetic field on the optimized values for Cs, without major losses on the efficiency of slowing down Rb.

3.1.2 Glass cell and magnetic fields

Our main experimental chamber is a glass cell with the dimensions 238mm × 45mm × 60mm. This glass cell was developed by B. Engeser [Eng06] and specially designed for the investigation of trapped atoms close to a surface. The highlight of the glass cell is a prism with a super-polished surface, which is glued to the glass cell with epoxy seal², and allows the implementation of evanescent waves. Figure 3.4 shows a picture of the glass cell including the glued-in glass prism. For the current experimental setup the prism is not used.

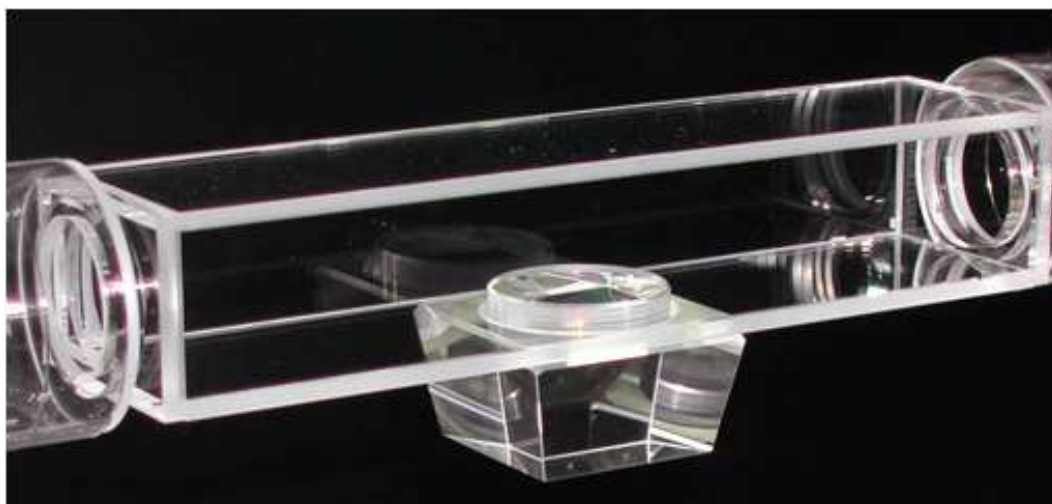


Figure 3.4: Main experimental chamber: Glass cell with integrated super-polished prism, which allows for production of evanescent waves.

Generally a vacuum system, which supports UHV is necessary to prevent the cold atomic samples from being lost due to collisions with the background gas (see section

²Epotek 353 ND

3 Rb-Cs mixture: Apparatus and experimental procedure

2.1.1). Pressures around a few 10^{-11} mbar allow lifetimes of the trapped atoms on the order of 100 seconds, providing enough time to prepare and investigate the gas. Figure 3.5 shows the remaining atom number of Cs over time in a magnetic trap in the glass cell. The $1/e$ -lifetime of the sample in the magnetic trap is about 100s. In the previous setup, which was used to investigate an ultracold sample of Cs atoms close to a surface, we have observed lifetimes on the order of 20s [Eng06]. Later we realized the presence of residual resonant light, which could pass an optical fiber because of a broken mechanical shutter. We got rid of this problem and obtain lifetimes now, which are consistent with the pressure of 2×10^{-11} mbar.

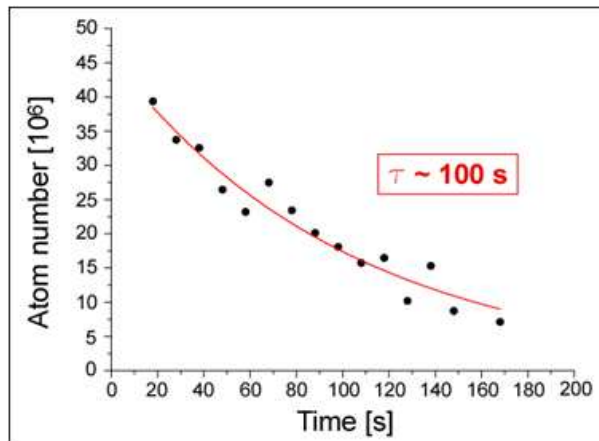


Figure 3.5: Number of remaining Cs atoms over time in a magnetic trap. The exponential fit to the decay curve results in a $1/e$ -lifetime of the sample of around 100s.

In addition the use of a glass cell has several advantages. Obviously the use of a glass cell of this size offers great optical access. This is especially important for more complex systems, like the combination of two or more atomic species, of which each needs different lasers for cooling and trapping. Furthermore the advantage of a glass cell compared to a steel chamber is obvious for the use of magnetic fields. We do not suffer from eddy currents, therefore fast switching times and accurate control of magnetic field values on a precise level are possible.

For preparation and control of the atomic sample we need homogenous magnetic fields and gradient fields. The magnetic gradient field can be used to realize a magnetic trap or to hold the atoms against gravity. The force compensating for gravity is associated with an atom carrying a magnetic moment in a gradient magnetic field. Atoms in an external magnetic gradient field see the following potential

$$U_{\text{mag}} = m_F g_F \mu_B B, \quad (3.1)$$

where m_F and μ_B are the magnetic quantum number and the Bohr magneton, respectively. The Landé g -factor is $-\frac{1}{4}$ for Cs and $-\frac{1}{2}$ for Rb in their respective lowest hy-

3.1 Apparatus and magnetic fields setup

perfine states. Rb and Cs in their lowest internal state can be levitated by the magnetic force, since they are *low-field seekers*. Because of *incidentally* shared properties of the species the magnetic gradient field can be used for both species without change. In the case of ^{87}Rb and ^{133}Cs the difference of this ratio in between the species is only a few percent without regarding the quadratic Zeeman effect

$$\frac{\mu_{\text{Cs}}/m_{\text{Cs}}}{\mu_{\text{Rb}}/m_{\text{Rb}}} \approx 0.98, \quad (3.2)$$

where μ_{Cs} and μ_{Rb} denote the magnetic moments of Cs in the state ($F = 3, m_F = 3$) and Rb in the state ($F = 1, m_F = 1$), respectively. In the case of Rb and Cs in their absolute internal ground states, we calculate the value for the equilibrium between gravitational force and magnetic gradient force to be $\approx 31\text{G/cm}$. The small difference of magnetic moment to mass ratios for the states used allows for levitation of both species with the same magnetic gradient field. As an important consequence we do not suffer from a mismatch in between the two-species clouds due to the gravitational sag, when we compensate for gravity using the gradient field.

The magnetic moment to mass ratio changes when we apply homogeneous magnetic-offset fields, since the quadratic Zeeman effect has to be taken into account. Therefore the levitation condition can not be fulfilled for both species simultaneously, when a strong homogeneous magnetic offset field is present. Figure 3.6 shows the deviation of the optimum magnetic gradient field from its value at zero magnetic-offset field for both species.

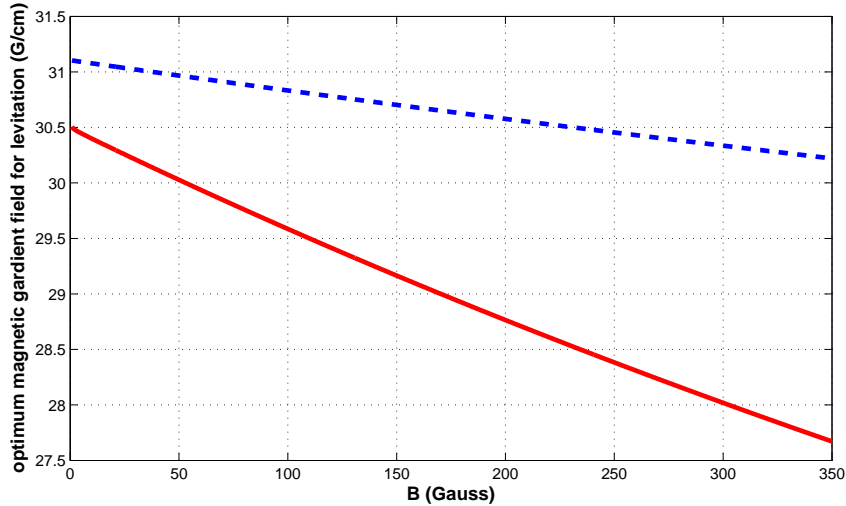


Figure 3.6: Optimum magnetic gradient field in the presence of a homogeneous offset field. The solid (red) line corresponds to the Rb case, where the dashed (blue) line shows the optimum magnetic gradient field for Cs.

3 Rb-Cs mixture: Apparatus and experimental procedure

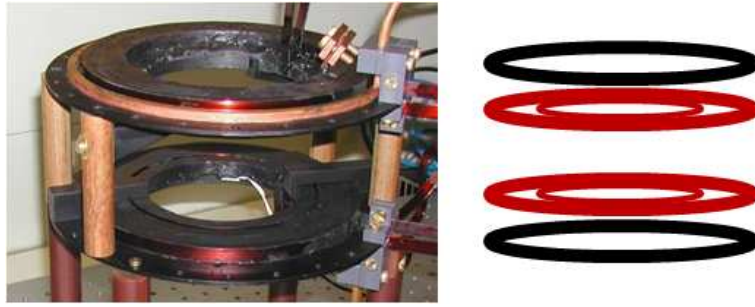


Figure 3.7: Photograph of the magnetic field coils setup on the left. On the right the schematic distribution of the six available magnetic field coils is indicated by colors, red for homogenous field and black for gradient field.

Homogenous magnetic fields are used to control the interactions between the atoms, as already introduced in section 2.3.1. When we started building up the experiment, nothing was known about the positions of interspecies Feshbach resonances between Rb and Cs. For the search of Feshbach resonances experiments usually require homogenous magnetic fields on the order of 1000G. The old magnetic field setup (working with single species Cs) was designed to reach homogenous magnetic field values of up to only 70G. Therefore we improved the magnetic field setup to enlarge the range of operation. In more detail the old magnetic field configuration consisted of six single water-cooled coils. We redistribute the interconnections of the coils and upgrade the power supplies to maximum currents of 100A for the gradient field and 200A for the homogenous field. A schematic of the six-coil configuration and a picture of the coils setup is displayed in figure 3.7. Further details on the exact configuration of the single coils can be found in [Pil05].

To summarize we are able to reach homogenous magnetic fields up to 670G in the presence of the levitation field. A restriction has to be made, since the homogeneous magnetic field cannot be operated steady state at high values, because water cooling is not sufficient enough to permanently carry away the heat produced by the power dissipation of the coils. Up to now we are e.g. limited to pulse durations of about 5s for the homogeneous magnetic field at values of around 300G, when the levitation field is switched on. Longer pulse durations will lead to extensive heating of the coils and produce instabilities of the atom numbers due to thermal effects.

3.2 Two-color magneto-optical trap

This section provides an overview of the technical realization of a double-species magneto-optical trap (MOT). Nowadays a MOT is a well established key technique in the field of ultracold quantum optics [Raa87]. It provides cooling and trapping of atoms down to a few tens of microkelvin. Basically a MOT relies on the force of near-resonant laser radiation acting on the motion of the atoms. In the presence of a

quadrupole magnetic field these light forces are depending on the polarization and get spatially dependent (because of the Zeeman effect), consequently providing confinement of the atomic gas. Even though a MOT is a well established technique today, the simultaneous cooling of two different atomic species gives rise to new technical challenges. The first subsection will briefly summarize the basic laser setup for ^{133}Cs and ^{87}Rb . Additionally the technical realization of the double species MOT is presented. In the end the experimental procedure and the results of loading the atoms into the MOT including the subsequent compression- and molasses-phase are discussed.

3.2.1 Rb and Cs laser setup

A closed atomic transition is necessary to continuously cool and trap atoms in a MOT. For alkali atoms the transition between the upper hyperfine levels in the ground ($S_{1/2}$) and in the excited state ($P_{3/2}$) is basically closed. Off-resonant excitations can cause the atoms to decay into the lower hyperfine state. To depopulate the lower hyperfine state a repumper laser is needed in addition to the cooling laser. Therefore we basically need two different wavelengths for each species to realize a MOT.

Cs laser system

Figure 3.8 shows the relevant level scheme for Cs. The cooling light for Cs is resonant to the $F = 4 \rightarrow F' = 5$ transition, where else the repumper-laser runs on the $F = 3 \rightarrow F' = 3$ manifold.

In the case of Cs the lasers light at a wavelength of 852nm is provided by a rather complex diode laser system (details are found in [Pil05]). The underlying structure of the diode laser system is based on a combination of grating stabilized laser diodes, which are themselves directly used for the experiment or used to seed so-called slave lasers, which are able to deliver more optical power. Acousto-optical modulators (AOM) shift the frequency of the laser light and thus provide control over detuning and optical power. Fast switching of the laser intensity is enabled by the control of the radio-frequency power applied to the AOM.

Rb laser system

To provide a closed transition for cooling and trapping rubidium, two grating stabilized so-called master lasers are spectroscopically locked on the $F = 2 \rightarrow F' = 3$ and the $F = 1 \rightarrow F' = 2$ transitions. Figure 3.9 shows the relevant level scheme of Rb.

In contrast to the Cs diode laser system, the detuning for the cooling transition is not produced with an AOM, instead we beat-lock [Sch99] another grating-stabilized laser diode to the master reference. The advantage of this setup is the larger tuning range of the laser, which is basically limited by the bandwidths of the radio-frequency electronics used. Furthermore, we amplify the light delivered by the beat-locked laser with a commercial tapered amplifier setup³, which has a maximum output power of 1W

³BoosTA 780, Toptica

3 Rb-Cs mixture: Apparatus and experimental procedure

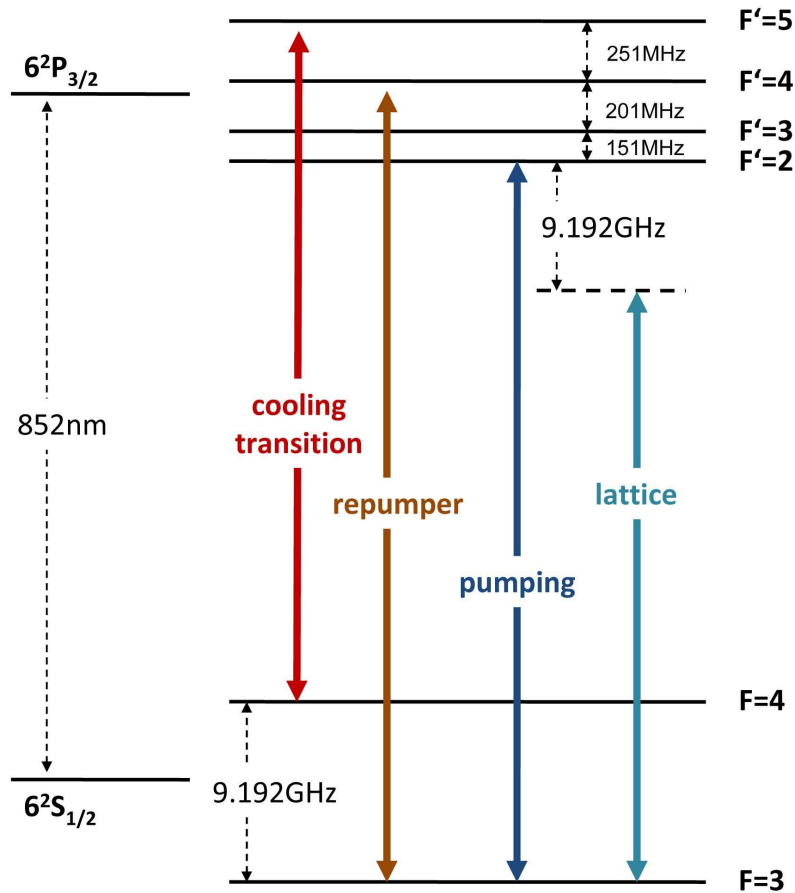


Figure 3.8: Relevant level scheme of Cs atoms (frequencies not to scale). The arrows indicate the laser transitions used for the MOT (cooling transition and repumper). In addition the wavelengths for the lattice and the pumping beam used for degenerate Raman-sideband cooling (see 3.3) are shown.

at an amplification factor of 100. The available power for the Rb cooling transition is more than sufficient to run a MOT. Similar to the Cs laser setup we seed two slave lasers to provide enough optical power for the Zeeman slower. Further details on locking schemes and the mechanical setup of the home-built lasers can be found in [Tha01, Unt05].

The setup of the diode laser systems for the near resonant light used for a MOT is placed on a different optical table apart from the main experimental apparatus, to protect the atomic cloud against resonant stray light. The laser radiation needed for trapping, cooling and imaging of the atomic clouds is delivered to the main experimental table with single-mode polarization-maintaining optical fibers. As already mentioned, fast switching is provided by the use of AOMs. In addition mechanical shutters are used to guarantee full shut-down of the laser power. Polarization-maintaining fibres can suffer from fluctuations induced by thermal instabilities. To compensate for fluctu-

3.2 Two-color magneto-optical trap

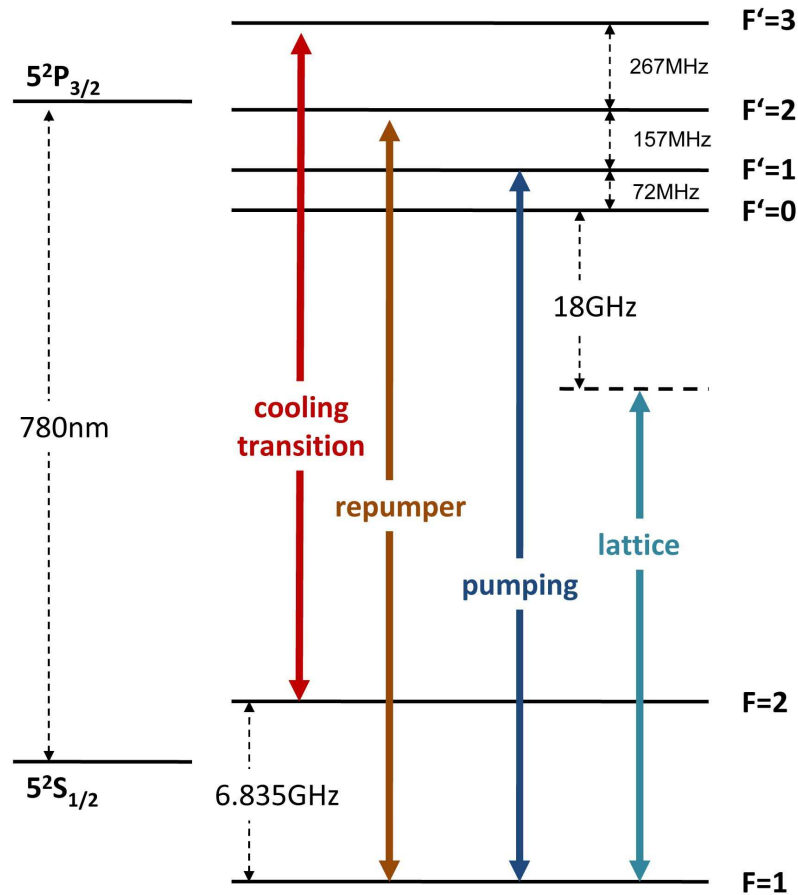


Figure 3.9: Relevant level scheme of Rb atoms (frequencies not to scale). The arrows indicate the laser transitions used for the MOT (cooling transition and repumper). In addition the wavelengths for the lattice and the pumping beam used for degenerate Raman-sideband cooling (see 3.3) are shown.

ations of the polarization we clean the polarization after the fibre by using a polarizing beam-splitter. Fluctuations of the polarization will thereby be translated into intensity instabilities. To stabilize the intensity we couple a few percent of the light after the beam splitter out and actively control the laser power by tuning the radio-frequency power applied to the AOM. This technique is usually used for all laser light going to the experimental chamber, increasing significantly the shot-to-shot and long-term stability of the measured atom numbers.

3.2.2 Two-color magneto-optical trap setup

We realize the double-species MOT with a single optical setup. We use six two-color counterpropagating laser beams. One advantage of using a single optical setup for the two-color MOT is to save space and thus provide maximum optical access around the

3 Rb-Cs mixture: Apparatus and experimental procedure

main experimental chamber. Another important point is the relative position between the Rb and Cs MOTs. To have both wavelengths coming out of a single-mode fibre automatically gives almost perfect overlap between the clouds of different species. Consequently after alignment of a single species MOT (e.g. Cs), we just need to find the optimum laser detunings for the other species (e.g. Rb) to get both MOTs loading.

We combine both wavelengths for the cooling transitions, 780nm for Rb and 852nm for Cs, on a dichroic mirror⁴ in front of a polarization-maintaining single-mode optical fibre, which delivers the laser light to the main table. On the main table we use broadband optics suitable for both wavelength. As already mentioned in the previous subsection, we actively control the laser intensities. To do so independently for both colors, we again use a dichroic mirror after picking off a few percent of the overall light power. The two different wavelength components are separated again and can be monitored on different photodiodes.

For sure we have to be careful with the selection of optical components. Already a slightly angled output facette of the optical fibre turns out to result in a visible mismatch in between the mode profiles of the two wavelength components after a few meters, because of the dependence of the refractive index on the wavelength. Furthermore we pay attention to use optical components like polarizing beam-splitters and broadband waveplates, of which the specifications promise very little deviation from the nominal values.

For the Zeeman-slower laser beam we combine the two wavelengths for the cooling transition directly on the main optical table on a dichroic mirror, which allows independent control of the beam alignment. For efficient Zeeman slowing the repumper light for both species is overlapped with the cooling light.

We optimize the values of the magnetic gradient field, the detuning of the cooling transition for the MOT and the Zeeman slower independently for both species on maximum atom numbers and fast loading. The case of simultaneous loading of both species will be discussed in the following subsection. Each of the six two-color MOT beams has a waist of about 1cm and an optical power of 8mW for Cs and 13mW for Rb. The optimum detuning of the cooling light for Cs (Rb) is -8MHz (-10MHz). The optical power of the Zeeman slower beam, which has a waist of about 1cm, is 40mW for Cs and 25mW for Rb. The repumper laser is superimposed on the beams of the MOT and the Zeeman slower. The detunings and optical powers for the repumper are -10MHz and 20mW for Cs and -12MHz and 25mW for Rb, respectively. The detuning of the repumper lasers are optimized on maximum loading efficiency of the MOT. At a gradient magnetic field of about 7G/cm we are able to load 5×10^8 atoms of Cs or Rb.

⁴Laseroptik Garbsen, custom order: one side of the mirror is coated for high reflectivity of 852nm and high transmission for 780nm under 45° , where the other side of the mirror is has a high transmission coating under 45° .

3.2.3 Experimental procedure and results

This subsection explains the experimental sequence used to load the double-species MOT including the subsequent combined compression and molasses phase. Furthermore, we developed a way to selectively control the atom number of Rb and Cs collected in the MOT. Finally the experimental results will be shown including a discussion of inelastic losses in the MOT caused by light-assisted inelastic collisions.

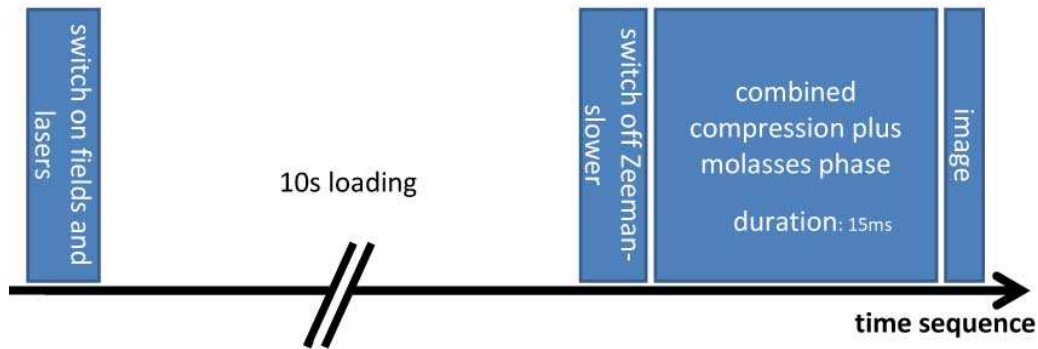


Figure 3.10: Timing sequence of loading the MOT including combined compression and molasses. The MOT is loaded for 10s before the Zeeman slower is switched off. For the compression and molasses phase we increase the value of the gradient magnetic field during we further shift the detuning of the MOT lasers to the red. As a last step the atom numbers and temperatures of the sample are extracted by standard absorption imaging [Ket99].

Timing sequence

Simultaneous loading of two species into a MOT requires a full control over several parameters. We are able to control basically all tunable experimental parameters such as laser light intensities and detunings, magnetic field values, etc. by a home-made computer-control interface. The timing sequence in figure 3.10 shows the procedure of loading the MOT plus subsequent molasses and compression phase. First the magnetic gradient field and the lasers for MOT and Zeeman slower are switched on. After a MOT loading phase of around 10s we switch off the Zeeman slower and start the combined compression and molasses phase. During this sequence (duration of about 15ms) we increase the strength of the magnetic gradient field by a factor of two to about 14G/cm. At the same time we increase the detunings of the MOT beams to -80MHz for Cs and to -110MHz for Rb. During the combined compression plus molasses phase we reduce the temperature of both species by nearly one order of magnitude to about $30\mu\text{K}$ for Cs and $40\mu\text{K}$ for Rb.

To extract the atom numbers we use standard absorption imaging. To measure the temperature of the atomic samples, we perform expansion measurements [Ket99]. Besides absorption imaging, we are also able to recapture the atoms into the MOT and record the fluorescence signal. We apply absorption imaging, when we need to know

3 Rb-Cs mixture: Apparatus and experimental procedure

the exact atom number, or when we measure temperatures. The recorded fluorescence signal is used to measure relative atom numbers. With the recapture method we are not able to extract the absolute atom number, but it is a powerful tool for measurements with low atom numbers. Depending on the experimental sequence we choose either to do absorption imaging or to recapture the atoms in the MOT.

Selective control of the atom number

For certain experiments we face the necessity to adjust the relative atom number of rubidium and cesium. For this purpose we developed a way, to selectively control the atom number of each species loaded into the two-color MOT. We use two photodiodes which record the fluorescence signal of the atoms already collected in the MOT. Each photodiode is species-selective, as we apply narrowband wavelength filters in front of each photodiode. The voltage output of the photodiode is proportional to the atom number in the MOT. We use a PI-circuit [Tie93] to selectively load and stabilize a single species MOT up to a certain value of voltage, which corresponds to a certain atom number. The control output of the PI-circuit is applied to the radio-frequency amplifier, which tunes the laser intensity via an AOM.

We have to take into account for an offset error on the photodiodes recording the fluorescence, as stray light of the MOT- or Zeeman-laser beams will also pass the narrowband filters. In this case we choose to control the laser intensity, which affects the offset on the photodiode least. In the case of Rb we actively control the Zeeman-slower laser intensity to keep the fluorescence signal at a certain level. If the voltage output of the fluorescence photodiode is corresponding to the setpoint, the laser power of the Zeeman slower is reduced. Therefore we balance the number of atoms loaded into the MOT region with the number of atoms getting lost from the atomic cloud. Hence we are able to stabilize the atom number collected by the MOT. The disadvantage of using the Zeeman-slower to control the atom number is the reduced speed of control, which relies on the rather long lifetime of a MOT on the order of several tens of seconds. In the case of Cs we use the repumper intensity to control the level of MOT loading. As the atoms will decay to a dark state regarding the cooling transition in the absence of the repumper light, they are no longer under the effect of the light force and can therefore leave the trap.

Figure 3.11 shows the stabilization of the fluorescence signal and the Cs atom number by controlling the fluorescence signal. Note that the atom number is measured after the combined compression plus molasses phase. Fluctuations introduced during this phase cannot be compensated by the control of loading the MOT. We observe a reduction of the shot-to-shot fluctuations to below 0.5% for the fluorescence signal, where the fluctuations of the atom numbers reduce to below 5%.

Light-assisted inelastic collisions

There are two main limitations to temperature and density which are associated with conventional laser cooling in a MOT or optical molasses [Wei99]. The first one is known as the reabsorption of photons. Near resonant photons, which need to be scat-

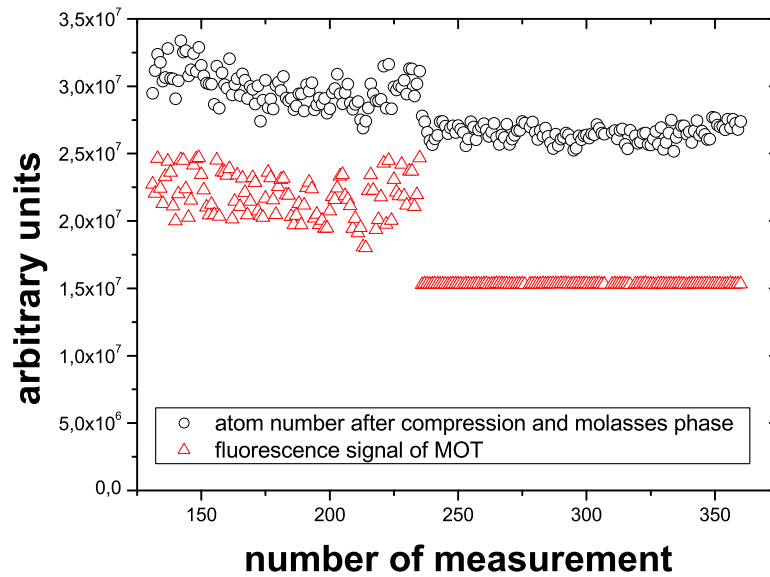


Figure 3.11: Stability of the Cs atom number (open circles) and the fluorescence signal (open triangles) with and without the use of the active control of the fluorescence signal. Note that the atom number is recorded after the compression and molasses phase, during which additional fluctuations limit the atom-number stability.

tered in the process of laser cooling, can be rescattered by other atoms before they leave the cloud. This leads on average to a force outwards the center of the cloud, therefore preventing the density from further increasing. Additionally the recoil momentum of the rescattered photons produces heating, limiting lowest achievable temperatures. The other contribution to temperature and density limitations is the loss of atoms due to light-assisted collisions. The near resonant light needed for cooling induces an atomic dipole moment, which allows the atoms to interact strongly on a long range. Two atoms colliding in the presence of near resonant photons can be coupled to an excited molecular bound state, which will decay back to the ground state threshold of the atom pair potential. The energy gain for such a process is typically much bigger than the depth of the trap and will therefore lead to losses, thus limiting the density of the MOT.

We observe strongly reduced loading of the double-species MOT compared to the single-species case, because of light-assisted collisions in the presence of both species. The group of Simon Cornish in Durham observed similar behavior in their experiment [Har08]. They quantitatively evaluate the loss rates by measurements of the lifetime of the MOT with and without the presence of the respective other species. Figure 3.12 shows the decay of a Cs MOT in the presence of Rb atoms. They conclude that the

3 Rb-Cs mixture: Apparatus and experimental procedure

Table 3.1: Table of the strength of light-assisted inelastic collisions. β_{CsCs} is associated with the loss rate of Cs for the single species case, where β_{CsRb} is associated with the loss rate of Cs in the presence of Rb.

	β ($10^{-11} \text{cm}^3 \text{s}^{-1}$)
β_{CsCs}	1.5(2)
β_{RbRb}	2.1(1)
β_{CsRb}	10(6)
β_{RbCs}	16(4)

interspecies light-assisted inelastic collisions are almost one order of magnitude larger than the single-species ones. Table 3.1 summarizes their results.

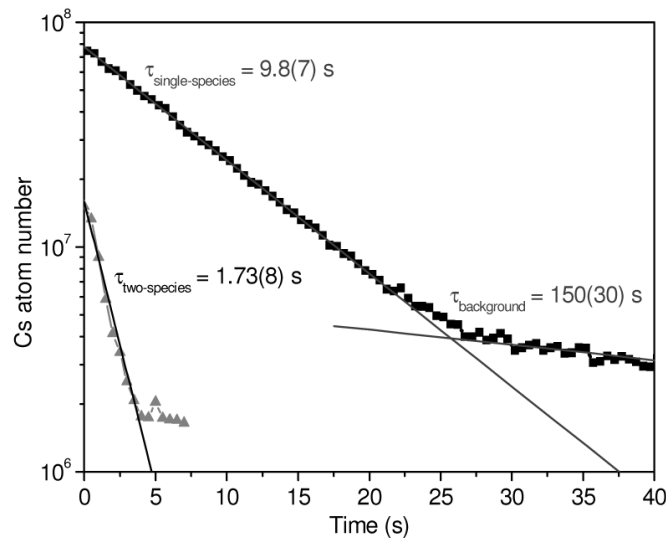


Figure 3.12: Decay of the Cs atom number in the MOT phase with (triangles) and without (squares) Rb present. Measurements taken at Durham University in the Cornish group [Har08].

As the inelastic interspecies losses are related to the overlap in between the two species, the loss rate β will significantly reduce by displacing one cloud with respect to the other. In our experiment we are able to selectively displace one or the other cloud by changing the detuning of the Zeeman-slower laser beam. By introducing a displacement, we do not observe a significant difference of atoms in the MOT if a single or both species are loaded.

With the technique of selective displacement of the two MOTs, we are able to simultaneously load and precool about 5×10^8 atoms of each species within 10s to a temperature of about $30\mu\text{K}$ and $40\mu\text{K}$ for Cs and Rb, respectively.

3.3 Two-color degenerate Raman-sideband cooling

A way to overcome the limitations on density and temperature in a MOT is the use of degenerate Raman-sideband cooling (DRSC). The implementation of this technique for both species is a major step towards the achievement of an ultracold mixed sample of Rb and Cs in an optical dipole trap. First we will explain the basic concept of Raman-sideband cooling, while in subsection 3.3.2 the technical realization is presented. Finally the experimental procedure and the results will be discussed.

3.3.1 Degenerate Raman-sideband cooling - basic concepts

Degenerate Raman-sideband cooling (DRSC) is a powerful technique to cool the atoms. Simultaneously both species get polarized in their lowest internal state. Up to now degenerate Raman-sideband cooling has been used for both Rb and Cs in a few single-species experiments dealing with ultracold atoms [Vul98, Ker99, Han00, Föl03, Wei05]. Especially for Bose-Einstein condensation of Cs it serves as a key tool, since efficient loading of an optical dipole trap is relying on starting conditions with high phase-space densities [Web03a]. It shows, that temperatures one order of magnitude below the temperatures achievable with optical molasses are obtainable with the technique of DRSC within an overall cooling duration on the order of 10ms [Tre01].

The substantial advantage of DRSC is the presence of a dark state, into which eventually all atoms will be pumped. The atoms are optically transferred at the end of the cooling process into this dark state. Therefore atoms which are already cooled to the lowest achievable temperatures are no longer exposed to resonant photon scattering. DRSC uses a three-dimensional optical lattice, optical pumping and a small homogeneous magnetic field. The scheme for degenerate Raman-sideband cooling of Cs atoms in an optical lattice is given in figure 3.13.

The atoms experience an array of micro-harmonic traps in the presence of the lattice potential. As the atoms are loaded into the lattice, they will be distributed among different vibrational states and different Zeeman states. A small homogeneous magnetic field is applied to the sample in such a way, that two adjacent vibrational levels of neighboring Zeeman levels, described by the quantum numbers (m_F, ν) and $(m_F + 1, \nu + 1)$, are degenerate. The laser light of the lattice itself is used to drive two-photon Raman transitions between the degenerate levels. Another important ingredient to make cooling possible is the pumping light. Particularly the polarization and direction of the pumping laser beam regarding the magnetic field is chosen in a clever way. The pumping light has to drive optical transitions towards the lowest Zeeman substate. In addition the state $(m_F = 3, \nu = 0)$ has to be dark with respect to the pumping laser field and the light used for the lattice. The cooling originates from the spontaneous decay of the atoms pumped to the excited level ($F = 2$). If the atoms will decay to an energetically lower lying state, the transfer of energy will be equal to the vibrational energy splitting. The cooling cycle is repeated until the atom reaches the state $(m_F = 3, \nu = 0)$. There it will remain since this state is dark regarding the pumping light and the two-photon

3 Rb-Cs mixture: Apparatus and experimental procedure

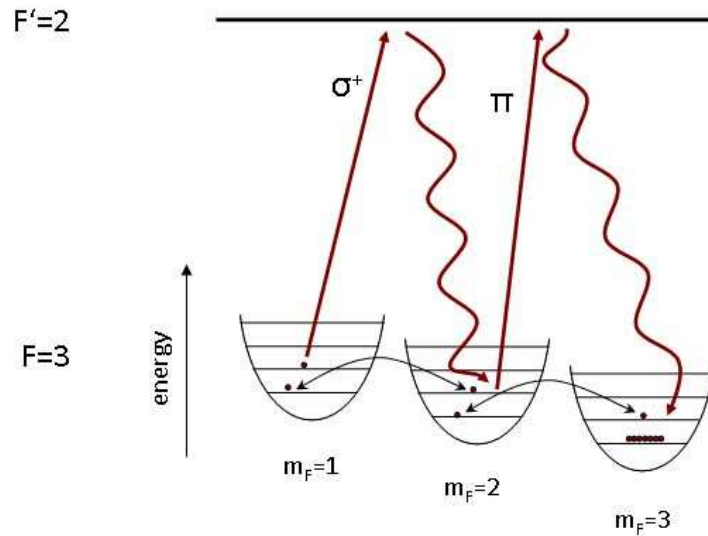


Figure 3.13: Degenerate Raman-sideband cooling for Cs. The atoms are loaded into an optical lattice and a small homogenous magnetic field is applied. The magnetic field strength is chosen in such a way, that the vibrational levels of neighboring Zeeman states (m_F, ν) and $(m_F + 1, \nu + 1)$ are degenerate. The laser light used to generate the optical lattice is able to drive two-photon Raman transitions between adjacent Zeeman levels of different vibrational quanta. The additional optical pumping is chosen in such a way, that the state $(m_F = 3, \nu = 0)$ is dark. The combination of two-photon Raman transitions and optical pumping will repeat until all atoms are collected in the dark state.

Raman transition.

3.3.2 Technical setup

We extend the basic concept of single-species DRSC to simultaneous cooling and polarizing Rb and Cs. For efficient loading of an optical dipole trap, we have to perform two-color degenerate Raman-sideband cooling on both species at the same time and in the same place. Besides facing technical challenges, we had to find a solution to fulfill the degeneracy condition for the two-photon Raman transition for both species at the same value of the homogenous magnetic field. To compensate for a mismatch when using optimized parameters of the magnetic field strength for one species, we match the vibrational splitting of the other species by tuning the lattice depth.

Figure 3.14 schematically shows the basic concept of two-color DRSC analogue to the single species case. Neighboring vibrational levels have to be energetically degenerate for both species.

3.3 Two-color degenerate Raman-sideband cooling

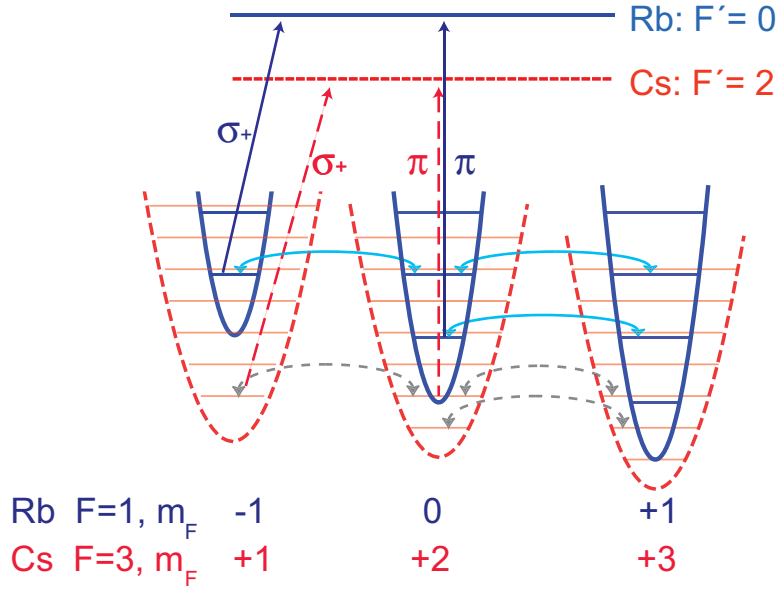


Figure 3.14: Illustration of two-color DRSC. The red color (dashed) corresponds to the Cs case, blue (solid) to the Rb case. DRSC works for both species, when neighboring vibrational levels are energetically degenerate for both Rb and Cs.

Two-color optical lattice

We use two different wavelengths to produce the three-dimensional optical lattices. Similarly to the realization of the two-color MOT we use dichroic mirrors and broadband optical components to overlap the lasers for both species. The combined light is directed to the main experimental table with a single-mode polarization-maintaining optical fibre. The intensities of both light fields are independently controlled and stabilized. To realize a three-dimensional optical lattice we use a four-beam configuration. Two beams are propagating in the x - z -plane perpendicular to each other. The third beam is directed along the y -axes, and retroreflected, see figure 3.15. With respect to a six-beam configuration the use of a four-beam lattice is insensitive to phase fluctuations of the single beams with respect to each other. While phase fluctuations in a six-beam lattice change the geometry of the lattice potential, fluctuations in the case of a four-beam lattice will only result in an overall translation [Gry93]. All four beams of the two-color Raman lattice are linearly polarized. To enable Raman coupling between states with different m_F quantum numbers, the polarizations of the beams are slightly tilted with respect to each other, see figure 3.15. We basically copy the lattice configuration including the relative orientation of the polarizations from the setup used in reference [Tre01].

The light for the Cs lattice is provided by a home-built diode laser. This laser is operated in slave configuration [Unt05], seeded by a laser running close to the Cs $F = 4 \rightarrow F' = 4$ transition. The maximum output power after the optical fibre on

3 Rb-Cs mixture: Apparatus and experimental procedure

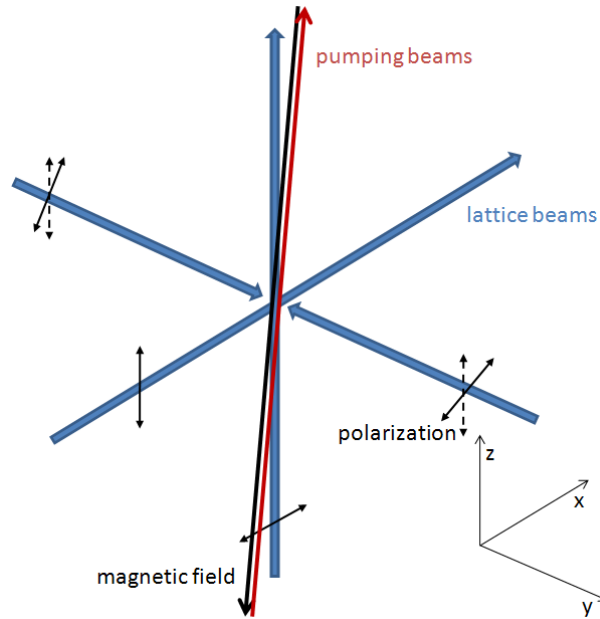


Figure 3.15: Configuration of the four beam three-dimensional two-color lattice. Two single beams are traveling within the x - z -plane under a relative angle of 90° . The third lattice beam is pointing in y -direction and reflected to generate a counterpropagating beam. The polarizations of each lattice beam have to be adjusted as described in reference [Tre01]. In addition the relative orientations of the homogenous magnetic field and the direction of the pumping beam are shown. The polarization of the pumping laser has to be mainly σ^+ with a small admixture of π with respect to the quantization axes given by the magnetic field, to drive transitions towards the dark state.

the main experimental table is about 60mW. For Cs atoms in the lowest hyperfine manifold ($F = 3$) this laser is red detuned with respect to the next possible optical transition ($F = 3 \rightarrow F' = 2$) by the hyperfine splitting of the ground state (9.2GHz). Cs atoms loaded into the three-dimensional lattice will occupy different vibrational levels. The light of the lattice itself drives two-photon Raman transitions between the vibrational levels of neighboring Zeeman states in the presence of a suitable magnetic field strength.

The light for the Rb lattice is generated by a grating-stabilized master diode laser in Littrow configuration [Tha01]. The wavelength of this laser can easily be tuned over a range of about 100GHz by tilting the grating with a piezo-electric crystal. The center frequency of the master laser is set to be 18GHz detuned to the red of the $F = 1 \rightarrow F' = 0$ optical transition. The optical output power of about 25mW is used to seed a commercial tapered amplifier laser⁵, which provides a maximum out-

⁵Toptica, BoosTA 780

3.3 Two-color degenerate Raman-sideband cooling

put power of 1 Watt. The high power and large tuning range of the Rb lattice laser gives us the possibility to slightly adjust the splitting between the vibrational levels. Since we have to fulfill the degeneracy condition for the two-photon Raman transition, the tunability of the vibrational splitting is crucial for simultaneous degenerate Raman sideband cooling of both species.

The homogenous magnetic offset field

A small homogenous magnetic field is applied, which shifts the magnetic sublevels in such a way, that vibrational levels with a difference $|\Delta\nu| = 1$ of the vibrational quantum number are degenerate. This magnetic field is produced by three pairs of coils, of which each pair is generating either a field in x -, y - or z -direction. Each pair of coils supports a maximum magnetic field of 10G in its direction. The magnetic field pointing parallel to the direction of the pumping beam can be actively controlled by the computer control system.

The pumping lasers

For Rb the pumping laser is tuned 11MHz below the $F = 1 \rightarrow F' = 0$ transition, where else the Cs pumping laser runs 9MHz below the $F = 3 \rightarrow F' = 2$ transition. Both pumping lasers are combined on the main experimental table with the help of a single dichroic mirror. The polarization of each pumping light is adjusted independently with $\lambda/2$ and $\lambda/4$ waveplates. The combined pumping light is directed to the atomic cloud pointing in the direction of the homogenous magnetic field. The polarizations of the pumping beams are chosen such that transitions towards the dark states are driven. Therefore the polarization is mainly σ^+ -polarized with a small π admixture with respect to the magnetic field axes, see figure 3.15. The waveplates are independently optimized recording the atom number and the width of the cloud after a fixed time of free expansion.

3.3.3 Experimental procedure and results

The implementation of degenerate Raman sideband cooling turned out to be challenging, since basically all tunable parameters (lattice alignment, homogenous magnetic field, polarization of the pumping lasers, timing sequence, ...) have to be at least close to optimum to experimentally obtain a signature of cooling the atoms. The optimization procedure is comparable to a search within a multi-dimensional parameter space. The window within DRSC works, is very narrow. Therefore we will present a recipe, which we find helpful to subsequently reduce the dimension of the parameter space providing fast discovery of the signature of DRSC.

Alignment of the three-dimensional optical lattice

The alignment of the four-beam lattice is done by using light resonant to an atomic transition. As mentioned before, the laser for the Cs lattice is basically resonant to the

3 Rb-Cs mixture: Apparatus and experimental procedure

MOT transition. We use the light force originating from resonant photon scattering to overlap every single beam with the position of the MOT. If the position of the laser coincides with the MOT, the light force imposed by the additional beam will displace the cloud. We subsequently align one beam after the other and try to see a displacement with respect to the absence of the additional laser beam. For the counterpropagating beam pair we will see a return of the position of the cloud to its original one, when the overlap between the counterpropagating beams is perfect. We set the appropriate polarizations of the single lattice beams to enable Raman transitions between two states associated with different m_F quantum numbers. The orientation of the small homogeneous magnetic field defines the main orientation-axes for the polarizations of the four lattice beams. As already mentioned, we align the relative tilt of the linear polarizations of each beam according to the setup described in reference [Tre01]. We use a commercial polarization-meter, which displays all relevant parameters of the polarization of a laser beam. We fine-tune the polarizations using the full sequence of DRSC optimizing the atom number after the cooling cycle.

Alignment of the pumping beams

As a next step we are able to independently optimize the direction and polarization of the pumping beams. Since the pumping beam is near-resonant to the repumper transition of the MOT, we again use the light force to overlap the pumping beam with the position of the MOT. The rough direction is chosen to be according to figure 3.15. More difficult but feasible is the optimization of the polarizations of the beams. We use Stern-Gerlach separation to split the cloud into different Zeeman components. The magnetic gradient field is set to levitate the absolute ground state of the respective species. Without optical pumping of the atoms the population will be distributed among all substates. We can use the pumping beam to optically pump the atoms to the ground state. Therefore we apply a small homogeneous magnetic field in z -direction after the combined molasses and compression phase and shine in the pumping beam for a few milliseconds. An increase of the atom number levitated by the magnetic gradient field indicates the appropriate polarizations of the pumping beams. This procedure has to be done for both species independently.

With the procedure described above we reduce the parameter space to three remaining dimensions, namely the homogeneous magnetic offset field needed to fulfill the degeneracy condition. In the absence of the earth magnetic field the optimization procedure of the magnetic field will reduce to one variable parameter, since the direction of the pumping beam and the orientation of the z -magnetic field axes coincide. This last remaining parameter is optimized using the full sequence of DRSC.

Timing sequence

Figure 3.16 shows schematically the full procedure of degenerate Raman sideband cooling after loading the two-color MOT. During the last stage of the two-color MOT we switch off the laser for the repumping transitions, therefore the atoms will accu-

3.3 Two-color degenerate Raman-sideband cooling

mutate in the lowest hyperfine manifold. After the combined optical molasses and compression phase we switch off the gradient field and turn on the two-color lattice, the pumping beams and a small homogenous magnetic field. The overall optimum duration of DRSC is 15ms. During the cooling process the magnetic field is tuned from about 600mG to 450mG. This procedure turns out to increase the efficiency of the cooling process, since the atom number increases by almost 30%. We believe, that the sweep of the magnetic field takes account for the Gaussian shape of the lattice beams, which produces a slightly different vibrational splitting along the geometry of the lattice. Atoms which are pumped to the upper hyperfine levels by non-resonant photon scattering, will no longer be available for the cooling procedure. Hence, in addition to the optical lattice and the pumping beams we shine in low intensities of the cooling transitions of both species. In the end the atoms have to be released from the lattice in a way which does not cause heating, i.e. achieving a minimum possible temperature in free space after the lattice is extinguished. This situation corresponds to the case, where the wavefunction changes adiabatically during the lattice potential is lowered [Kas94]. We release the atoms from the optical lattice by adiabatically ramping down the intensities of the lattice beams.

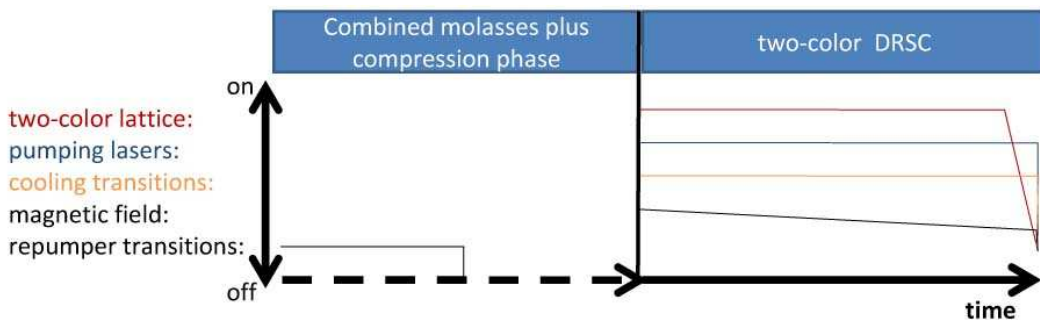


Figure 3.16: Timing sequence of DRSC. The atoms are pumped into the lower hyperfine state after the repumper laser is switched off during the last stage of the MOT. At the beginning of the DRSC procedure the magnetic field, the lattice lasers, pumping lasers and the cooling lasers are switched on. The homogenous magnetic field is ramped to lower values during the cooling procedure. In the end the atoms are released by adiabatically ramping down the lattice potentials.

Results

We independently optimized all variable parameters of the DRSC for both species following the recipe described above. In the absence of the respective other species we achieve temperatures as low as $1.5\mu\text{K}$ for cesium and $2.5\mu\text{K}$ for rubidium after adiabatic release from the two-color lattice. The number of atoms accumulated in the lowest Zeeman substate during the cooling procedure is about 10^8 for both species. Therefore we are able to decrease the temperature by a factor of 20 for both species after the molasses and compression phase. Nevertheless the tempera-

3 Rb-Cs mixture: Apparatus and experimental procedure

tures are still a factor 5 higher than already achieved by comparable experimental setups [Gus08, Tre01, Web03a]. We are not yet able to ascribe the limited efficiency of cooling to a specific problem. We currently investigate the influence of the noise performance of the pumping and lattice lasers on the cooling efficiency, since fluctuations of frequency and intensity might lead to heating of the sample and may empty the dark state.

To combine single-species DRSC to simultaneous cooling of both species, we optimize the magnetic field strength for Cs. Actually all the other parameters, which are independently optimized, lead to the same values for both species. This is somehow expected, as the use of broadband optical components will result in optimum lattice alignment for both species. Furthermore the pumping beams can be tuned independently. The only major difference occurs in the degeneracy condition of the vibrational levels. To compensate for a mismatch when using the optimized parameter of the magnetic field strength for Cs, we match the vibrational splitting of the Rb atoms in the lattice by tuning the lattice depth. Additionally we checked the influence of the presence of a two-color optical lattice for each species. Since one laser is detuned by several tens of nanometers with respect to the other, we could not measure any influence on the cooling efficiency. We did not observe any difference between cooling a single species or both species together. Nonetheless the lowest achievable temperatures are well above comparable experiments. This cannot be attributed to the presence of two species, moreover instabilities seem to limit the efficiency of the cooling procedure.

3.4 Levitated optical dipole traps

We use the concept of a combination of optical dipole traps and a magnetic gradient field to trap and cool the mixture of Rb and Cs similar to the single species setup of reference [Web03a]. As already mentioned inelastic two-body processes limit highest achievable phase-space densities for Cs atoms in excited states. The lowest internal state of Cs ($F = 3, m_F = 3$), which is stable against inelastic two-body collisions, is not trappable by magnetic forces since it is a high-field-seeking state. The use of optical dipole forces allows for trapping of atoms in their lowest internal state, for which the dominant loss processes are three-body inelastic collisions [Web03b].

The optical dipole force relies on the interaction of the induced dipole moment with the intensity gradient of the light field [Gri00]. Similar to a classical forced harmonic oscillator the ac electric field of the laser drives oscillations of the induced dipole moment. If the frequency of the electric field is red-detuned (blue-detuned) with respect to an atomic resonance the resulting optical potential is attractive (repulsive). We work with attractive optical potentials which are far-detuned from atomic resonances of both Rb and Cs. For far-detuned light the excitations caused by the laser field are small enough (low photon scattering rates) to consider the optical potential conserva-

3.4 Levitated optical dipole traps

tive. With the resonant transition frequency ω_0 , the speed of light c and the detuning Δ of the laser frequency from the atomic resonances we can write [Gri00]

$$U_{\text{Dip}}(r) = \frac{3\pi c^2 \Gamma I(r)}{2\omega_0^3 \Delta}, \quad (3.3)$$

$$\Gamma(r) = \frac{3\pi c^2 \Gamma^2 I(r)}{2\hbar\omega_0^3 \Delta^2}. \quad (3.4)$$

U_{dip} is the optical dipole potential, $\Gamma(r)$ is the photon scattering rate and $I(r)$ is the intensity of the light field.

We combine the optical dipole traps with the force produced by a magnetic gradient field. The magnetic gradient field is used to support trapping of the atoms in the presence of the gravitational force. Especially for large volume optical traps the levitation of the atoms by using a magnetic gradient field is essential to provide confinement of the sample in all directions [Web03a]. The force seen by an atom moving in the magnetic gradient field is proportional to the magnetic moment of the atom in its specific substate, see equation 3.1. In this context the combination of optical dipole traps with magnetic gradient fields represents a possibility for state selective trapping.

We work with two different sets of dipole traps: the "reservoir" and the "dimple". The concept of combining a large volume trap (reservoir) with a local modification of the trapping potential (dimple) gives the ability to locally increase the phase-space density [SK98]. An adiabatic change of the strength of the trapping potential without changing its shape will in general not lead to an increase of phase-space density. If the sample is compressed, the temperature will rise and vice versa. In the case of a combined reservoir plus dimple trap the phase-space density in the dimple trap can significantly increase, since the reservoir compensates for the rise of temperature gained during the change of the potential shape. After thermalization of the atomic sample the reservoir trap is removed and the dimple is loaded with the number of remaining atoms at much higher phase-space densities compared to the pure reservoir. Figure 3.17 illustrates the functionality of the combined reservoir plus dimple trap. This concept was successfully used to produce the first BEC of Cs atoms [Web03a].

The following subsection describes the general trap configuration and gives details on the lasers used to produce the potentials. Thereafter several aspects and problems of the current setup are discussed. Finally we present the experimental sequence including the results.

3.4.1 The reservoir and the dimple

The reservoir

The reservoir is a large-volume optical dipole trap, which is supported by a magnetic gradient field levitating the atoms.

3 Rb-Cs mixture: Apparatus and experimental procedure

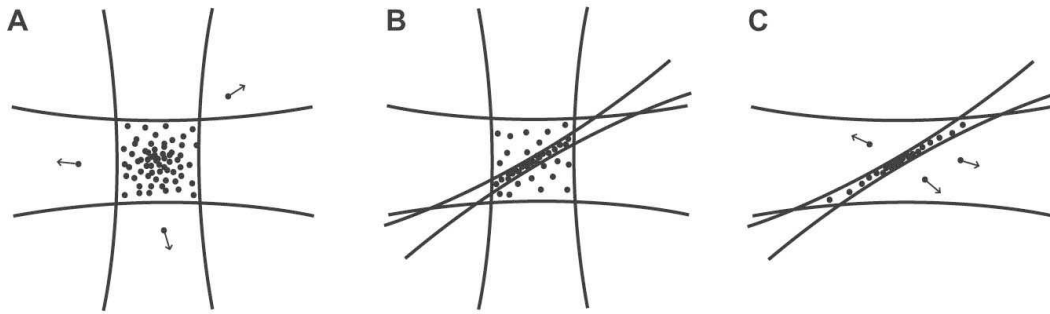


Figure 3.17: Reservoir plus dimple. The three steps A,B and C illustrate how to increase the phase-space density. First the reservoir is loaded, then the trapping potential is modified by an additional tightly focused laser beam (dimple). Some atoms will accumulate in the dimple, resulting in a local increase of phase-space density. Finally the reservoir is removed. Figure from [Web03a].

The reservoir is generated by an ytterbium-fibre laser⁶ with a central wavelength of 1070nm and a linewidth of about 3nm. This spatially single-mode fibre-coupled laser has a maximum output power of 100W. The waist of the beam after the fibre-output is approximately 2.5cm. We use a two-lens telescope to reduce the waist to 800 μm to pass through the AOM⁷, which allows to control and rapidly switch the power of the laser beam. Another telescope is used to produce a waist of about 500 μm at the position of the atoms, where the Rayleigh length is about 690mm. The laser beam passes the glass cell and is redirected through another pair of lenses to pass the glass cell a second time. The waist of the second beam is again approximately 500 μm . The two beams are crossing under a relative angle of about 78°. The schematic setup of the large volume optical dipole trap is shown in figure 3.18.

Because of the different polarizability and the different detunings of the dipole trap with respect to the different species, we obtain different optical trap depths for Rb and Cs, see equation 3.3. Cesium atoms are exposed to a trapping potential which is about a factor of 1.7 deeper than the trap depths for rubidium. Figure 3.19 shows the difference of trap depths for the species. For the calculated potential of figure 3.19 we assume a wavelength of 1070nm, a waist of 500 μm and a power of 20W for each beam, which corresponds to the parameters we use in the experiment. The photon scattering rates at the center of the trap are 0.07s⁻¹ for Cs and 0.03s⁻¹ for Rb.

The value of the magnetic gradient field along the z -direction is set to compensate gravity for the lowest internal states of both species. As already discussed in subsection 3.1.2 the magnetic moment to mass ratios of the absolute ground states of both species are almost equal for low homogeneous magnetic offset fields, which allows for simultaneous levitation. We calculate the trap depths for Cs in the states ($F = 3, m_F = 3$)

⁶IPG YLR-100

⁷the aperture of the AOM is approximately 2mm

3.4 Levitated optical dipole traps

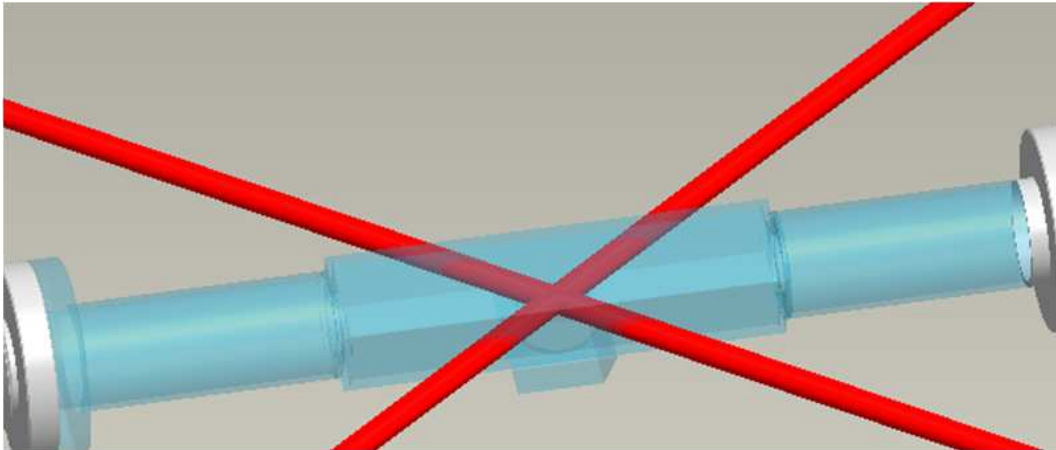


Figure 3.18: Large volume reservoir trap. The beam at a wavelength of 1070nm is passing the glass cell once and redirected to pass the glass cell a second time to produce a crossed optical dipole trap. The waist of the beams at the position of the atoms is approximately $500\mu\text{m}$.

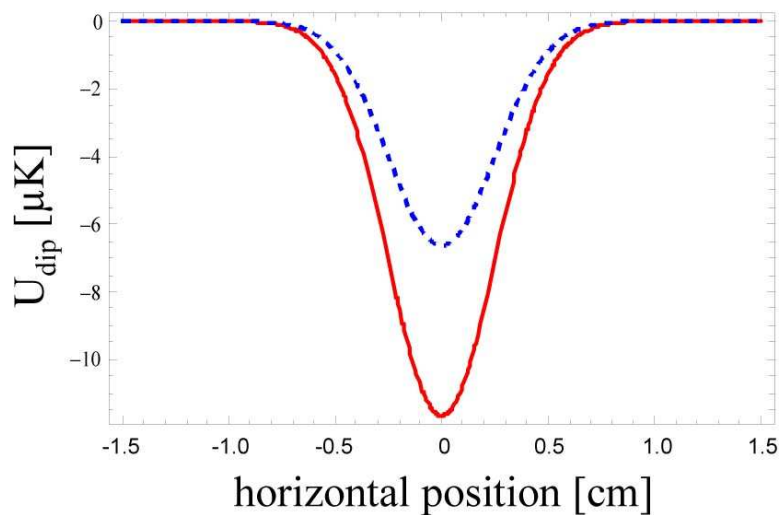


Figure 3.19: Calculated trapping potential for rubidium (dashed) and cesium (solid) in the horizontal direction. The trap depth for cesium is about a factor of 1.7 higher than for rubidium.

and ($F = 3, m_F = 2$) in the absence and presence of the magnetic gradient field at a value of about 31G. Figure 3.20 shows the dipole potential for Cs in the vertical direction for a crossed dipole trap. In the absence of the levitation field, the potential curve is too shallow to trap atoms. For a magnetic gradient field of about 31G the gravitation is fully canceled for Cs in the absolute ground state, while the trap is still not strong enough to support trapping of the ($F = 3, m_F = 2$) state. For Rb the state-selectivity of the trapping potential is even stronger, as the ($F = 1, m_F = 0$) state does not carry a magnetic moment. Thus the levitated optical dipole trap acts as state-selective filter

3 Rb-Cs mixture: Apparatus and experimental procedure

providing pure spin polarization of the two species.

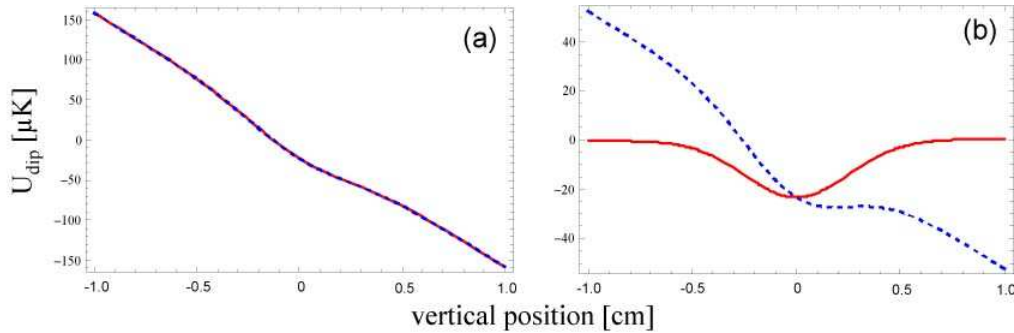


Figure 3.20: Trapping potential in the vertical direction for Cs in the states ($F = 3, m_F = 3$) (red solid line) and ($F = 3, m_F = 2$) (blue dashed line). Figure (a) shows that no trapping of atoms is supported in the absence of the magnetic gradient field. Figure (b) illustrates the state-selectivity of the trapping potential in the presence of the magnetic levitation field.

The dimple trap

The dimple trap is based on a commercial fiber laser⁸ which has a central wavelength of 1064nm and a linewidth of about 1nm. Similarly to the optical setup of the reservoir trap, we send the laser beam through an AOM, which allows for intensity stabilization and fast switching. To circumvent problems regarding the shape of the beam after passing through the AOM, we couple the deflected beam into a single-mode polarization-maintaining optical fibre. After the optical fibre we use a two-lens telescope and a single lens to focus the beam through the center of the reservoir trap. The waist of the dimple beam is $38\mu\text{m}$. The maximum available power for the dimple trap is 800mW. In analogy to the reservoir trap, the dimple potential is a factor of 1.7 deeper for Cs than for Rb. With the maximum power available we can produce a trapping potential for Cs(Rb) on the order of $75(42)\mu\text{K}$.

3.4.2 Aspects and problems of the current dipole trap setup

One major technical problem we have to face arises from the high optical power of the laser used for the reservoir trap.

Operating with high power lasers needs a clean environment, since optical components get soiled or damaged if e.g. dust particles are burned on them. We clearly observe contamination of the optical components by time. About every week we need to clean all optical surfaces, which are exposed to the high-power laser beam. In the experiment we clearly observe the contamination of the optics as a change of the shape of the optical potential. Figure 3.21 illustrates the effect of the severe distortion of the

⁸IPG PYL-10-LP

3.4 Levitated optical dipole traps

beam shape. After we clean the optics, the density distribution of the atoms does not show those irregularities.

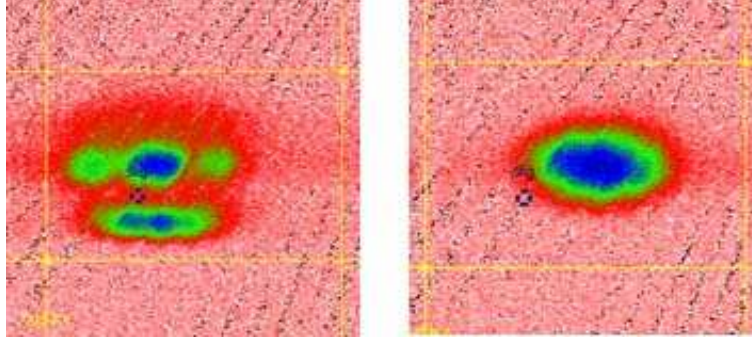


Figure 3.21: Illustration of the distorted dipole trap potential. The photograph on the left shows an absorption image of Cs atoms in the distorted reservoir trap. The absorption image on the right shows the density profile of the atoms after cleaning the optical components. The field of view is 2×2 mm.

The high power of the fibre laser can lead to thermal lensing, which is induced by a temperature gradient in the optical medium. In reality absorption of photons by the material cannot be prevented, when the laser beam is passing through an optical component. Typically the material is hotter near the beam axes compared with the outer region. This transverse temperature gradient can cause a gradient of the refractive index.

To reduce the effect of thermal lensing, materials with lowest possible absorption coefficients should be used. We plan to substitute the current optical components used for the optical setup of the reservoir trap by components with a more advanced selection of material. Even though the dominant destructive process can be attributed to the lack of a clean environment. We are currently about to install a flow box, which will strongly reduce the amount of dust particles. Moreover we have the possibility to enclose the whole optical setup for the reservoir beam and flood its volume with nitrogen, which would further reduce the risk of contamination. We also plan to substantially increase the minimum waist along the path of the light outside the vacuum chamber, since both effects related to the high power of the laser will decline with a reduction of the maximum intensity per unit area. In this context we think about substituting the AOM with an electro-optical modulator or an acousto-optical deflector, which offer much bigger apertures compared to an AOM.

We have to point out, that the waist of the reservoir trap has not been optimized on maximum loading efficiency. The use of a waist of about $500\mu\text{m}$ for the reservoir beams is an advance to perform measurements of Feshbach spectroscopy of the mixture. For more efficient loading of the reservoir trap, the spacial extension and the trap depth has to be matched with the properties of the atomic cloud released from DRSC,

3 Rb-Cs mixture: Apparatus and experimental procedure

see section 3.3. This so-called phase-space matching between the released sample and the reservoir trap will be necessary to obtain a quantum degenerate mixture. Prospects towards a degenerate mixture of Rb and Cs are given in chapter 5.

3.4.3 Experimental procedure and results

The atoms are loaded into the levitated crossed reservoir trap by adiabatically ramping down the lattice potentials after DRSC. Right after the power of the lattice lasers is switched off, the magnetic gradient field and a small homogenous magnetic offset field are applied. The strength of the magnetic gradient field is chosen to compensate for gravity regarding the lowest spin states of both species. The laser providing the trapping potential of the large volume trap is already switched on during the loading phase of the MOT. With this procedure we circumvent thermal drifts caused by the use of an AOM⁹. We do not observe any influence of the cooling efficiency of DRSC on the presence of the large volume optical dipole trap.

In single-species experiments, we are able to trap either 2.5×10^6 atoms of Rb or Cs. Note that the configuration of the optical dipole traps is not designed for optimum phase-space matching, as already stated in the previous subsection. We expect a significant increase of atom numbers for a trapping potential, which matches the atomic clouds released from DRSC. The temperatures of both species are determined by expansion measurements [Ket99] to about $4.5\mu\text{K}$ for Cs and $3\mu\text{K}$ for Rb. We extract the lifetime of the species in the reservoir trap by recording the remaining atom number after a variable hold time in the trap. Figure 3.22 shows the data on a lifetime determination of Cs in the dipole trap. We measure the lifetimes in single species experiments to be 3.3s for Cs and 18s for Rb.

The lifetime of the atoms in the dipole trap can be limited by inelastic collisional losses (three-body losses in the case of atoms in the absolute ground state) and losses caused by off-resonant photon scattering. We perform the lifetime measurements for Cs at a value of the s -wave scattering length of about $210a_0$, which corresponds to a minimum of the three-body recombination coefficient [Kra06]. We calculate the photon-scattering rate to be 0.07/s, see equation 3.4. The reduced lifetime of the sample can therefore not be attributed to three-body losses or off-resonant photon scattering. We assume to be unfortunately resonant to a two-photon transition between the levels $6S_{1/2}$ and $7S_{1/2}$. Further details on the level scheme are found in appendix B. In addition we can not attribute the limited lifetime of Cs to heating caused by e.g. fluctuations of the laser power of the reservoir, since the lifetime of Rb is about a factor of 6 higher. The frequency component of instabilities of the dipole trap causing heating and trap loss is usually on the order of the trap frequency of the atoms. In the case of Rb and Cs the trap frequencies are almost equal, because of fortuitous coincidences. The

⁹The power of the radio-frequency heats up the AOM, thus changing the lattice geometry of the crystal, which leads to thermal drifts.

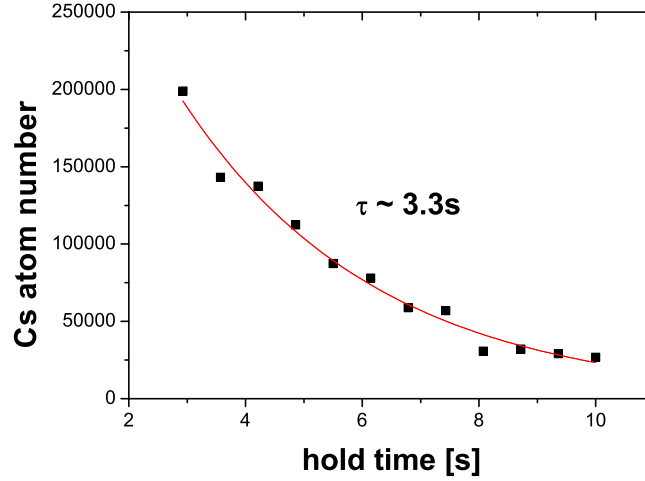


Figure 3.22: Lifetime of Cs in the reservoir trap. We record the remaining atom number of Cs after a variable hold time in the dipole trap. The lifetime is extracted by fitting a single exponential decay. The lifetime of Cs in the reservoir is about 3.3s.

trap frequency (regardless corrections for the presence of homogeneous and magnetic gradient fields) of the atoms is proportional to $\sqrt{U_{\text{dip}}/m}$. Since the mass ratio of Rb and Cs nearly corresponds to the ratio of optical trap depths for the two species, the trap frequencies only differ by less than 10%.

For double-species loading of the dipole trap, we observe enhanced losses of Rb from the reservoir trap in the presence of Cs. We do not attribute the reduced atom number of Rb to inelastic Rb-Cs collisions, since a decrease of the Rb atom number goes together with an increase of the Cs atom number. The loss of Rb is explained by the reduced trap depth for Rb compared to the trapping potential of Cs combined with a large interspecies elastic scattering rate. In other words, Rb is used to sympathetically cool the Cs sample. Our experimental configuration can be compared to an experiment done by reference [Mud02], where they observed enhanced losses of ${}^7\text{Li}$ in the presence of ${}^{133}\text{Cs}$, while the temperatures of the two species are equilibrating. The thermalization rate between the species is proportional to the collision rate of the atoms

$$\gamma_{\text{therm}} \propto \xi \gamma_{\text{el}}, \quad (3.5)$$

with

$$\gamma_{\text{el}} = n\sigma v, \quad (3.6)$$

3 Rb-Cs mixture: Apparatus and experimental procedure

Table 3.2: Table of lifetimes τ and temperatures T of Cs and Rb in the reservoir for single-species loading and for double-species loading. In the case of both species in the reservoir, we reduce the atom number of Cs loaded into the MOT by a factor of 10 compared to Rb. In the presence of Rb the lifetime of Cs increases by almost a factor of 2, while the temperature of both species equilibrates.

	τ_{Cs} [s]	τ_{Rb} [s]	T_{Cs} [μK]	T_{Rb} [μK]
single-species	3.3	18.0	4.5	3.0
double-species	6.5	17.5	3.0	3.0

where σ is the scattering cross section, v the average relative velocity and n the particle density. The ξ -factor is mass dependent and can be calculated from energy and momentum conservation to

$$\xi = \frac{4m_A m_B}{(m_A + m_B)^2}, \quad (3.7)$$

where m_A and m_B denote the mass of the atomic species A and species B , respectively. To get an estimation of the interspecies thermalization rate, we evaluate the factors of equation 3.7. In the case of a mixture of ^{87}Rb plus ^{133}Cs the factor ξ would be almost unity, where else in the case of ^7Li plus ^{133}Cs the factor would be approximately 0.2. Regarding this simple argument a mixture of Rb and Cs is expected to show fast thermalization between the two species. What remains unknown is the scattering cross section σ , which can hardly be predicted by theory.

After loading both species into the reservoir trap we observe an increase of the atom number and lifetime of Cs compared to single-species loading, while Rb, the cooling agent, experiences enhanced atom-number losses. Table 3.2 compares the lifetimes and temperatures of Rb and Cs for single- and double-species measurements. We observe a decrease of the Rb atom number in the reservoir after a thermalization time of 500ms by a factor of 3, when we initially load an equal number of atoms of both species into the MOT. We artificially decrease the number of Cs atoms in the MOT by the procedure described in 3.2.3. Loading both species into the reservoir we measure the lifetimes listed in table 3.2 for an atom number ratio of $N_{\text{Cs}} : N_{\text{Rb}} = 1 : 10$. We observe an increase of the lifetime of Cs in the trap by a factor of 2, while the lifetime of Rb stays almost uninfluenced because of the large atom number imbalance. The temperatures of both species equilibrate at about $3\mu\text{K}$.

4 Heteronuclear Feshbach resonances in an ultracold mixture of Cs and Rb

In single-species experiments with ultracold Cs or Rb many interesting physical phenomena have been observed. The investigation of Rb or Cs quantum gases lead to many breakthroughs in quantum physics. Although laser cooling has been applied already for many years on both ^{87}Rb and ^{133}Cs very little about their interspecies collisional properties and interatomic potentials is known. Early experiments on a Rb-Cs mixture studied the interspecies collisional properties in a magnetic trap [And05, Haa07, Har08]. Sympathetic cooling of Cs and the rethermalization of the mixture after species-selective heating was investigated. From the theoretical side reference [Jam03] calculated the interspecies scattering lengths for similar-looking potential curves, for which even small changes of the shape of the potential lead to changes of the s -wave scattering length by two orders of magnitude. Furthermore references [Ker04b, Ker04a, Sag05] investigated the ro-vibrational structure of RbCs molecules by using photoassociation. Reference [Tie06] extracted scattering lengths from the measurements of [And05] to be $700^{+700}_{-300}a_0$ or $(176 \pm 2)a_0$, the first value being the more likely one. The extracted information is still far-off being sufficient to gain an appropriate description of the mixture.

A powerful tool to gain information on interspecies collisional properties is the location of interspecies Feshbach resonances. We perform Feshbach spectroscopy on the Rb-Cs mixture for two different spin combinations of the species. We locate more than 23 interspecies resonances associated with different partial-wave characters. We provide data, which will allow to enhance the knowledge on the interspecies molecular potentials. The knowledge of the molecular potentials makes a prediction of the interspecies scattering lengths and further positions of Feshbach resonances possible. The procedure of mixed-sample preparation is described in section 4.1. The results of Feshbach spectroscopy in the lowest spin channel and in a higher spin channel are given in sections 4.2 and 4.3, respectively. Section 4.4 discusses the results of the Feshbach spectroscopy and presents general aspects of collisions between Rb and Cs. In the end of this chapter the progress of the theoretical assignment of the Feshbach

4 Heteronuclear Feshbach resonances in an ultracold mixture of Cs and Rb

resonances using a coupled channel calculation [Kot08] or the asymptotic bound state model [Wil08] will be discussed.

4.1 Sample preparation

A Feshbach resonance manifests itself in an enhancement of trap loss [Chi08]. In the energetically lowest spin channel, such losses can be fully attributed to three-body collisions. In our mixture, three-body collisions involving one Cs and two Rb atoms and collisions with one Rb and two Cs atoms are both possible. The rate coefficients for these two processes can in general be different, with one process dominating over the other. The visibility of heteronuclear resonances can be enhanced by creating an imbalance between the atom numbers of the two species [Wil08]. In this way, one species can be used as a probe and the other one as a collisional bath. For large enough atom imbalance, the minority component will be fully depleted, while the majority component will remain nearly unaffected. By a selective control of the MOT loading, we create a majority species (either Rb or Cs) and a minority species (thus either Cs or Rb) with an imbalance ratio of about 1 : 10.

To perform Feshbach spectroscopy an ultracold atomic sample has to be prepared. Typically temperatures below $10\mu\text{K}$ are necessary to be sensitive to Feshbach resonances. Higher temperatures decrease the visibility of the loss signature, increase the width of the resonance feature and lead to contributions of higher partial waves (see sections 2.1 and 4.4).

4.1.1 Experimental procedure

To prepare an ultracold mixture of Rb and Cs we follow the scheme of trapping and cooling described in chapter 3. To summarize, the Rb and Cs atoms are first loaded into a two-color magneto-optical trap (MOT) from a Zeeman slowed atomic beam. The mixture is further cooled by applying two-color degenerate Raman-sideband cooling (DRSC), which also polarizes the atoms into their lowest spin state. The sample is then loaded into a levitated optical dipole trap, which is used to probe heteronuclear Feshbach resonances. We have a pure sample of $\text{Rb}|1, 1\rangle$ for Rb and $\text{Cs}|3, 3\rangle$ for Cs in this trap, where the first number indicates the total spin quantum number F and the second its projection m_F onto the magnetic field axis. The typical final temperature of the mixture is about $3\mu\text{K}$ with up to 6×10^5 atoms for each species at peak densities of a few 10^{10}cm^{-3} .

For Feshbach spectroscopy experiments, it is favorable to increase the atomic density of both species since the losses occur as a result of interspecies collisions. We compress the mixture by superimposing an additional tightly focused laser beam (see section 3.4), which acts as a dimple trap [Web03a, Kra04]. The optical field is generated by a second fiber laser (IPG PYL-10-LP) with central wavelength of about 1064nm and linewidth of about 1nm . The beam has a power of about 300mW and a

4.1 Sample preparation

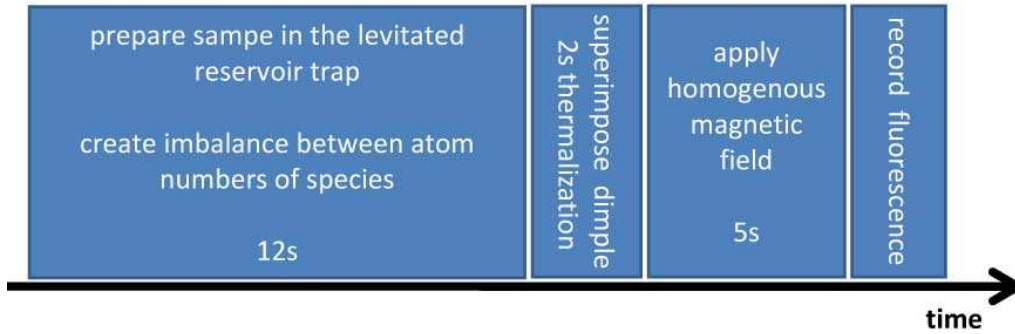


Figure 4.1: Experimental procedure for Feshbach spectroscopy. The atoms are loaded into the levitated crossed optical dipole trap after loading the two-color MOT and subsequent two-species DRSC. We create an imbalance ratio between the atomic species of $N_{Cs} : N_{Rb} = 1 : 10$. Probing the minority species of the imbalanced sample will increase the visibility of a loss feature, which indicates a Feshbach resonance. We let the imbalanced sample thermalize for 2s. To further increase the density, we superimpose the dimple beam onto the reservoir trap. After another two seconds of thermal equilibration, we set a certain value of the homogenous magnetic field and keep it for 5s. To record the remaining atom number of the minority species, we switch off the traps, recapture the atoms in the MOT and record the fluorescence signal. To obtain the Feshbach spectrum, we vary the value of the homogenous magnetic field between different cycles.

waist of $38\mu\text{m}$. The dimple trap depths are $18\mu\text{K}$ and $31\mu\text{K}$ for Rb and Cs, respectively. With the use of this additional optical field, we typically increase the peak density of both species by an order of magnitude to about $5 \times 10^{11} \text{ cm}^{-3}$ at a final temperature of about $7\mu\text{K}$.

Once the imbalanced mixture is produced in the combined reservoir-plus-dimple trap, we are in the position to perform Feshbach spectroscopy. We perform a magnetic field scan between 20 and 300G with a resolution of 250mG. At low magnetic fields our scan is limited by the horizontal forces induced by the magnetic levitation field, which pull the atoms out of the trap [Web03a]. A scan consists of more than 1000 experimental cycles of about 30s duration each. In each cycle, we let the mixture evolve at a specific value of the homogeneous magnetic field for 5s. In the next cycle, we change the magnetic field value in random order and we repeat the measurement. To determine the atom number of the minority species, we switch off the optical dipole trap, recapture the remaining atoms into the MOT, and record their fluorescence signal. The full procedure of a single experimental cycle for Feshbach spectroscopy is shown in figure 4.1.

4 Heteronuclear Feshbach resonances in an ultracold mixture of Cs and Rb

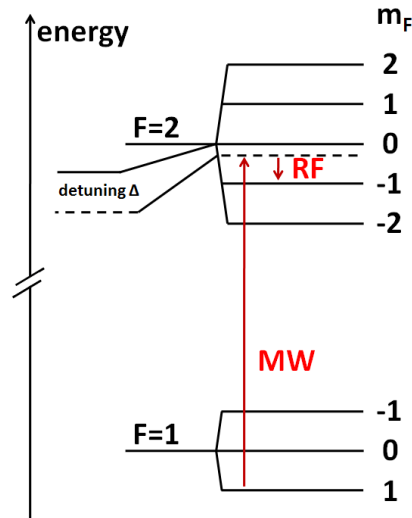


Figure 4.2: Rb state transfer. The Rb atoms are transferred into the $Rb|2, -1\rangle$ state by applying a two-photon microwave plus radio-frequency transition. The microwave is detuned from the $Rb|2, 0\rangle$ state by Δ . The radio-frequency is chosen to couple the atoms to the $Rb|2, -1\rangle$ level in a resonant two-photon process.

4.1.2 ^{87}Rb state transfer

In a second set of experiments, we perform Feshbach spectroscopy in another spin-channel combination. We keep the Cs atoms in the absolute ground state because of strong two-body dipolar losses for Cs-Cs collisions occurring in any higher spin state [GO98a, GO98b, Hop00]. For Rb, the $Rb|2, -1\rangle$ state is the only other state fulfilling the levitation condition. Atoms in the $Rb|2, -1\rangle + Cs|3, 3\rangle$ channel are stable against spin-changing collisions which do not involve a change in F as the relaxation channels are energetically closed. Two-body hyperfine-changing collisions are energetically possible and allowed under the conservation of the total orientation quantum number, but we do not observe any significant background loss that exceeds the observations in the other spin channel. Loss at Feshbach resonances may however include resonantly enhanced two-body loss.

To transfer the Rb atoms from the ground state to the $Rb|2, -1\rangle$ state, we start with Rb atoms prepared in the $Rb|1, 1\rangle$ state as described before. Then we apply a two-photon transfer scheme, which combines microwave and radio-frequency excitation. Figure 4.2 schematically shows the working principle of the transfer scheme. The microwave frequency is detuned by few MHz with respect to the $Rb|1, 1\rangle \rightarrow Rb|2, 0\rangle$ transition. The radio-frequency signal couples the $Rb|2, 0\rangle$ and the $Rb|2, -1\rangle$ state with the corresponding detuning that leads to the two-photon resonance. The pulse sequence has a duration of 400ms during which the magnetic field value is set at 20G. Using this scheme, we incoherently transfer almost 50% of the ground state Rb atoms into the excited state. The remaining atoms in the $Rb|1, 1\rangle$ state are selectively removed

4.1 Sample preparation

from the trap by applying a short light pulse resonant with the $F = 1 \rightarrow F' = 2$ transition, pumping the atoms into different magnetic sublevels of the $F = 2$ upper hyperfine state. Those atoms which do not end up in the target state $\text{Rb}|2, -1\rangle$ leave the trap as the levitation condition is not fulfilled. In this way spin impurities can be completely avoided.

The microwave frequency is produced by a home-build microwave setup (details see appendix A.3) and delivered to the atomic sample via a broadband waveguide. The radio-frequency is produced by a frequency generator¹, amplified² and applied to the atomic cloud by a single magnetic field coil. The coil to drive radio-frequency transitions is made with a copper wire and has three rounds and a diameter of 3.5cm. The orientation of the coil is chosen to be normal with respect to the coil pair producing the homogenous magnetic field.

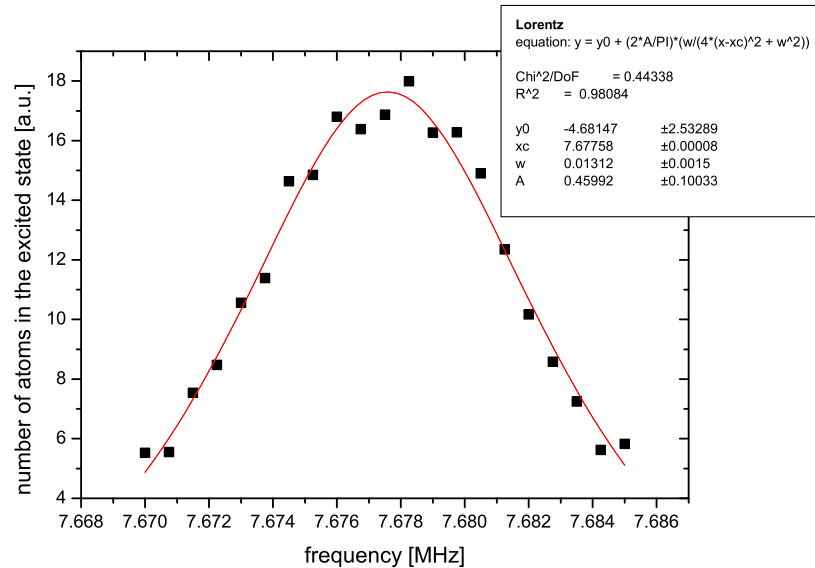


Figure 4.3: Populating the $\text{Rb}|2, -1\rangle$ state. The atom number of rubidium in the state $\text{Rb}|2, -1\rangle$ is plotted against the detuning of the radio-frequency. The maximum atom number corresponds to the two-photon resonant case, where the detuning Δ of the radio-frequency is equal to the detuning of the microwave frequency.

The transfer of the atoms to the $\text{Rb}|2, -1\rangle$ state is experimentally optimized by tuning the power of the microwave and radio-frequency, by varying the duration of the pulse and by varying the detuning Δ from the excited level. Figure 4.3 shows the number of atoms being in the excited state for different values of the radio-frequency. The optimum transfer is achieved, when the detuning Δ of the radio-frequency from the

¹Agilent 33250A

²FLL-75

4 Heteronuclear Feshbach resonances in an ultracold mixture of Cs and Rb

$\text{Rb}|2, -1\rangle \rightarrow \text{Rb}|2, 0\rangle$ transition corresponds to the detuning of the microwave from the $\text{Rb}|1, 1\rangle \rightarrow \text{Rb}|2, 0\rangle$ transition.

An adiabatic transfer [Mie00] by sweeping the magnetic field or equivalently the applied frequency would be a way to coherently populate the excited state. To realize an adiabatic sweep of the frequency, the square of the Rabi frequency has to be much bigger than the speed of the frequency change. In our case the Rabi frequency of the two-photon transition is on the order of 1kHz. The lower constraint on the speed of the frequency sweep is given by the trap frequency, since the atoms might get resonantly coupled during the transfer more often. Because of these restrictions we are not able to perform an adiabatic sweep to coherently populate the excited state.

4.2 Feshbach resonances in the lowest spin channel

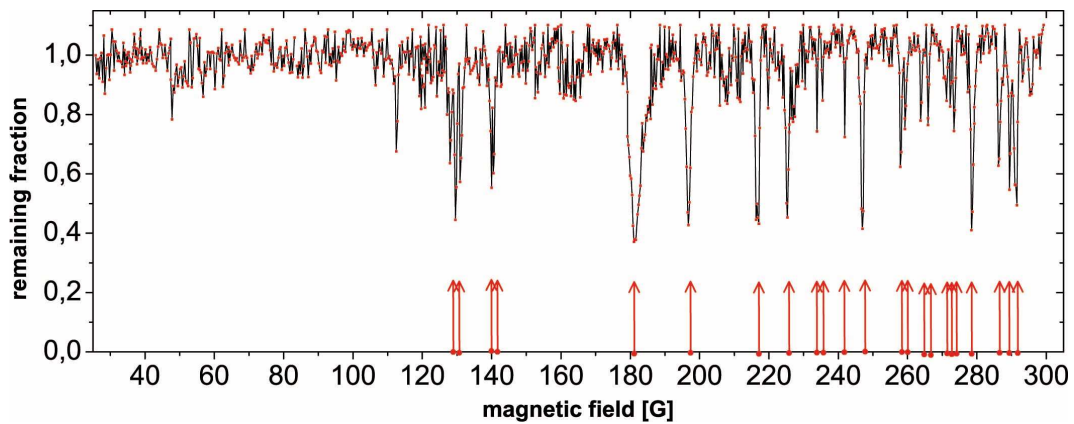


Figure 4.4: Observation of heteronuclear Rb-Cs Feshbach resonances in the lowest spin channel by loss spectroscopy. The spectrum is recorded for Cs atoms, being the minority component of the mixture. The remaining fraction represents the number of Cs atoms after a 5s hold time in the dipole trap normalized to the corresponding average number detected off any resonance. The arrows indicate the positions of the interspecies Feshbach resonances. Other loss features correspond to homonuclear Cs Feshbach resonances.

The Feshbach spectrum in the ground state of the mixture is obtained by measuring the three-body loss spectrum of the atomic mixture in the states $\text{Rb}|1, 1\rangle + \text{Cs}|3, 3\rangle$. Figure 4.4 shows the complete loss spectrum choosing Cs as the probe. Each point corresponds to an average of 5 to 10 different measurements. At specific values of the magnetic field, the Cs atom number decreases by at least 20%. Since the mixture contains an order of magnitude less Cs than Rb atoms, the latter species exhibits very small relative losses. To avoid any possible confusion with homonuclear resonances, we have repeated the magnetic field scan using samples of either pure Cs or pure Rb

4.2 Feshbach resonances in the lowest spin channel

atoms. The loss features, indicated by the arrows in Fig. 4.4, only appear using a two-species mixture, while the others can be attributed to Cs Feshbach resonances [Chi04]. In this way, we identify 23 interspecies Rb-Cs Feshbach resonances in the absolute ground state combination of the two species.

For some resonances we also perform consistency checks by monitoring the loss of Rb atoms prepared as a minority species. Figure 4.5 shows the loss spectrum of Cs in a mixture with Rb, where Rb is chosen to be the majority species. We expect that for interspecies Feshbach resonances the loss signature is present in both configurations, Cs or Rb being the minority species. In contrary, for homonuclear Feshbach resonances, we will not observe resonant losses for either the one or the other species. In Figure 4.5 we identify two interspecies Feshbach resonances, while the loss feature at 131G is corresponding to a homonuclear Cs *d*-wave resonance.

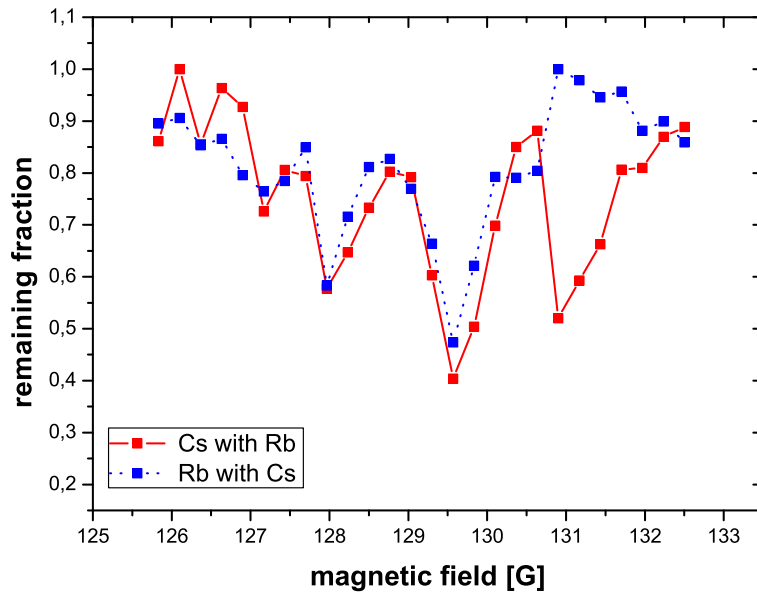


Figure 4.5: Changing the minority species for selected Feshbach resonances. The solid line (red) is the result of the Feshbach spectroscopy when probing Cs in a collisional bath of Rb. The dotted (blue) line corresponds to the same loss measurement but with an inverted atom number ratio when probing Rb. Two interspecies Feshbach resonances at the magnetic field values of 128G and 129, 6G are present for both settings of the atom number ratio, while the loss feature at 131G is clearly induced by a homonuclear Cs *d*-wave resonance [Chi04].

4.3 Feshbach resonances in a higher spin channel

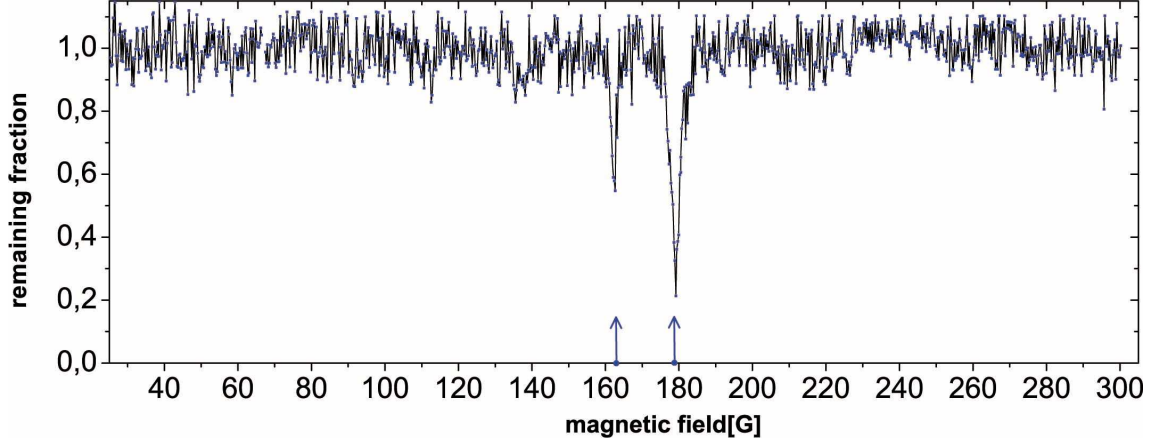


Figure 4.6: Observation of heteronuclear Rb-Cs Feshbach resonances in the higher spin channel by loss spectroscopy. The spectrum is recorded for Cs atoms, being the minority component of the mixture. The arrows indicate the positions of the interspecies Feshbach resonances.

The Feshbach spectrum of the excited channel is obtained by a measurement of the loss spectrum of the atoms being in the states $\text{Rb}|2, -1\rangle + \text{Cs}|3, 3\rangle$. We prepare the mixed sample similar to the procedure for the ground state Feshbach spectrum. After loading the reservoir trap, we transfer the Rb atoms from the ground state to the $\text{Rb}|2, -1\rangle$ state according to the procedure described in subsection 4.1.2.

Figure 4.6 shows the loss spectrum for the mixture in the excited channel. We observe two interspecies Feshbach resonances within a magnetic field ranging from 20G to 300G. We checked the origin of the loss features by single-species Feshbach scans. Table 4.1 summarizes the positions of the interspecies Feshbach resonances and maximum losses observed for the ground and the excited spin combination.

In sum we observe 23 interspecies Feshbach resonances in the ground and 2 in the excited spin channel of the mixture. The measured positions, widths and loss fractions are summarized in Table 4.1. Two main mechanisms can contribute to a broadening of the loss resonances. First, the levitation field gives rise to an inhomogeneous broadening. For a typical cloud size of $\sigma = 20\mu\text{m}$, we estimate the broadening caused by the field gradient B' to be $B'\sigma \approx 70\text{mG}$. Second, the temperature broadening can be estimated as $k_B T / \Delta\mu$, where $\Delta\mu$ is the relative magnetic moment between the atom pair state and the molecular state causing the resonance. The broadening typically varies between 50 and 200mG. Therefore we extract widths from our experimental data only for those resonances that appear wider than 100mG. To determine the full widths at half maximum, ΔB , we use Lorentzian fits.

4.4 General considerations and interpretation

Table 4.1: Feshbach resonances in collisions between ^{87}Rb and ^{133}Cs in a range from 20 to 300G. The locations, the widths ΔB and the fractional losses of the Feshbach resonances in both channels $\text{Rb}|1, 1\rangle + \text{Cs}|3, 3\rangle$ and $\text{Rb}|2, -1\rangle + \text{Cs}|3, 3\rangle$ are listed.

	B (G)	loss (%)	ΔB (G)	B (G)	loss (%)	ΔB (G)
$\text{Rb} 1, 1\rangle$	128.0	40	-	258.0	55	0.4
$+ \text{Cs} 3, 3\rangle$	129.6	60	-	259.3	30	0.5
	140.0	50	-	263.8	30	0.5
	140.5	50	-	265.9	30	-
	181.6	70	3.1	271.2	25	-
	196.8	60	1.2	272.3	25	0.3
	216.7	60	1	273.4	30	0.4
	225.3	60	1	278.4	65	0.95
	233.9	30	-	286.2	45	0.8
	235.5	25	-	289.4	50	0.5
	241.9	35	-	291.5	55	1.1
	246.9	65	0.7			
$\text{Rb} 2, -1\rangle$	162.3	50	1.4			
$+ \text{Cs} 3, 3\rangle$	179.1	80	2.8			

4.4 General considerations and interpretation

In this section we discuss some general aspects of the scattering properties of Rb and Cs. A major difference to other mixtures of alkali atoms are the high masses of the two species used in our mixture. Especially the second order spin-orbit interaction is expected to play a crucial role for the scattering of Rb and Cs. Furthermore we give an interpretation of the observed Feshbach spectra.

Dipolar interactions

Dipolar interactions are expected to play a crucial role for a mixture of Rb and Cs, similar to single-species Cs case. Since the first creation of a BEC in 1995, several attempts to condensate cesium have failed. Due to high inelastic two-body losses for excited states including magnetically trappable states, it has not been possible to get a condensate of cesium atoms in a magnetic trap. In 2002 the first realization of a BEC of Cs in its absolute ground state was realized by the use of an optical dipole trap [Web03a], which is capable of trapping the absolute internal ground state of Cs. The absolute ground state is immune against spin- or hyperfine-changing collisions, nevertheless one has to take care of the extraordinary high three-body losses [Web03b].

As already mentioned in 2.1.4 the dipolar interactions are stronger for heavy alkali atoms. Therefore strong effects are present for Cs. Rb on the other hand, which has a mass number of 87, shows very weak dipolar interactions. This is due to the fact that

4 Heteronuclear Feshbach resonances in an ultracold mixture of Cs and Rb

the two contributions, the magnetic spin-spin and the second order spin-orbit interaction, almost cancel [Mie96, Leo98].

In a mixture of ^{133}Cs and ^{87}Rb dipole-dipole interactions are expected to play a major role, especially second order spin-orbit coupling gains importance because of the high masses of the species, as we can see in figure 4.7. The figure, which originates from a calculation provided to us by S. Kotochigova [Kot08], displays the contrast between the pure magnetic spin-spin and the second order spin-orbit dipolar interaction depending on the interatomic distance for a ^{87}Rb - ^{133}Cs mixture.

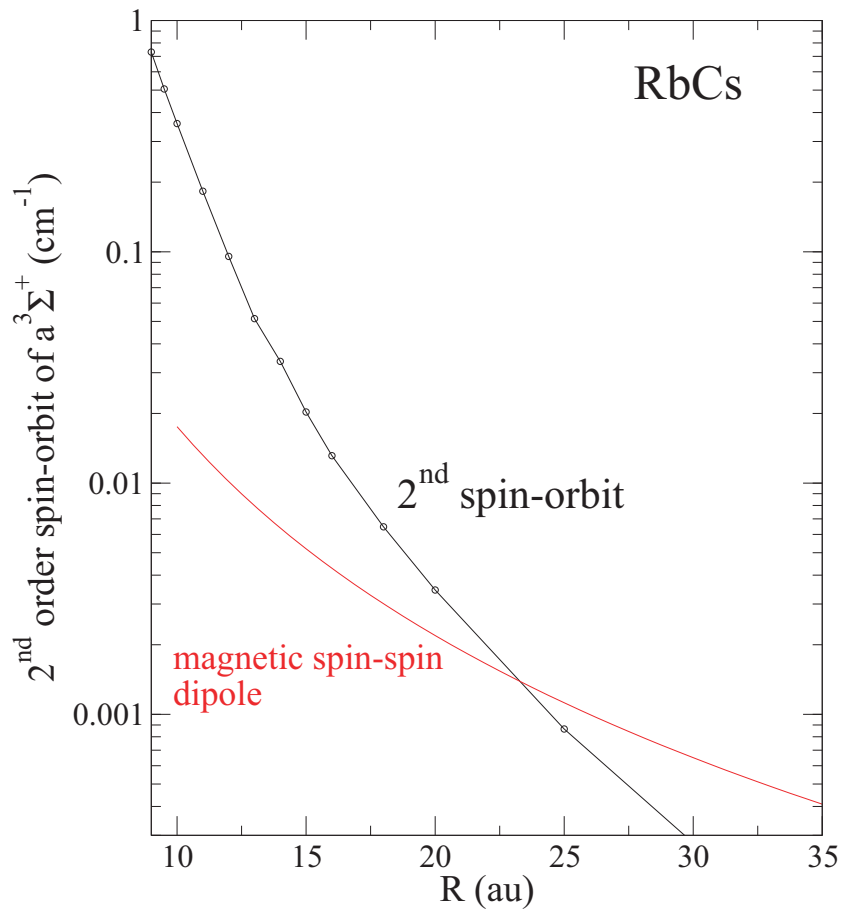


Figure 4.7: Strengths of the magnetic spin-spin and the second order spin-orbit dipolar interaction for a mixture of ^{133}Cs and ^{87}Rb . For larger separations between the different species the magnetic spin-spin interaction is the dominating term, where else for small interatomic distances the second order spin-orbit interaction is much stronger than the magnetic spin-spin interaction [Kot08].

The presence of 23 interspecies Feshbach resonances within a magnetic field ranging from 20 to 300G is unusual for alkali mixtures [Sta04, Ino04, Fer06, Wil08]. Our observations indicate contributions of higher partial waves, since due to the relatively

4.4 General considerations and interpretation

high dipole-dipole interactions for a mixture of Rb and Cs, coupling from incoming s waves to higher partial waves is likely. Therefore some of the discovered loss resonances may also be attributed to d or even g states in the closed scattering channel.

Higher partial wave contributions

Because of symmetry reasons indistinguishable bosons (fermions) are restricted to even (odd) numbers of the quantum number l (see subsection 2.2). In the case of a mixture of ^{87}Rb and ^{133}Cs odd and even numbers of the partial wave quantum number are allowed. For sufficiently low temperatures scattering in between one species is restricted to incoming s waves. For collisions between different atomic species at higher temperatures p waves have to be taken into account in addition to interspecies s -wave scattering.

The interaction between neutral particles is dominated by the van-der-Waals potential, which plays a major role when the atoms approach each other sufficiently closely. To take p waves for the scattering process into account, a closer look into equation 2.3 shows, that a repulsive term is added to the attractive van-der-Waals potential. The repulsive part of the scattering potential for higher partial waves is given by $\hbar^2 l(l+1)/2\mu r^2$ and is usually denoted by the centrifugal barrier (μ is the reduced mass). If the kinetic energy of the colliding atoms is smaller than the height of the barrier, the probability to tunnel through the barrier drops with decreasing temperature. Thus the atoms are reflected back outwards before they reach the non-negligible part of the van-der-Waals potential. To estimate the energy threshold, at which higher partial waves contribute to a collision, we calculate (from a classical point of view) the energy of the local maximum in the potential which contains the attractive and the centrifugal term

$$E_l = \frac{\hbar^2 l(l+1)}{2\mu R_l^2} - \frac{C_6}{R_l^6}, \quad (4.1)$$

with

$$R_l = \sqrt{\frac{6\mu C_6}{\hbar^2 l(l+1)}}. \quad (4.2)$$

For a mixture of Rb and Cs this estimate results in the height of the potential barrier being around $55\mu\text{K}$ for a p wave. Figure 4.8 shows the typical shape of a scattering potential for a p wave.

In the case of a Rb-Cs mixture p -wave collisions are particularly important, since the temperature of the mixed sample is on the order of the height of the centrifugal barrier for $l = 1$. In a first approximation incoming p waves couple to p -wave molecular states, while more complex coupling possibilities are again allowed via dipolar interactions. A p -wave resonance can lead to a doublet structure because of the spin-spin dipole interaction, which splits the resonance into two components based on the partial-wave

4 Heteronuclear Feshbach resonances in an ultracold mixture of Cs and Rb

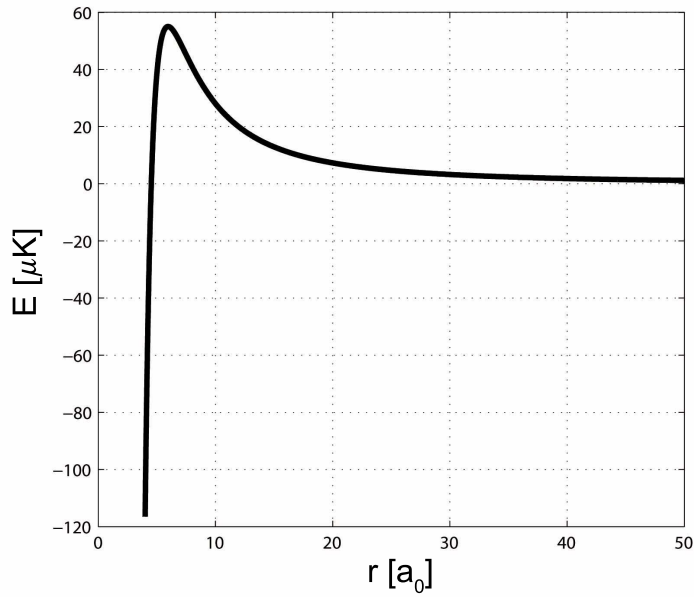


Figure 4.8: Van-der-Waals potential including the centrifugal barrier corresponding to a p wave.

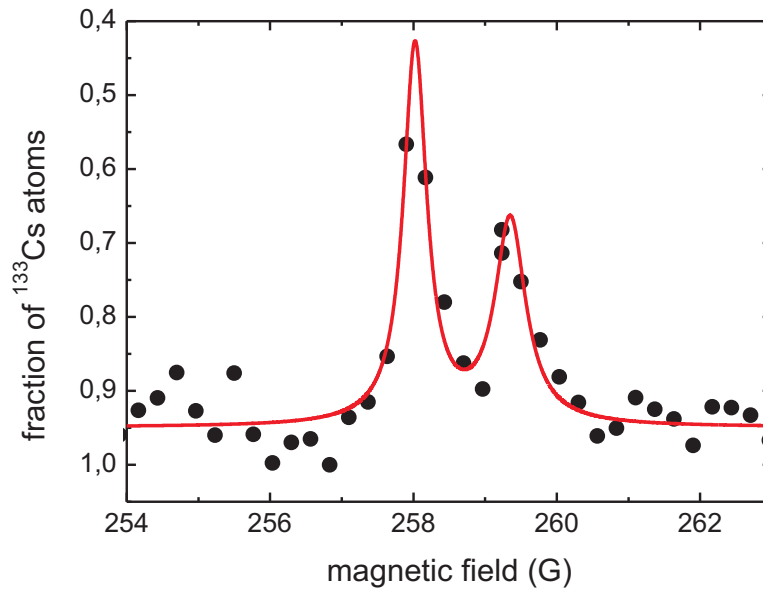


Figure 4.9: Doublet structure. We observe several loss features which show a pair of resonances. This observation may indicate the p -wave nature of the loss resonance.

projection onto the magnetic field axis, $m_\ell = 0$ and $|m_\ell| = 1$ [Tic04, Reg03b]. In our Feshbach scan, we observe several resonances that come in pairs. Such a feature could be fortuitous but could also be evidence of the p -wave character. In particular, four res-

4.4 General considerations and interpretation

onance pairs are candidates for p -wave resonances, namely the resonances near 140, 234, 259, and 273G. We typically observe a splitting of about 1G, which indicates a strong spin-spin interaction between Rb and Cs atoms. Doublets with a splitting of this order have been predicted for the specific Rb-Cs system [Kot08]. Figure 4.9 gives an example of such a doublet structure. Here, the splitting between the two peaks is about 1.3G.

Resonances based on higher incoming partial waves exhibit a split structure of the resonances [Tic04], since the projection m_l of the angular momentum of the relative motion onto the magnetic field axes removes the degeneracy. Figure 4.10 schematically explains the splitting of a p -wave resonance, associated with the projections $m_l = 0$ and $|m_l| = 1$. In the figure two classical spins are shown, which are aligned along the external magnetic field. When the dipoles are aligned head to tail, they will attract each other. When the dipoles are aligned in parallel, they will repel each other. For $m_l = 0$ the spins rotate in plane with the magnetic field, and will thus sometimes repel and sometimes attract each other. For $|m_l| = 1$ the dipoles rotate in the plane normal to the magnetic field axes and are predominately repelling each other. This effect leads to an additional contribution based on dipole-dipole interactions to the Hamiltonian describing the interaction. This dipole-dipole interaction removes the energetic degeneracy and will lead to distinct loss features observable in the Feshbach spectrum.

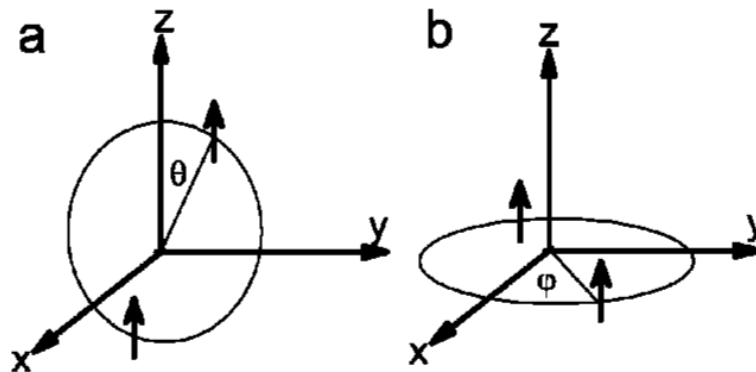


Figure 4.10: Schematic representation of classical dipoles interacting in different circular orbits. In figure (a) the dipoles sometimes attract and sometimes repel each other, corresponding to $m_l = 0$. In figure (b) the dipoles rotate in the plane perpendicular to the magnetic field axis ($|m_l| = 1$) and will hence predominately repel each other. Figure from [Tic04].

Widths of resonances

Particularly interesting is e.g. the interspecies Feshbach resonance for the lowest spin channel combination located at about 180G, since it appears broader than the other loss features. This resonance could be a good candidate to efficiently Feshbach associate RbCs molecules and for precise control of the interspecies scattering length by means of magnetic field. Note that the magnetic gradient field together with the

4 Heteronuclear Feshbach resonances in an ultracold mixture of Cs and Rb

comparatively high temperature of the mixed sample result in a broadening of the loss signal. Considering a typical cloud size of $20\mu\text{m}$, we estimate both contributions to lead to a broadening on the order of about 100mG .

In the limit of zero collision energy the widths of Feshbach resonances depend on the coupling strengths between the entrance and the molecular bound state and on the difference of the magnetic moments $\delta\mu$ between the channels. If the coupling strength is high, the resonances will be broad. Typically *s*-wave resonances show the largest widths [Chi08, Köh06], since the coupling between the channels is induced by the strong exchange interaction (see chapter 2.1). Feshbach resonances which are classified by higher partial waves, usually show small widths, because of the comparatively low coupling strength. Therefore the interspecies Feshbach resonance at 180G could be interpreted as a *s*-wave resonance. On the other hand the width of the resonance also depends on the difference of the magnetic moments $\delta\mu$. The smaller $\delta\mu$, the larger is the width of the loss feature. In the mixture experiment of [Wil08] they observe a *p*-wave Feshbach resonances with a width exceeding the widths of the measured *s*-wave Feshbach resonances. To get a reliable assignment of the observed interspecies Feshbach resonances, a full theoretical treatment is necessary, since classification of the observed loss features by the arguments mentioned above is speculative.

4.5 Status of theoretical assignment

The measured Feshbach spectra including more than 23 interspecies Feshbach resonances in a mixture of Rb and Cs provides experimental input to characterize Rb-Cs scattering properties. An appropriate theoretical treatment of the scattering problem will unambiguously assign the observed resonances in terms of different partial-wave molecular states. The theory will reproduce the positions of the observed interspecies Feshbach resonances and will in addition enable the prediction of further locations of interspecies Feshbach resonances. Furthermore the dependence of the *s*-wave scattering lengths on the magnetic field can be calculated and be used to experimentally control the scattering properties.

Two different theoretical models are currently used to investigate the scattering properties of Rb and Cs using our data of the Feshbach spectra. One, the asymptotic bound state model (ABM), locates the Feshbach resonances via the use of a two-body bound state model, which includes exchange interaction (see section 2.1). The ABM model is a relatively new method to make an assignment of Feshbach resonances. It was recently used to characterize the scattering properties of a heteronuclear Fermi-Fermi mixture of ${}^6\text{Li}$ and ${}^{40}\text{K}$ [Wil08]. The accuracy and computational simplicity of this model makes the assignment very efficient, allowing rapid feedback between the experiment and theory during the search for Feshbach resonances. Because of the presence of strong dipole-dipole interactions in a mixture of Rb and Cs the ABM model is up to

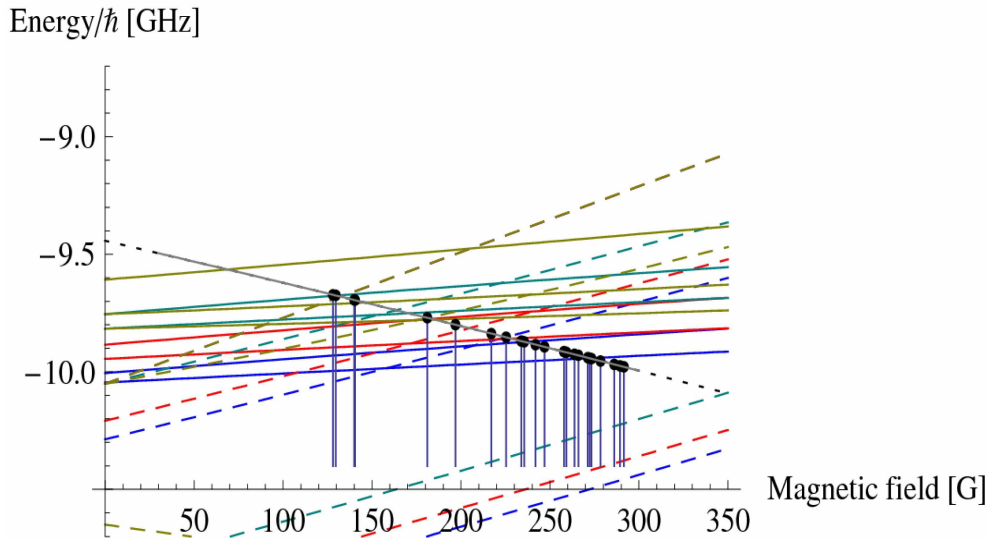


Figure 4.11: Preliminary result of the assignment of the experimentally observed interspecies Feshbach resonances in the ground state channel calculated by the ABM model. The grey line corresponds to the threshold of the entrance channel, where the black dots are marking the experimentally obtained magnetic field positions of the Feshbach resonances. The solid and dashed lines correspond to different partial-wave molecular bound states. If a molecular bound state crosses the entrance channel threshold, a Feshbach resonance should occur. Up to now the model is not able to reproduce the locations of the Feshbach resonances observed in our experiment. Figure from [Goo08].

now not applicable for our purpose. However the model is currently being adapted and expanded to include also coupling to higher partial-wave molecular states. A preliminary result of a calculation done by M. Goosen and S. Kokkelmans [Goo08] is shown in figure 4.11. The grey line corresponds to the threshold of the entrance channel $\text{Rb}|1, 1\rangle + \text{Cs}|3, 3\rangle$. The black dots on the gray line are corresponding to the experimentally located magnetic field values of the interspecies Feshbach resonances. The solid and dashed lines in the figure are associated with different partial-wave molecular bound states, which cross the threshold of the entrance channel, causing a Feshbach resonance. Up to now, the ABM model is not sufficient to assign the experimentally observed Feshbach resonances.

The other method used to assign the experimentally observed Feshbach resonances is a coupled channels calculation, in which the short range parts of the scattering potentials are varied to reproduce the positions of Feshbach resonances [Sto88]. The coupled channels calculation is known to give very accurate results, however the high computational load is time-consuming. Preliminary calculations done by S. Kotochigova [Kot08] on the assignment of the Feshbach resonances in the ground state channel are shown in figure 4.12. The energy threshold of the incoming channel is given by the

4 Heteronuclear Feshbach resonances in an ultracold mixture of Cs and Rb

zero-energy line in the graph. The blue line above the threshold displays the invert of the Feshbach spectrum, which has been obtained in our experiment. The black, red and green lines below the threshold are associated with s -, p - and d -wave molecular bound states, respectively. The crossings of molecular bound states with the threshold of the incoming channel should correspond to the positions of experimentally observed locations of interspecies Feshbach resonances.

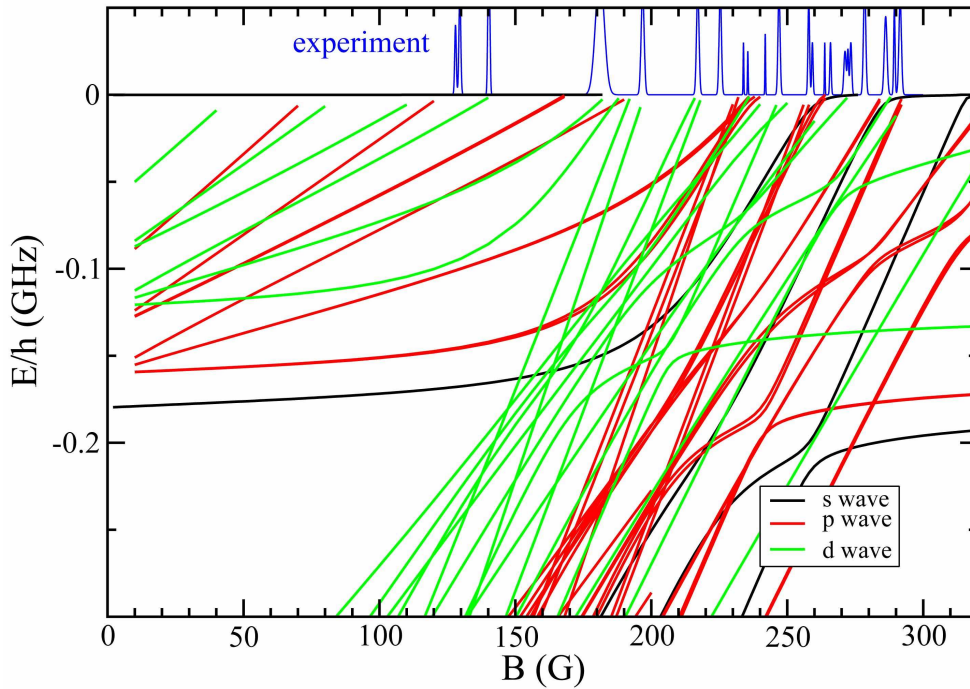


Figure 4.12: Preliminary result of the multichannel calculation. The x axis at zero energy corresponds to the energy threshold of the entrance channel $\text{Rb}|1, 1\rangle + \text{Cs}|3, 3\rangle$. The blue line above the threshold displays the inverted result of the experimental Feshbach spectrum. The black, red and green lines below the threshold are associated with s -, p - and d -molecular bound states. The crossing points of the molecular bound states with the energy threshold of the entrance channel are not corresponding to the experimentally observed positions of the Feshbach resonances. Figure from [Kot08].

In summary the complexity of the scattering problem of a mixture of Rb and Cs has up to now prevented the assignment of the observed Feshbach resonances. Particularly the presence of relatively high dipole-dipole interactions causing contributions of higher partial-wave molecular states challenges the theoretical models. Further experimental input will probably decrease the possible scattering scenarios and reduce the effort and computational time to obtain the appropriate assignment.

5 Towards molecules and double-degenerate mixtures

In our Rb-Cs mixture experiment we follow two main goals. First, the achievement of a double-species BEC and, second, the creation of heteronuclear ground-state molecules, which carry a permanent electric dipole moment. Additionally we perform Feshbach spectroscopy of loosely bound RbCs dimers, which is aim of the first section. In following section we discuss the progress towards a double-degenerate mixture, as well as the recently obtained BEC of Cs atoms in our apparatus. The last section will show the path towards ground state RbCs molecules via a combined technique of Feshbach association of molecules and a ground-state transfer via a two-photon stimulated Raman adiabatic passage (STIRAP).

5.1 Magnetic field association

The association of molecules by using magnetic fields is a powerful tool to produce molecular samples or to perform molecular spectroscopy. Besides the association of molecules by means of a magnetic field sweep across a Feshbach resonance, molecules can be associated applying an oscillatory magnetic field (wiggle). The following subsections explain the basic concepts of the wiggle technique and show preliminary results on molecular spectroscopy of RbCs dimers.

5.1.1 The wiggle technique - basic concepts

The wiggle technique was introduced as a novel atom molecules formation technique by [Tho05]. The association of molecules by applying a sinusoidal modulation of the homogeneous magnetic field close to a Feshbach resonance is presented as an alternative to conventional formation techniques, which use a sweep of the magnetic field across a Feshbach resonance to produce molecules. Association of molecules by sweeping the magnetic field across a Feshbach resonance may give rise to heating and loss of particles for ultracold samples at high densities. Close to a Feshbach resonance, where the scattering length diverges, three-body recombination leads to heating of the sample and to loss of atoms, limiting the maximum achievable phase-space densities. In contrary the wiggle technique can be applied sufficiently far away from a Feshbach

5 Towards molecules and double-degenerate mixtures

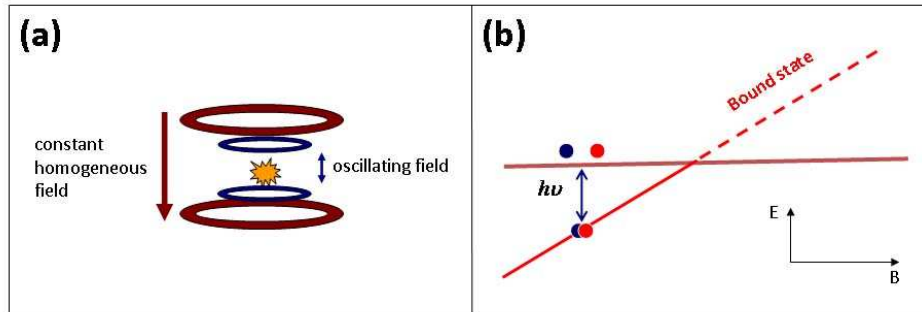


Figure 5.1: Basic concept of the wigggle technique. Molecules are associated close to a Feshbach resonance by applying a sinusoidal magnetic field. Figure (a) schematically shows the setup of the magnetic field coils. In addition to the coil pair creating the homogeneous dc magnetic field (red), we superimpose a sinusoidal modulation with the other coil pair (blue). Figure (b) displays the energy difference of the threshold of free atoms at zero kinetic energy and the molecular bound state. In the limit of zero collision energy the free atoms will be coupled to the molecular bound state, if $h\nu$ is corresponding to the molecular bound state energy.

resonance to circumvent limitations caused by the divergence of the scattering length. Furthermore the wigggle technique allows to determine precisely the binding energies of weakly bound molecules.

The basic concept of the wigggle technique is presented in figure 5.1. The homogeneous magnetic field is set to a value close to a Feshbach resonance, where a molecular bound state exists. The threshold is defined by the energy of two colliding free atoms. The energy difference between the free atoms and the molecular bound state can be bridged by applying an oscillating magnetic field in addition to the constant magnetic field. If the frequency ν of the oscillating field is chosen to fulfil the following condition

$$h\nu = E_b + E_{\text{therm}}, \quad (5.1)$$

molecules can be associated [Han07]. E_b denotes the binding energy of the molecular bound state at the specific value of the magnetic field, and E_{therm} is associated with the average thermal energy of the free atoms.

We use the wigggle technique to perform high-precision spectroscopy of Cs dimers. Details on the experimental setup and the sequence can be found in reference [Lan08b]. For specific values of the homogenous magnetic field we scan the frequency of the oscillatory magnetic field. If the modulation frequency ν is close to the binding energy value $E_b = h\nu$, the oscillating magnetic field couples atom pairs to molecules. The atoms are converted into molecules, and the resulting association is detected as reso-

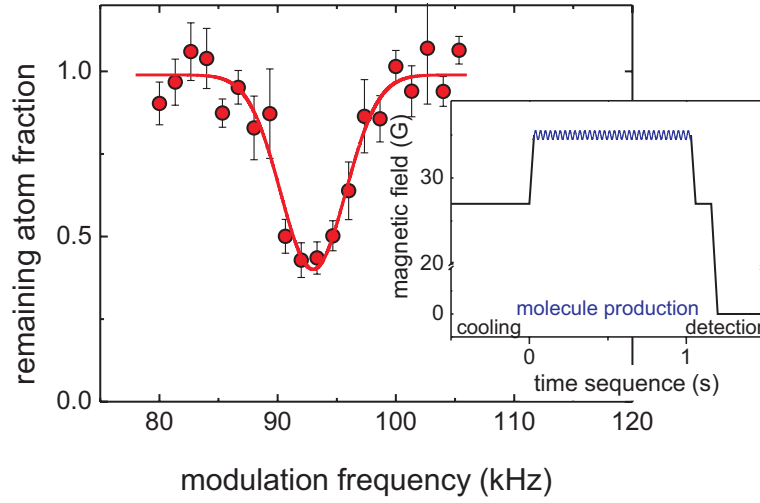


Figure 5.2: Example of a loss resonance at 48.2G for Cs atoms at a temperature of about 100nK. The losses are due to the coupling between atom pairs and d-wave molecules. The solid line is a gaussian fit to the data. The inset shows the typical magnetic field sequence used to associate Cs dimers with an oscillating magnetic field.

nant loss in the atom number. A typical loss signal is shown in figure 5.2. The resonant frequency is determined by fitting the data with a Gaussian profile.

We determine the resonant loss frequency for different values of the magnetic field. Figure 5.3 shows the measured molecular spectrum (open circles) in the magnetic field range between 25G to 60G. Here, three weakly bound molecular states, namely *s*-, *d*-, and *g*-wave bound states, overlap near threshold. We usually observe losses of Cs atoms up to 50%. The largest loss rate is observed when *g*-wave molecules are associated. This observation is consistent with the results of reference [Han07], which predict higher conversion efficiencies for larger relative magnetic moments $\delta\mu$.

The analytic model presented in reference [Lan08b] is used to calculate the atomic scattering length near a Feshbach resonance from data on the molecular binding energy. From fitting the binding energy data (red solid line in figure 5.3), the magnetic-field dependent scattering length can be determined with high precision.

5.1.2 Preliminary results and discussion

We extend the wiggle technique to the mixture of Rb and Cs. Measurements of the molecular binding energy of RbCs dimers will deliver spectroscopic information. The obtained data can be used as an additional input for theoretical models, which determine the scattering properties between Rb and Cs, see section 4.5.

To perform molecular spectroscopy on the mixture, we use the following experimental sequence: We load the mixture into the levitated crossed optical dipole trap, analogue to the procedure for Feshbach spectroscopy. We let the sample thermalize

5 Towards molecules and double-degenerate mixtures

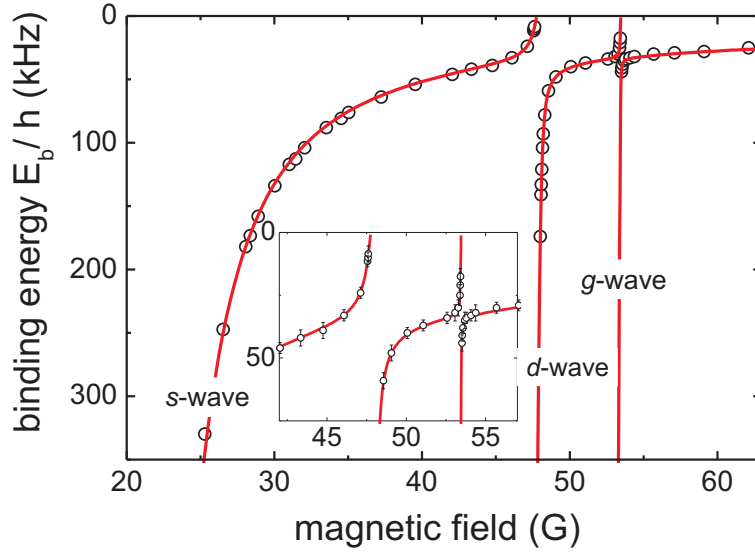


Figure 5.3: Binding energy of cesium molecules near three Feshbach resonances as a function of the magnetic field. Zero energy corresponds to two Cs atoms in the absolute hyperfine ground-state sublevel. The measurements are shown as open circles. The fit (solid line) is based on the theoretical model described in reference [Lan08b]. The inset shows an expanded view in the region of the two d - and g -wave narrow resonances.

for 2s. The waist of the reservoir is approximately $500\mu\text{m}$ and has an intensity of about 23W. The temperature and the peak density of the mixed sample is $3\mu\text{K}$ and a few 10^{10}cm^{-3} , respectively. We artificially create an imbalance between the atom number of both species, to increase the contrast of the loss signal, similar to the settings used for Feshbach spectroscopy. We ramp the homogeneous magnetic field to a specific value close to a heteronuclear Feshbach resonance. In addition we apply a modulation of the magnetic field. For each experimental cycle we vary the frequency of the sinusoidal modulation of the magnetic field. If the frequency ν is close to the corresponding binding energy value of the heteronuclear dimer ($E_b = h\nu$), the free atoms are coupled to the molecular bound state. The association of molecules will lead to trap losses caused by inelastic atom-molecule collisions. We apply the oscillating magnetic field for a duration between 1s and 5s. The association of molecules in combination with inelastic atom-dimer collisions opens a continuous atom number loss channel. We measure the remaining fraction of atoms after we switch off the traps by recapturing the atoms of the minority species in the MOT and recording their fluorescence signal.

To extract the value of the molecular binding energy for a specific value of the homogeneous magnetic field, we record the fraction of remaining atoms for different frequencies applied to the radio-frequency coil. We observe a strong asymmetric broadening of the resonance feature, which can be explained by the finite temperature

5.1 Magnetic field association

of the sample and by the presence of the magnetic gradient field. The asymmetric broadening of the loss signal caused by the non-zero temperature of the atoms can be attributed to the asymmetric Boltzmann distribution of the kinetic energy of the particles. A theoretical model recently published by reference [Kle08] is able to reproduce the shapes of the resonances at finite temperatures obtained in an experiment associating $^{41}\text{K}^{87}\text{Rb}$ molecules [Web08]. Figure 5.4 shows the number of associated molecules versus the radio-frequency for different temperatures. The data is obtained at LENS in Florence in the group of F. Minardi [Web08]. The solid lines in the graphs correspond to the theoretical model of reference [Kle08].

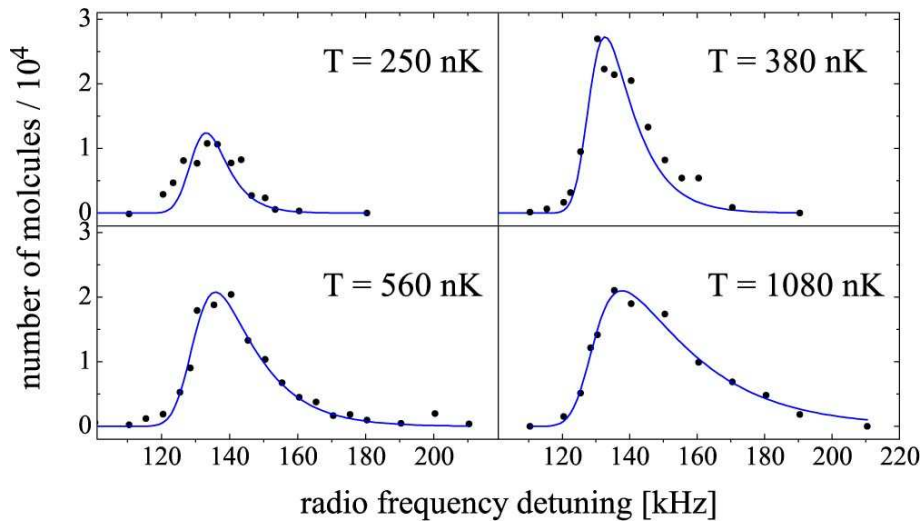


Figure 5.4: Number of molecules versus the radio-frequency for various temperatures and a fixed value of the magnetic field. The solid lines show the theoretical model, which takes into account the finite temperature of the sample. Measurements and theory were done by reference [Kle08].

Another mechanism which broadens the shape of the loss feature can be attributed to the presence of the magnetic gradient field. Sufficiently far away from the position of the Feshbach resonance, where the binding energy of the molecule scales linearly with the magnetic field, we can estimate the broadening of the loss resonance. For typical widths of the atomic sample in the optical trap of about $300\mu\text{m}$ and a magnetic gradient field of about 31G the broadening of the loss resonance is on the order of 14kHz for a difference of the magnetic moment between the entrance and the molecular bound state channel of $1\mu_B$ (μ_B is the Bohr magneton). The situation gets more complicated when we approach the position of the Feshbach resonance, where the binding energy scales quadratically with the scattering length. An inhomogeneity of the magnetic field will lead to an asymmetric shape of the loss signal. In this region, the interpretation of the loss spectrum is speculative in the presence of the gradient magnetic field. Figure 5.5 clarifies the additional broadening mechanisms caused by the presence of the magnetic gradient field in the regime of linear dependence of the binding energy on the magnetic

5 Towards molecules and double-degenerate mixtures

field and in the regime close to the Feshbach resonance, where the binding energy scales quadratically.

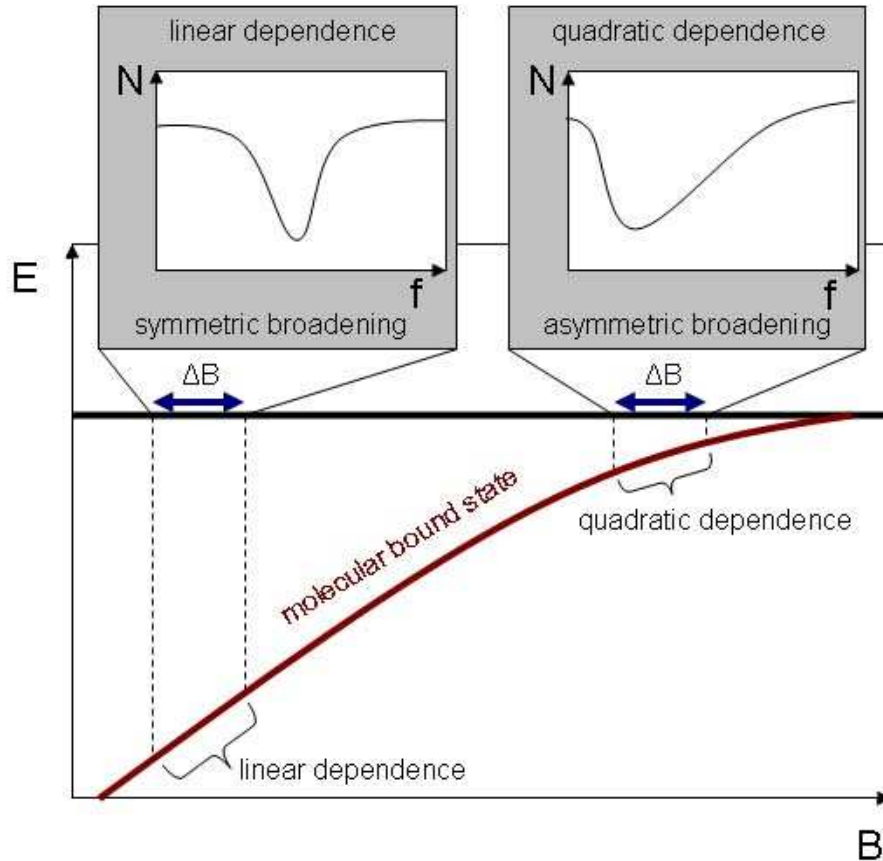


Figure 5.5: Influence of the magnetic gradient field on the lineshape of the loss signal. The inhomogeneity of the magnetic field leads to a symmetric broadening of the loss resonance in the regime, where the binding energy depends linearly on the magnetic field (left inset). Close to the Feshbach resonance, where the binding energy depends quadratically on the magnetic field, the shape of the resonant loss feature is asymmetrically broadened (right inset).

As a first estimate we assume the binding energy of the RbCs molecule to be associated with the minimum value of the remaining atom number. Figure 5.6 shows the preliminary result of the wiggle spectroscopy. The upper two graphs show typical loss resonances, which are recorded by applying a radio-frequency pulse with a duration of 5s for a specific value of the homogeneous magnetic field. The amplitude of the oscillating magnetic field is approximately 500mG. The upper graph on the left shows a loss signature, where two resonances overlap at their corresponding minimum frequencies of 50kHz and 120kHz. The lower graph of figure 5.6 displays the data of the binding energy depending on the value of the magnetic field. Note that we cannot determine the sign of the binding energy. Since there is no way to determine the sign

5.1 Magnetic field association

of the frequency associated with the maximum losses, the data points are arbitrarily arranged below or above the threshold.

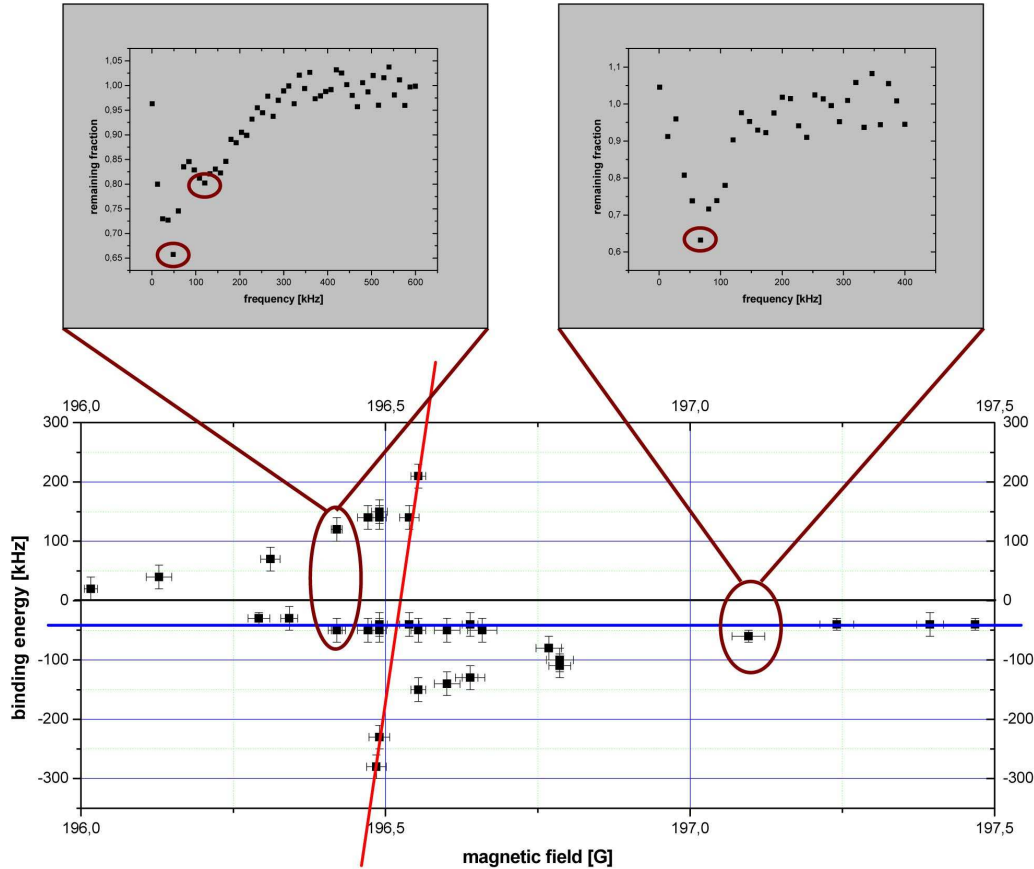


Figure 5.6: Preliminary data of the binding energy of RbCs dimers close to the 196G Feshbach resonance. The binding energies are measured using the wiggle technique. The threshold corresponds to the energy of two colliding free atoms of different species. The single data points are revealed by the determination of the molecular binding energy for a specific homogeneous magnetic field. The red line indicates a molecular bound state crossing the threshold at the position of the Feshbach resonance. The blue line is associated with a bound state, which is almost parallel to the threshold. The two insets on the top show typical loss measurements for specific values of the magnetic field.

The red line in the graph indicates a molecular bound state, which is crossing the threshold at the position of the interspecies Feshbach resonance at about 196G. We observe bending of the molecular bound state close to the threshold, corresponding to the coupling between the bound state and the entrance channel. Furthermore, the binding energy extends above threshold into the continuum, which could indicate the higher partial-wave character of the molecular bound state, since the presence of the centrifugal barrier of the molecular potential supports a finite lifetime of the molecules. In addition, we see a strong indication for a molecular bound state, which is almost paral-

5 Towards molecules and double-degenerate mixtures

level to the threshold (blue line in figure 5.6). The presence of a heteronuclear molecular bound state with an approximate binding energy of about $E_b = h \times 50\text{kHz}$ will correspond to an interspecies background scattering length of $a_{\text{bg}} = \sqrt{\hbar^2/(2\mu E_b)} \approx 800a_0$, μ is the reduced mass.

Even though the preliminary results on the measurement of the binding energies of RbCs molecules close to a heteronuclear Feshbach resonance are up to now speculative, the basic ability to obtain spectroscopic data looks promising. We are currently improving the experimental procedures to decrease the temperature of the sample. Furthermore we work on a trap configuration, which allows trapping of both species in the absence of the magnetic gradient field. These efforts will enhance the precision of the determination of the binding energy and lead to a conclusive energy spectrum of RbCs molecules.

5.2 Towards a double-degenerate atomic mixture

Two-component degenerate quantum gases exhibit new physical properties, which are not accessible in single-species experiments. The first experiment working with a two-component quantum gas studies the interactions between two condensates of different spin states of the same species in a magnetic trap [Mya96]. Furthermore reference [Hal98] investigates the dynamics of a two-spin component gas, where they observe a local separation between the spin components in the steady state. The experimental control over the inter-component interactions is presented in reference [Pap08]. In a two-spin component mixture of ^{87}Rb atoms the use of a single-component Feshbach resonance modifies the miscibility of the condensates. The first double-species BEC is reported in [Mod02a] on a mixture of ^{41}K and ^{87}Rb . They study the dynamics of two-component degenerate gas in an elongated magnetic trap, and find scissor-like oscillations as a result of off-axes collisions.

If a two-component quantum gas is miscible or immiscible is one fundamental property [Jez02, Rib02]. The miscibility of a quantum degenerate mixture is determined by the relative strength of single-species and interspecies interactions. Spatial separation of two immiscible quantum fluids in a trap is typified by a ball-and-shell ground-state structure in which one fluid forms a low density shell around the other. We can quantify the miscibility by introducing the parameter

$$\Delta = u_{11}u_{22} - u_{12}^2. \quad (5.2)$$

u_{11} and u_{22} are associated with the single-species interactions of species 1 and species 2, respectively. u_{12} denotes the interspecies interaction. The interactions can be written in the following form, e.g. for single species interaction of particles 1

$$u_{11} = \frac{4\pi\hbar^2 a_{11}}{m_1}. \quad (5.3)$$

5.2 Towards a double-degenerate atomic mixture

a_{11} is the single-species s -wave scattering length, and m_1 denotes the mass of particle 1. Correspondingly we write the interspecies interaction

$$u_{12} = 2\pi\hbar^2 a_{12} \frac{m_1 + m_2}{m_1 m_2} = u_{21}. \quad (5.4)$$

a_{12} is the interspecies s -wave scattering length, m_2 denotes the mass of particle 2. Note that $a_{12} = a_{21}$. We can distinguish between two regimes. If Δ is positive, the species are miscible. If Δ is negative, they are immiscible.

For a mixture of Rb and Cs the miscibility should be tunable at the position of an interspecies Feshbach resonance. Since we observe a strong indication for a large interspecies background scattering length (see section 5.1.1), the parameter Δ will be negative. By adjusting the interspecies scattering length with the help of a heteronuclear Feshbach resonance the miscibility can be modified.

5.2.1 Production of a Cs BEC

The ability to produce a BEC of Cs atoms is a benchmark on the present experimental setup. Furthermore the experimental procedure used to achieve a BEC of Cs atoms can be helpful for the production of a mixed-species BEC. The first creation of a Cs BEC [Web03a] was achieved within an optical dipole trap with Cs atoms in the lowest internal state. We basically follow the experimental procedure described by references [Web03a, Kra04] to obtain a BEC of Cs atoms.

Experimental procedure

We optimize every single step of cooling and trapping on highest phase-space densities. According to the experimental procedure used to obtain a Feshbach spectrum, we trap and cool Cs atoms in a MOT, followed by a combined compression and molasses phase. Afterwards we perform single-species degenerate Raman-sideband cooling and obtain about 10^8 atoms at a temperature of $1.5\mu\text{K}$. To achieve higher phase-space density (PSD) in the levitated reservoir trap, we change the waist of the single optical dipole trap beams to approximately $780\mu\text{m}$, which allows for a better phase-space matching between the cloud released from DRSC and the dipole trap. We operate the reservoir trap at an intensity of 26W per beam. The trap depth and trap frequency are about $6.2\mu\text{K}$ and 9Hz , respectively. With 8×10^6 atoms we achieve a PSD on the order of 1.4×10^{-4} . To further increase the PSD we overlap the dimple beam with a waist of $33\mu\text{m}$ onto the reservoir. During the next 2s the dimple trap is loaded via elastic collisions. Afterwards we switch off one beam of the reservoir trap, therefore we create an elongated crossed dipole trap. With this method we increase the PSD by almost three orders of magnitude. The temperature of the sample with 4×10^5 atoms is 440nK , the peak density is approximately $1 \times 10^{13}\text{cm}^{-3}$. This is the starting point for a three-step forced evaporation. Important parameters of the three steps of evaporation are listed in table 5.1.

5 Towards molecules and double-degenerate mixtures

The values listed in table 5.1 are partially measured and partially derived values. We measure the atom number N , the temperature T of the sample, the trap frequency ν , and the laser powers P_1 and P_2 of the beams. We derive the other quantities assuming a harmonic potential. The peak density n_0 and the mean density n are calculated by

$$n_0 = N \left(\frac{m(2\pi\nu)^2}{2\pi k_B T} \right)^{3/2} \quad (5.5)$$

and

$$n = \frac{n_0}{\sqrt{8}}, \quad (5.6)$$

where m and k_B are the mass of the Cs atom and the Boltzmann constant, respectively. The phase-space density (n_{PS}) is calculated as follows

$$n_{\text{PS}} = N \left(\frac{2\pi\nu\hbar}{k_B T} \right)^3. \quad (5.7)$$

The elastic scattering rate γ and the three-body loss rate l_3 are evaluated by the formulae

$$\gamma = n \sqrt{\frac{16k_B T}{\pi m}} \frac{8(\pi a \hbar)^2}{\pi \hbar^2 + 4ma^2 k_B T} \quad (5.8)$$

$$l_3 = L_3(a) \frac{n_0^2}{\sqrt{27}}, \quad (5.9)$$

where $L_3(a)$ is the three-body loss coefficient

$$L_3(a) = 3C(a) \frac{\hbar a^4}{m}, \quad (5.10)$$

which depends on the forth power of the scattering length a [Web03b] and shows an oscillatory behavior of $C(a)$ with the scattering length [Esr99, Bra01, Kra06]. For the evaluation of the three-body loss rates listed in table 5.1 we assume a constant value for $C(a) = 40$.

Note that the large high power beam changes its shape with time as already discussed in section 3.4. The change of the shape results in a change of the trap frequency. We observe drifts of the value of the trap frequency on the order of 25%. Furthermore the distortion of the beams does not simply correspond to a reduction of the waist, moreover the trap can no longer be approximated by Gaussian beams. An error of the trap frequency of 25% leads to an uncertainty on the calculated values of n_0 and n_{PS} on the order of 80%. Furthermore, we cannot exclude an additional error on the determination of the atom number.

5.2 Towards a double-degenerate atomic mixture

Table 5.1: Table of parameters used to achieve a BEC of Cs. Atom number N , trap frequency ν , temperature of the sample T , magnetic field B and the laser powers of the large beam P_1 and the dimple beam P_2 are measured quantities. The phase-space density n_{PS} , the peak density n_0 , the elastic scattering rate γ and the three-body loss rate l_3 are calculated values. Note that all the values carry a systematic error, which is mostly induced by the uncertainty of the atom number and the waist of the trapping beams (for details, see text).

	$N(10^5)$	$T(\text{nK})$	n_{PS}	$\nu(\text{Hz})$	$n_0(10^{12})$
reservoir	80	1200	3.6×10^{-5}	9	0.14
dimple trap	3.5	440	0.17	72.3	14
1st ramp	1.9	175	0.56	52.3	12
2nd ramp	1.0	70	1.0	34.8	7.3
3rd ramp	0.2	10	-	20.1	4.0

	$\gamma(\text{s}^{-1})$	$B(\text{G})$	$l_3(\text{s}^{-1})$	$P_1(\text{W})$	$P_2(\text{mW})$
reservoir	34.7	67.5	0.003	26	-
dimple trap	862	27.4	0.89	26	63
1st ramp	472	27.4	0.6	24	25
2nd ramp	64.0	22.5	0.03	23	8
3rd ramp	67	22.5	0.008	16	2

As already mentioned, for Cs atoms a high three-body loss coefficient is present, which scales with the fourth power of the scattering length [Web03b, Kra06]. We have to carefully adjust the scattering length to overcome limitations induced by three-body recombination. In addition efficient forced evaporation relies on high elastic scattering rates. We therefore have to balance between sufficient thermalization rates and moderately low three-body loss rates. The values for the magnetic field used for the different evaporative steps, as well as the elastic scattering rate and the rate of the three-body recombination are listed in table 5.1. We reduce the scattering length at the end of the first evaporative ramp from $480a_0$ to $280a_0$.

Figure 5.7 illustrates the timing sequence of the three evaporative steps. All three linear ramps of the laser powers have a duration of 5s, while the final values of the powers of the large and the dimple beam are optimized experimentally on maximum PSD. We assume the reduced power of the large beam is necessary to keep photon scattering rates moderate. At the beginning of the forced evaporation the heating rate associated with photon scattering is on the order of 5nK/s. Figure 5.8 shows the increase of the PSD for different steps of the evaporation.

If we further decrease the optical power of the dimple beam by about 10% in the last stage of the evaporation, we observe the emergence of the Cs BEC. We take an absorption image of the atomic cloud after 80ms of free expansion at a magnetic field

5 Towards molecules and double-degenerate mixtures

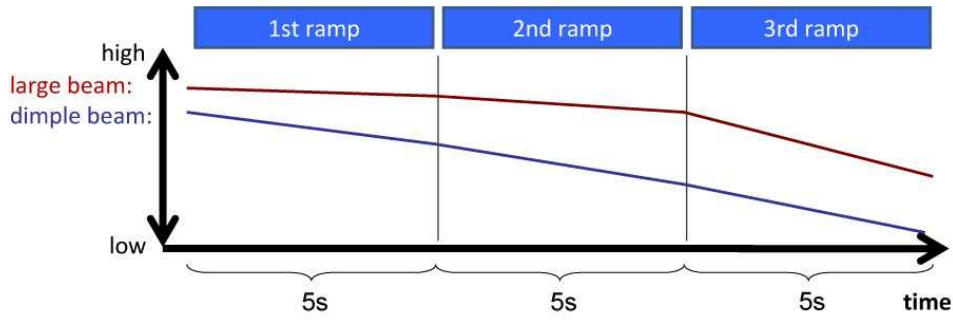


Figure 5.7: Timing sequence of the three steps of the evaporation. We linearly lower the optical powers of the large and the dimple beam according to table 5.1. Each of the three steps has a duration of 5s.

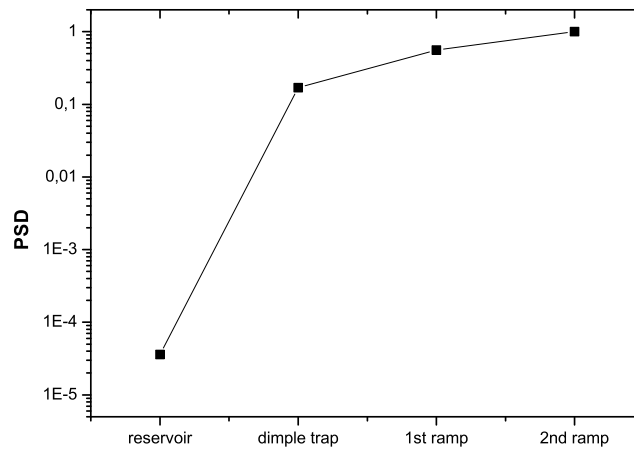


Figure 5.8: Diagram showing the PSD during the single steps of evaporation.

of about 17G, which correspond to a zero-crossing of the scattering length. During the expansion the magnetic gradient field is compensating for gravity. Figure 5.9 displays the bimodal distribution of the atom number density. The graphs correspond to the linear integrated atom number densities along the horizontal and the vertical directions, respectively. The width of the cloud in the horizontal direction is broadened by the presence of the gradient magnetic field. From the width $(110 \pm 10)\mu\text{m}$ of the Gaussian thermal background of the cloud in the vertical direction we extract a temperature of about $(15 \pm 3)\text{nK}$. We calculate the critical temperature for our trapping parameters to be about $T_c = 21\text{nK}$. The corresponding condensate fraction

$$\frac{N_c}{N} = 1 - \left(\frac{T}{T_c}\right)^3 \quad (5.11)$$

is between 0.4 and 0.8, which agrees to the results obtained from fitting a bimodal distribution.

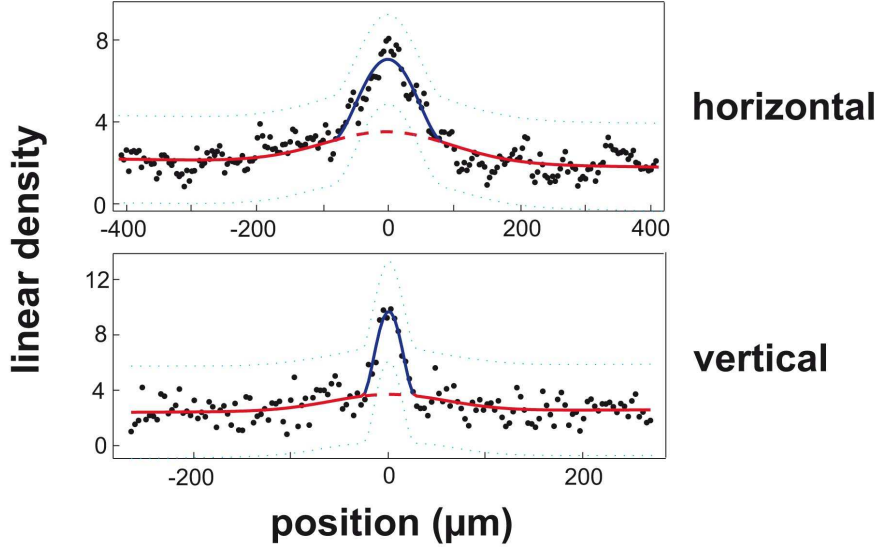


Figure 5.9: Bimodal distribution of a Cs BEC emerging from a thermal cloud. The absorption image is taken after 80ms of free expansion at zero scattering length. The levitation field during expansion is holding the atoms against gravity. The upper and the lower graphs display the integrated linear atom number densities along the horizontal and the vertical direction, respectively. The blue and the red lines are resulting from a fit-function, which reproduces the bimodal distribution by fitting a Gaussian shape to the thermal background and a Thomas-Fermi shaped function to the condensate fraction. We extract a condensate fraction of 50% for an overall atom number of 1.2×10^4 .

We are able to produce a BEC of Cs atoms within an overall experimental cycle time of about 40s. The condensate fraction is approximately 50%. Since we are able to obtain a BEC of Cs atoms, we can exclude systematic problems (apart from the distortion of the reservoir beams) of our experimental apparatus.

5.2.2 Ways to obtain a double BEC

Different requirements on the trapping configuration have to be met to obtain a BEC of Cs or Rb in single-species experiments. For the production of a Cs BEC the strategy is to use a large volume optical dipole trap combined with a tightly focus laser beam [Kra04]. To obtain a Rb BEC in an optical dipole trap, the strategy is different. Reference [Kin05] shows the production of a Rb BEC in an optical dipole trap, by

5 Towards molecules and double-degenerate mixtures

reducing the volume of the trap after loading within the first 600ms by a factor of 200. The reduction of the waist of the beams and therefore the increase of the atom number density is necessary for efficient evaporation in the case of Rb, since the background scattering length is too low to allow for fast thermalization in large volume traps.

If we want to obtain a double-species BEC, we have to merge both strategies. On one hand side we need to have a large volume trap to efficiently load the atoms released from the DRSC lattice into the optical dipole trap. On the other hand the big trap size prevents the Rb sample from fast thermalization, which is necessary for efficient evaporation. The thermalization rate basically depends on the elastic scattering rate, which is itself proportional to the trap frequency and the scattering length. In contrary to the Cs atoms we do not have the ability to change the scattering length for Rb, since there is no Rb Feshbach resonance within the accessible magnetic field range and the background scattering length is basically constant at a value of about $100a_0$ up to 1000G.

Another important fact is the difference of the trap depths for the different species. For the laser we use to produce the optical dipole trap, the trap depth for Rb is a factor of 1.7 smaller than for Cs (see section 3.4). Since the Cs atoms are located in a deeper trapping potential and the interspecies collision rates are high, we will predominantly evaporate Rb while the Cs atoms are sympathetically cooled.

If we perform forced evaporation by ramping down the optical trap depth in the current experimental setup, we will lose all Rb atoms. The presence of Cs in the trap will together with the lower trap depth for Rb deplete the number of Rb atoms very fast.

We present two main paths to overcome these difficulties: First we can load each species into separated traps, which we merge to a single trap after the condensation of both species. Second, we keep the current setup of the levitated optical dipole trap, but we artificially decrease the trap depth for Cs, or increase the trap depth for Rb.

To realize the separated traps idea, we basically have two possibilities. First, we use two different laser beams of which one can be locally moved with respect to the other (e.g. with the use of an AOM). We independently design and optimize the trap depths and waists for each species. Irrespective the other trap we perform evaporative cooling on the single species. After we obtained BEC of the two species, we merge both traps and get a double-species BEC within a single trap.

Second, we could realize a *trap-in-trap* design, in which a small volume trap is surrounded by a large volume reservoir trap, see figure 5.10. For a mixture of Rb and Cs the large volume trap could be simply similar to the reservoir trap we are currently using. Both species will be loaded into this trap, similar to the actual trap configuration. The second trap will be a tightly focused laser beam, which is blue detuned for Cs and red detuned for Rb, and which is directed through the center of the reservoir trap. In this way we produce an attractive dimple trap for Rb and just a small repulsive perturbation for the Cs trap. The light used for the dimple is chosen to create an attractive

5.2 Towards a double-degenerate atomic mixture

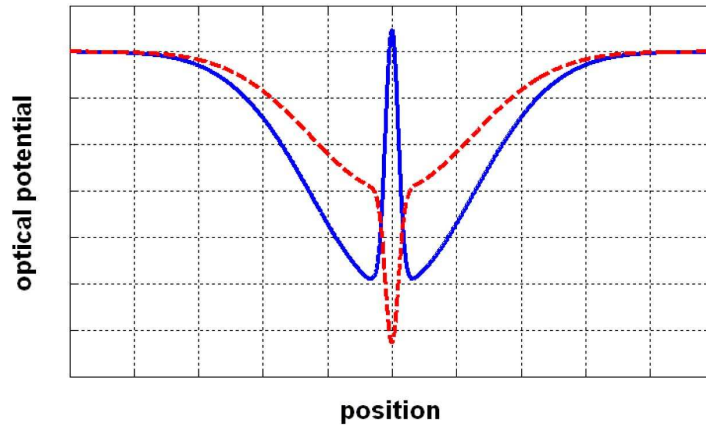


Figure 5.10: Trap-in-trap configuration: The blue solid line corresponds to the trapping potential for Cs, which is composed of a large volume reservoir trap, which is disturbed by the presence of the blue detuned dimple trap. The red dashed line denotes the optical dipole potential for Rb. Both the reservoir laser and the laser producing the dimple beam are red detuned with respect to the transition frequencies of Rb, therefore producing attractive potentials. This configuration of the trapping potentials might allow for efficient evaporation for both Rb and Cs.

potential for Rb and a repulsive one for Cs. For a wavelength of 820nm, a waist of $80\mu\text{m}$ and an optical power of 50mW we create a trap depth of about $5\mu\text{K}$ for Rb. In this trap the thermalization rate for Rb is much higher because of the tighter confinement. On the other hand the photon scattering rate keeps moderately low at a value of about 0.11s^{-1} for Rb and 0.093s^{-1} for Cs. The dimple will be loaded via single- and interspecies collisions in the reservoir trap. We can now independently perform forced evaporative cooling in both traps. After we obtain BECs in each of the traps, we ramp down the dimple beam, and merge the traps again. One open question is in which respect the presence of the repulsive optical potential distorts the reservoir trap for Cs.

To artificially modify the trap depths for Rb and Cs, we can apply two techniques: First we are able to artificially reduce the trap depth for the Cs atoms by applying a microwave frequency, similar to the so-called *radio-frequency knife* used to evaporate atoms from a magnetic trap, see figure 5.11. Since the optical dipole trap is combined with a magnetic gradient field, we create a state selective trap. Similar to atoms in magnetic traps, hot atoms will on average experience higher magnetic fields. We can use a selected microwave frequency to cut the optical potential at a certain level corresponding to a maximum temperature of the atoms. Effectively we will reduce the trap depth selectively for the Cs species. The disadvantage of this method is the extensive loss of Cs atoms, since we simply cut down the trap depth.

A more evolved technique reduces the trap depth for Cs by tilting the trap reducing

5 Towards molecules and double-degenerate mixtures

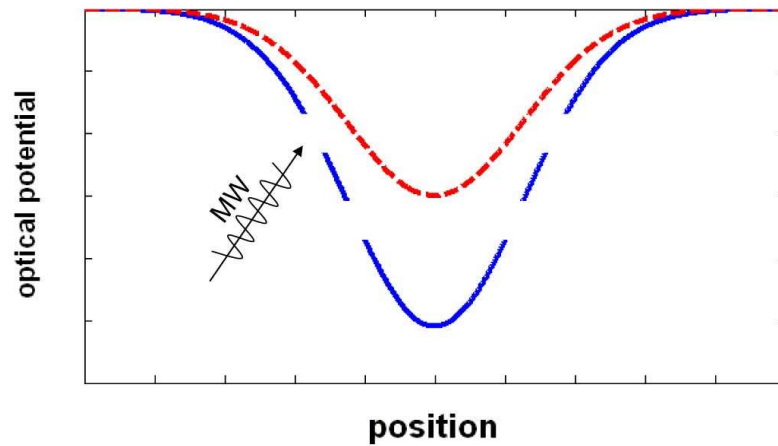


Figure 5.11: Reduction of the Cs trap depth (blue solid line) by applying a microwave frequency. The microwave will pump the atoms to a state which is not levitated by the magnetic gradient field.

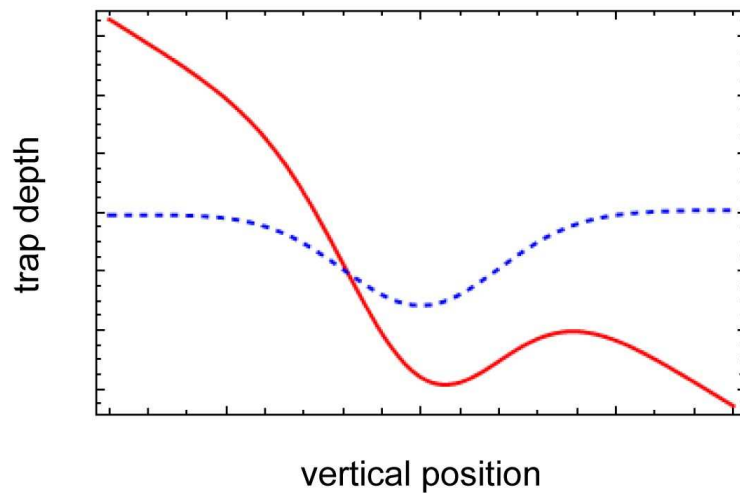


Figure 5.12: Reduction of the Cs trap depth by applying the magnetic gradient field to levitate the Rb $|2, -2\rangle$ state. Since the magnetic gradient field is optimized on compensating for the gravitational sag of Rb, the trap depth in the vertical direction will be reduced for the Cs atoms.

the magnetic gradient field used for levitation. At the same time the trap depth for Rb has to be almost kept constant. Figure 5.12 illustrates this technique. We can realize such a trap configuration with a mixture of Rb in the state $F = 2, m_F = -2$ and Cs in its ground state. Since the magnetic moment to mass ratios for these states differ by a factor of two, we effectively reduce the trap depth for Cs, when the magnetic gradient field is operated to compensate for gravity on the Rb species. Furthermore a mixture

of Rb and Cs in the states mentioned are stable against spin exchange. Recently a BEC of Cs atoms has been obtained by forced evaporation ramping down continuously the gradient magnetic field [Hun08].

5.3 Towards heteronuclear ground state molecules

In atomic samples, interactions are sufficiently short range to be approximated by contact interaction and they are spatially isotropic. For particles that show dipole-dipole interactions an expanded range of physical phenomena could be studied. Dipole-dipole interactions can be realized using atomic magnetic dipoles. Magnetic dipole-dipole interactions are typically much weaker than those which can be realized for molecules carrying a permanent electric dipole moment.

Quantum gases with dipolar interaction represent many-body quantum systems of increased complexity [Bar08]. Dipolar quantum gases confined in periodic potentials promise the realization of Hubbard-type Hamiltonians with extra spin degrees of freedom. The strength and the long-range nature of the electric dipole-dipole interaction remove the restriction to on-site interaction and allow processes where nearest-neighbor interactions are relevant. It is in principle possible to have full control over all external and internal (spin-) degrees of freedom, while the strength and the orientation of the interaction can be tuned by externally applied electric fields. A large variety of many different quantum phases beyond the well-studied Mott insulator phase has been suggested [Gór02], e.g. checker-board phases and different types of supersolid phases [Yi07]. Exotic pseudo-magnetic ordering is possible [Bar06], and dipolar gases in two-dimensional lattice geometry can serve as protected quantum memory and allow topological quantum computing [Mic06]. Quantum gases with externally controllable dipolar interactions are also expected to play an important role in ultracold coherent chemistry [JD04] and possibly in quantum information processing [DeM02] and for precision measurements.

The strength of dipole-dipole interactions in an ultracold gas depends basically on three parameters: the temperature, the number density of molecules and the dipole moment. To study the interactions, the thermal energy has to be comparable or smaller than the effect of the dipole-dipole interactions. Furthermore high density of the molecules is needed, since the dipole-dipole interaction scales like $1/r^3$, where r is the interparticle distance. The strength and orientation of the long-range dipole-dipole interaction of the dipolar gas can be tuned by externally applied electric dc and ac fields. Figure 5.13 compares permanent electric dipole moments for different heteronuclear alkali molecules.

The first ultracold samples of dipolar ground state molecules have been produced in the group of D. DeMille at Yale University via photoassociation and a combination of spontaneous and stimulated transfer [Sag05]. Yet, transfer efficiency and state selectivity are low, and the resulting phase-space densities are far away from the quan-

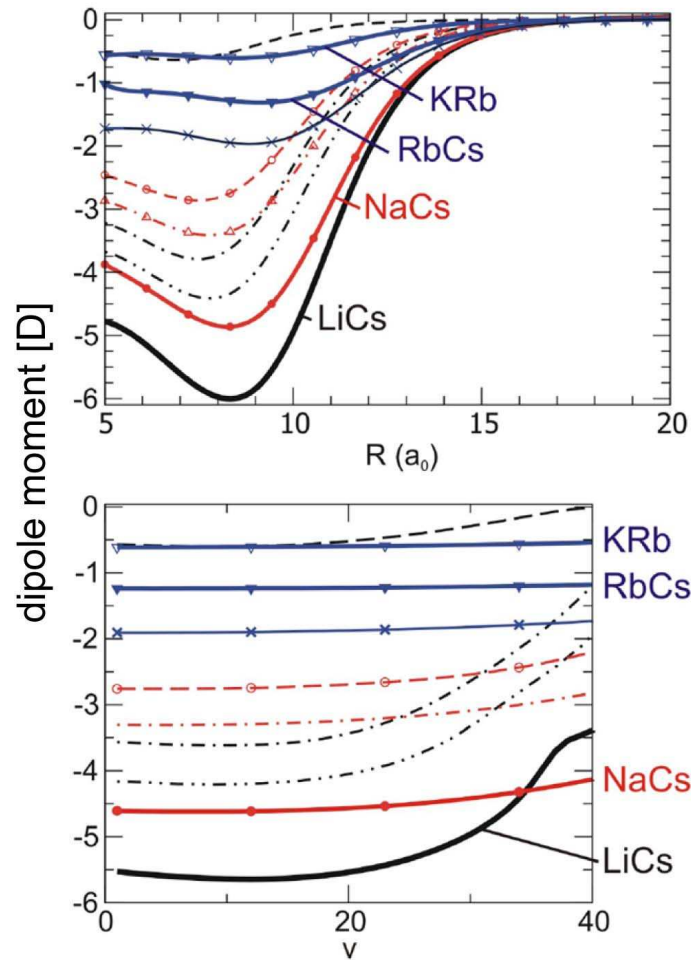


Figure 5.13: Permanent electric dipole moments for different mixed species. The dipole moments are calculated for the singlet ground state of the heteronuclear dimers. The upper graph shows the strengths of the dipole moments depending on the interparticle separation, while the lower graph displays the dependence on the vibrational quantum number [Kot06].

tum degenerate regime. Alternative approaches, relying on buffer gas cooling or Stark deceleration [JD04], are not yet capable of reaching the ultracold regime. Recently, heteronuclear Feshbach molecules of KRb have been transferred to the ro-vibrational groundstates of the triplet and singlet potentials [Osp08, Ni08].

Our goal is to produce a quantum gas of dipolar RbCs molecules in the ro-vibrational ground state of the singlet potential. These molecules are trapped in a periodic potential, that allows the investigation of possible dipolar quantum phases. We plan to first produce the molecules from a nearly degenerate or Bose-condensed sample of Rb and Cs by means of magnetic field association near an interspecies Fesh-

5.3 Towards heteronuclear ground state molecules

bach resonance. To shield the sample from inelastic losses, we perform the association in the presence of an optical lattice. The shallow bound molecules are transferred to the ro-vibrational ground state of the singlet potential via a stimulated two-photon Raman transition using STIRAP [Ber98]. In a three level system with the two electronic ground states $|a\rangle$ and $|b\rangle$, and the excited state $|e\rangle$ we apply two laser fields, of which the first couples the levels $|a\rangle$ and $|e\rangle$ and the second couples the states $|b\rangle$ and $|e\rangle$. The basic idea of STIRAP is to keep the molecules in a dark superposition state of the electronic ground state levels during the transfer. Ideally the transfer from state $|a\rangle$ to state $|b\rangle$ can be done coherently without losses, since the population is kept in the dark superposition state without any contribution of the excited level $|e\rangle$. If the molecules are transferred to the ground state with a dipole moment of $1.25D$ in the case of RbCs [Kot06], the strong long-range and anisotropic electric dipole-dipole forces dominate the interaction. The strength and the orientation of the interaction can be controlled by external dc and ac electric fields.

Molecular ground state transfer via 2-photon Raman transition using STIRAP

We plan to combine techniques of Feshbach association and coherent molecular state transfer to produce quantum gases of heteronuclear molecules in the ro-vibrational ground state, similar to the procedure used in reference [Dan08]. The molecules, produced in an optical lattice via a magnetic field ramp across a heteronuclear Feshbach are loosely bound. The presence of the optical lattice will shield the molecules against relaxational collisions. In the next step we transfer the loosely bound molecules to the ro-vibrational ground state according to figure 5.14. The transfer process involves an excited level. Population transfer into this level needs to be avoided to prevent loss due to spontaneous emission. One possibility is to use the technique of STIRAP [Ber98], which is very robust and largely insensitive to laser intensity fluctuations. The combined scheme of Feshbach association and STIRAP has several advantages. First, production of Feshbach molecules out of a quantum degenerate atomic sample can be very efficient. Second, the optical transfer rate starting from the Feshbach molecules is greatly enhanced in comparison to the free atom case. Further, the scheme is fully coherent, not relying on spontaneous processes. If losses and off-resonant excitations can be avoided, the scheme essentially preserves PSD and coherence of the initial particle wave function.

One possible ground-state transfer scenario could involve an intermediate level of the $A^1 \Sigma^+$ potential curve, see figure 5.14. This potential carries vibrational levels that should provide sufficient Franck-Condon overlap on the order of 10^{-5} with both the Feshbach molecules and the ro-vibrational ground state of the singlet $X^1 \Sigma^+$ potential. As a first step, we will perform optical spectroscopy on the RbCs Feshbach molecules in the range 1540 to 1570nm, more than 5000cm^{-1} to the red of the $S_{1/2}$ (Rb) - $P_{1/2}$ (Cs) asymptote. We will identify the appropriate excited states of the $A^1 \Sigma^+$ potential that have sufficient Franck-Condon overlap with the ro-vibrational ground state. The corresponding optical transitions for the second leg of the two-photon transition are in

5 Towards molecules and double-degenerate mixtures

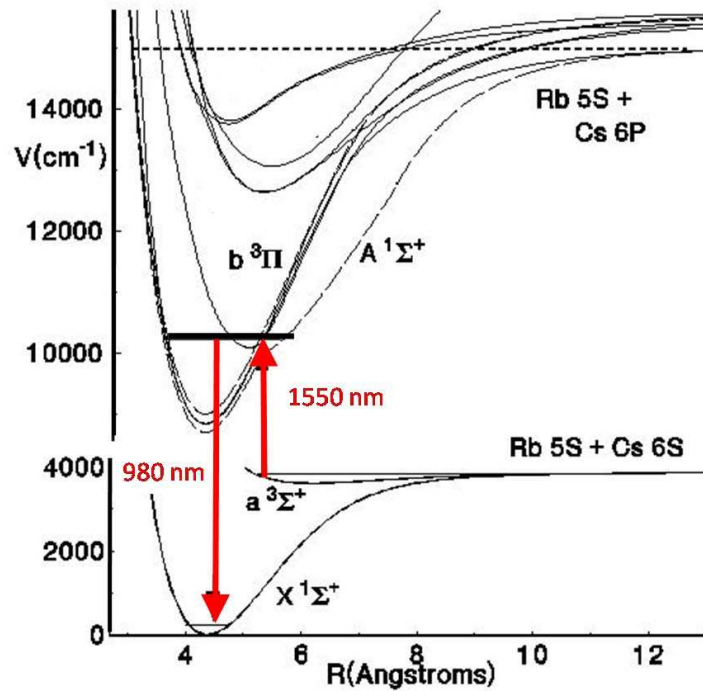


Figure 5.14: Relevant potential curves involved for the STIRAP ground state transfer. A single step Λ -type two-photon Raman transition using STIRAP starting from loosely bound Feshbach molecules seems to be promising. Potentials are calculated by [Stw04].

the range around 970nm for excitation at 1550nm on the first leg and can be addressed by a diode laser system.

Once the molecules are transferred to the singlet ro-vibrational ground state we are able to focus on the investigation of dipolar gases in optical lattices. As a result of the anisotropy and the long-range nature of the dipolar interaction, interesting exotic quantum phases ranging from the well-known Mott insulator phase to checkerboard, collapse and supersolid phases will be experimentally accessible [Gór02, Yi07]. Furthermore the way to achieve a BEC of ground state heteronuclear molecules will be open. The influence of the long-range dipolar interaction on the dynamic behavior and the stability of the degenerate quantum gas can be studied.

6 Conclusions

We have developed a new experiment for the simultaneous trapping of ultracold rubidium and cesium atoms in an optical dipole trap, and we have investigated the interspecies scattering properties by performing Feshbach spectroscopy. The localization of Feshbach resonances provides first insight into the energy structure of RbCs molecules near the dissociation threshold and is a major step towards the full understanding of the interspecies scattering properties.

We apply several stages of cooling and trapping to reach ultralow temperatures. First, we load both species into a two-color MOT providing 5×10^8 atoms at about $40\mu\text{K}$. We have the full control over the single-species atom number loaded into the MOT. We have extended the powerful technique of degenerate Raman-sideband cooling to a two-color version, resulting in final temperatures of about $2\mu\text{K}$ and $3\mu\text{K}$ for Cs and Rb, respectively. We obtain atom numbers of about 10^8 for both species fully polarized in their respective ground states. The use of an optical dipole trap combined with a magnetic levitation field is the key concept to trap and cool Rb and Cs and to reach the ultracold regime. Cs shows high rates of inelastic two-body collisions. The only state, which is immune against inelastic two-body collisions, is the absolute ground state, which cannot be trapped by magnetic forces. The use of an optical dipole trap enables us to cool and trap both Rb and Cs in their lowest internal states. The achievable atom numbers and phase-space densities are therefore no longer limited by inelastic two-body collisions. In addition the combination of the dipole force with the magnetic levitation field creates a highly state-selective potential, providing clean experimental conditions for the search of heteronuclear Feshbach resonances. With the concept of a levitated crossed optical dipole trap we can trap up to 2.5×10^6 atoms of Rb or Cs. For an equal mixture of the atomic species, we obtain atom numbers around 10^6 for both Rb and Cs at temperatures of about $3\mu\text{K}$.

With the current experimental setup we perform Feshbach spectroscopy of the Rb-Cs mixture. We find 23 interspecies Feshbach resonances for the collisional channel, in which both atoms are in their lowest internal spin state. We can attribute two more resonances in an excited spin-channel mixture. The measured Feshbach spectra represent fundamental experimental input to characterize the Rb-Cs scattering properties, and they also present suitable starting points for the association of ultracold heteronuclear RbCs molecules.

In addition we collect preliminary data on the determination of the molecular energy structure of RbCs dimers by using the technique of ac magnetic field association

6 Conclusions

of molecules. This spectroscopic data will further increase the knowledge of inter-species scattering potentials and will hopefully lead to a conclusive description of the collisional processes. Furthermore we recently obtained a BEC of cesium, which represents a benchmark for the performance of our current experimental setup.

We have identified some problems which presently limit the performance of the apparatus. One is related to the high-power laser used for the reservoir trap, since dust contaminates the optical components. This problem is solvable by providing a clean environment. To achieve a double-species BEC we also have to overcome the limit set by the different optical trap depths for the two species, which leads to predominant losses of Rb. We have identified several ways to deal with the current limitations, being confident of fast progress towards a two-species degenerate mixture.

For the future we follow two major objectives. First we plan the creation of a double BEC and second the production of ground-state polar molecules. In BEC mixtures interesting phenomena involving both single-species and heteronuclear interactions can be investigated as for example the miscibility of the two species. The production of polar ground state molecules will allow us to enter the regime of quantum degenerate gases that predominantly interact via the long-range anisotropic dipole-dipole interaction.

A Microwave spectroscopy and magnetic field calibration

The use of microwaves turned out to be very helpful for various purposes in our experiment. The basic idea is to drive transitions between different Zeeman states of two hyperfine levels ($F = 3 \rightarrow F = 4$ for Cs and $F = 1 \rightarrow F = 2$ for Rb) by applying a microwave frequency corresponding to the energy splitting of the two levels. We mainly use microwave spectroscopy to calibrate the magnetic fields. In addition we can remove a certain spin component of the gas or we prepare the sample in different substates, whether pure or in a mixture of Zeeman states.

For the species and magnetic field strengths we use, the Breit-Rabi formula [Cor77, Bre31] applies for the energy splitting between the Zeeman states of different hyperfine levels. For higher field strengths (when the Zeeman splitting is on the order of the hyperfine splitting), the Paschen-Back regime [Ale93] comes into play. We write the energy of two atomic states in different hyperfine levels as

$$E_{2mf_2} = -\frac{E_{\text{hfs}}}{2(2I+1)} + g_I \mu_B m_{f_2} B + \frac{E_{\text{hfs}}}{2} \sqrt{1 + \frac{4m_{f_2} x}{2I+1} + x^2}, \quad (\text{A.1})$$

$$E_{1mf_1} = -\frac{E_{\text{hfs}}}{2(2I+1)} + g_I \mu_B m_{f_1} B - \frac{E_{\text{hfs}}}{2} \sqrt{1 + \frac{4m_{f_1} x}{2I+1} + x^2}, \quad (\text{A.2})$$

with

$$x = (g_J - g_I) \mu_B \frac{B}{E_{\text{hfs}}}, \quad (\text{A.3})$$

Table A.1: Table of constants needed to evaluate the Breit-Rabi formula. Values taken from [Ste08].

	¹³³ Cs	⁸⁷ Rb
A_{hfs}	2298.1579425MHz	3417.341305452MHz
E_{hfs}	$A_{\text{hfs}}(I + 1/2)$ MHz	$A_{\text{hfs}}(I + 1/2)$ MHz
g_I	-0.00039885395	-0.000995141
g_J	2.00254032	2.00233113

A Microwave spectroscopy and magnetic field calibration

where $E_{2m_{f_2}}$ and $E_{1m_{f_1}}$ denote the energy of the atom in the state m_{f_2} and m_{f_1} , respectively. Note that the quantum number m_f is given by the sum

$$m_f = m_I + m_J, \quad (\text{A.4})$$

where the quantum numbers m_I and m_J are the projections on the total nuclear angular momentum \mathbf{I} and total electron angular momentum \mathbf{J} , respectively.

The microwave frequency needed to resonantly couple two Zeeman states of the different hyperfine ground states is given by the energy difference

$$\Delta E = E_{2m_{f_2}} - E_{1m_{f_1}}. \quad (\text{A.5})$$

The constants needed to evaluate these equations are given in table A.1.

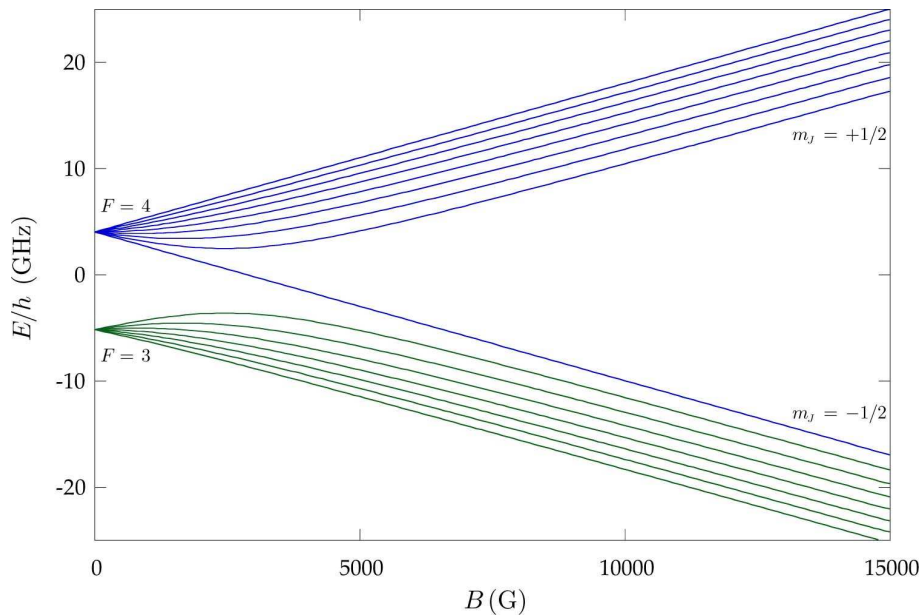


Figure A.1: $^{133}\text{Cs } 6^2\text{S}_{1/2}$ hyperfine structure in an external magnetic field. The levels are split according to the Breit-Rabi formula [Ste08].

Figures A.1 and A.2 show the energy splitting of the different Zeeman states of the two ground state hyperfine levels of Cs and Rb, respectively. In the region of low magnetic field strengths the states are grouped by the quantum number F , while for high magnetic fields (Paschen-Back regime) the states are split into two groups labeled by $m_J = \pm \frac{1}{2}$.

A.1 Microwave spectroscopy

This section explains the hardware setup for microwave spectroscopy of Rb and Cs. For the source frequency in the microwave regime, we use a frequency generator,

A.2 Magnetic field calibration

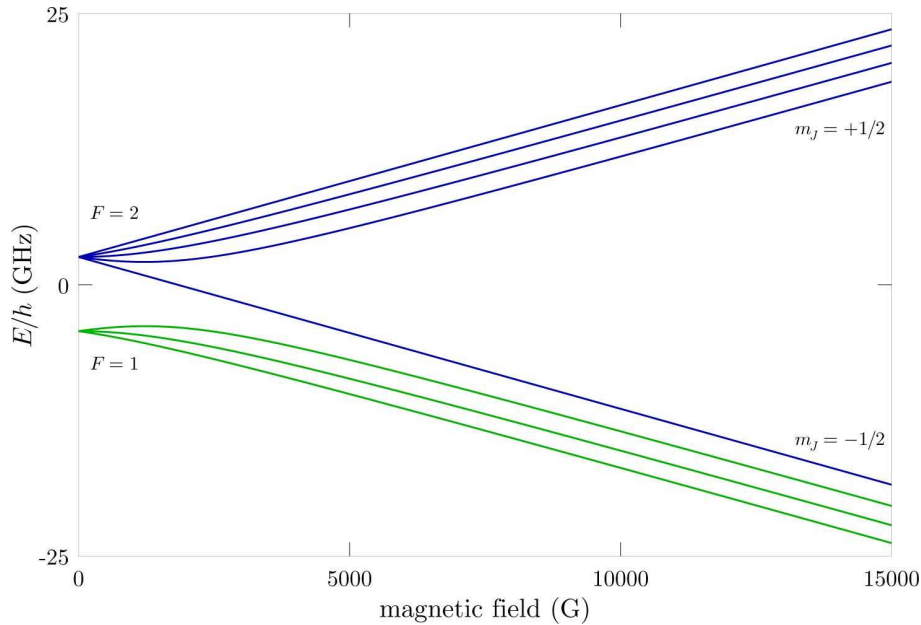


Figure A.2: $^{87}\text{Rb } 5^2\text{S}_{1/2}$ hyperfine structure in an external magnetic field. The levels are split according to the Breit-Rabi formula [Ste08].

which is programmable between 100kHz and 22GHz and has a maximum output power of 20dBm¹. In addition we mix² the source frequency with a computer controlled radio-frequency output of a programmable frequency generator³. Afterwards the signal is amplified⁴ up to 30dBm and applied to a broadband waveguide⁵, which is located as close to the position of the atomic clouds as possible. Figure A.3 displays the schematics of the microwave hardware setup. To switch the microwave on and off, a commercial high-frequency switch⁶ is used.

This hardware setup can be used for every single microwave-transition-based experiment for ^{133}Cs and ^{87}Rb . One application is the calibration of magnetic fields with the help of microwave spectroscopy.

A.2 Magnetic field calibration

We observe resonant microwave coupling between two levels by recording the remaining atom number in the trap after applying a microwave pulse. When the microwave frequency hits the resonance, atoms are transferred into a different level carrying a

¹Rohde&Schwarz, SMF100A

²mixer: Minicircuits ZMX-10G, 3.7 – 10GHz

³Agilent 33250A, 80MHz

⁴amplifier: Qunstar 10754001 6 – 18GHz, +30dB

⁵LAB.E.M 691.000.489

⁶Minicircuits ZYSWA-2 – 50DR

A Microwave spectroscopy and magnetic field calibration

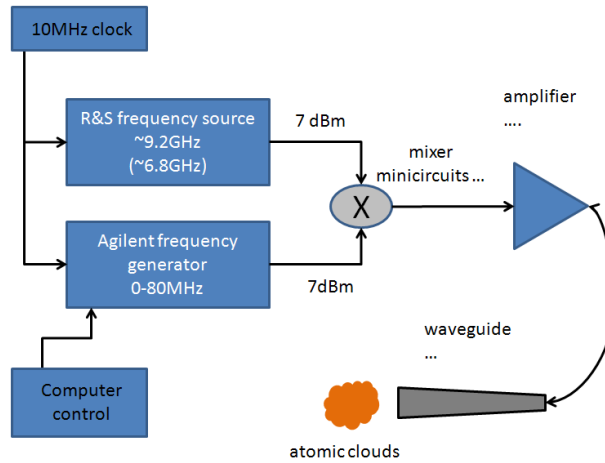


Figure A.3: Hardware setup for microwave spectroscopy. Two frequency sources, which are locked to an external 10MHz clock, are mixed and amplified. The broadband waveguide directs the microwave to the position of the atoms. Whether the microwave is applied on Cs or Rb, the frequency of the R&S is manually changed to the approximate values of 9.2GHz or 6.8GHz, respectively. The sidebands generated by the admixture of a radio-frequency signal are shifted by computer controlled radio-frequency generator.

different magnetic moment. As we trap the atoms in a levitated crossed optical dipole trap, atoms with different magnetic moments than the ground get lost from the trap. Figure A.4 shows a typical loss signature for Cs atoms transferred from the $F = 3, m_F = 3$ to the $F = 4, m_F = 4$ state. For this measurement the microwave signal is applied for 200ms at a power delivered to the microwave horn of about 18dBm. Note that the loss feature is broadened by the presence of the magnetic gradient field. From a Gaussian fit we extract a width of about 0.5MHz corresponding to a diameter of the thermal cloud in the vertical direction of about $320\mu\text{m}$.

For magnetic field calibration we simply record measured resonant microwave transitions depending on the externally applied magnetic field. Every shift of the transition frequency for different magnetic fields is calculated by evaluating the Breit-Rabi formula. Thus we are able to calculate the exact magnetic field for each current send through the magnetic field coils. Extrapolating will deliver the unknown parameters of the fit-function describing the magnetic field strength depending on the current.

A.2 Magnetic field calibration

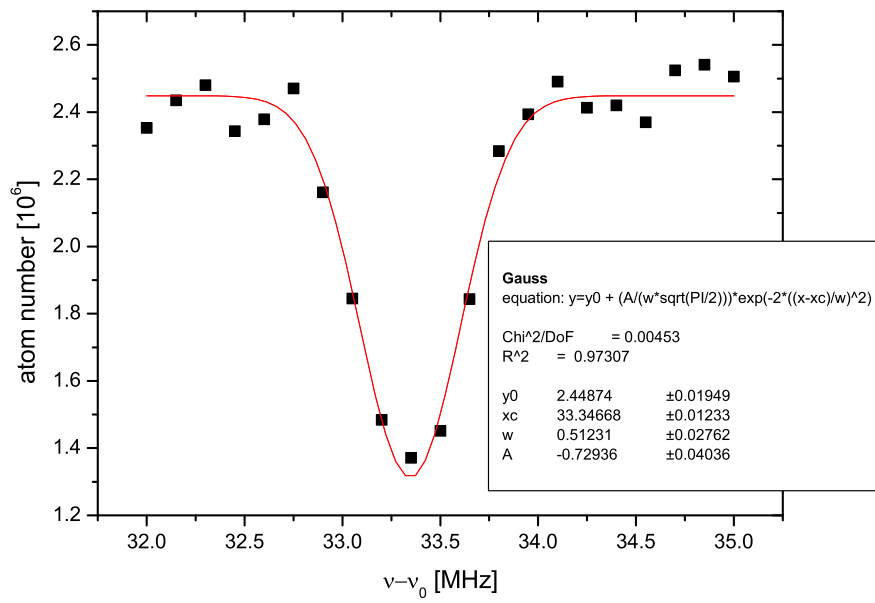


Figure A.4: Typical loss signature for resonant microwave excitation. The Cs atom number is recorded for different values of the radio-frequency ν , which is mixed onto the microwave source ν_0 . The data is fitted by a Gaussian, where the center frequency corresponds to the transition between the $F = 3, m_F = 3$ and $F = 4, m_F = 4$ levels.

B Extended level scheme of Cs

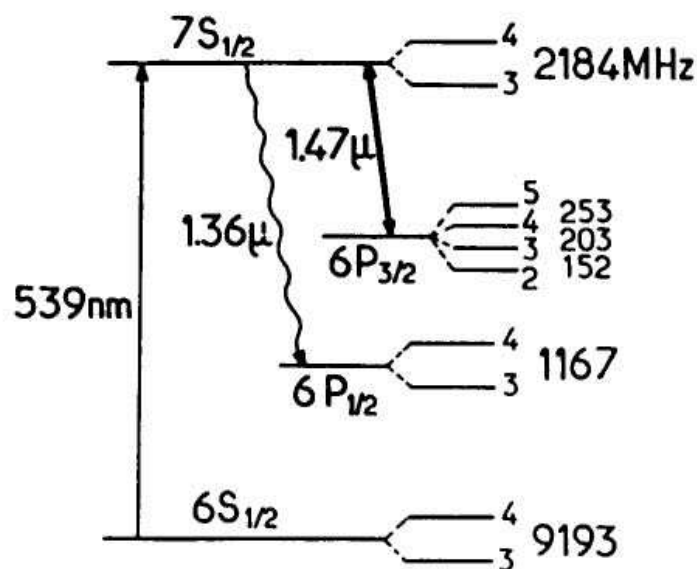


Figure B.1: Figure of relevant levels for a two-photon transition between $6S_{1/2}$ and $7S_{1/2}$ (not to scale). Figure from reference [Bou89].

As discussed in section 3.4 we observe a limited lifetime of Cs in the reservoir trap of about 3.3s. We believe that enhanced losses from the dipole trap can be partially attributed to a coincidence of a two-photon transition between $6S_{1/2}$ and $7S_{1/2}$ and the wavelength of the laser used to produce the trapping potential. The central wavelength of the laser is 1070nm and has linewidth of about 3nm. Figure B.1 shows the relevant spectrum of Cs including the transition between $6S_{1/2}$ and $7S_{1/2}$ at about 539nm [Bou89].

C Publications

Observation of interspecies Feshbach resonances in an ultracold Rb-Cs mixture

K. Pilch, A. D. Lange, A. Prantner, G. Kerner, F. Ferlaino, H.-C. Nägerl, R. Grimm
arXiv:0812.3287

Determination of atomic scattering lengths from measurements of molecular binding energies near Feshbach resonances

A. D. Lange, K. Pilch, A. Prantner, F. Ferlaino, B. Engeser, H.-C. Nägerl, R. Grimm, C. Chin
arXiv:0810.5503

Evidence for Efimov quantum states in an ultracold gas of caesium atoms

T. Kraemer, M. Mark, P. Waldburger, J. G. Danzl, C. Chin, B. Engeser, A. D. Lange, K. Pilch, A. Jaakkola, H.-C. Nägerl, and R. Grimm
Nature **440**, 315 (2006).

References

- [Abe98] F. A. van Abeelen, D. J. Heinzen, and B. J. Verhaar, *Photoassociation as a probe of Feshbach resonances in cold-atom scattering*, Phys. Rev. A **57**, (R)4102 (1998).
- [Ale93] E. B. Alexandrov, M. Chaika, and G. I. Khvostenko, *Interference of atomic states*, Springer-Verlag, Berlin, 1993.
- [And95] M. H. Anderson, J. R. Ensher, M. R. Matthews, C. E. Wieman, and E. A. Cornell, *Observation of Bose-Einstein condensation in dilute atomic vapor*, Science **269**, 198 (1995).
- [And97] M. R. Andrews, C. G. Townsend, H.-J. Miesner, D. S. Durfee, D. M. Kurn, and W. Ketterle, *Observation of interference between two Bose condensates*, Science **275**, 637 (1997).
- [And05] M. Anderlini, E. Courtade, M. Cristiani, D. Cossart, D. Ciampini, C. Sias, O. Morsch, and E. Arimondo, *Sympathetic cooling and collisional properties of a Rb-Cs mixture*, Phys. Rev. A. **71**, 061401(R) (2005).
- [Arl98] J. Arlt, P. Bance, S. Hopkins, J. Martin, S. Webster, A. Wilson, K. Zetie, and C. J. Foot, *Suppression of collisional loss from a magnetic trap*, J. Phys. B. **31**, L321 (1998).
- [Bar06] R. Barnett, D. Petrov, M. Lukin, and E. Demler, *Quantum magnetism with multicomponent dipolar molecules in an optical lattice*, Phys. Rev. Lett. **96**, 190401 (2006).
- [Bar08] M. Baranov, *Theoretical progress in many-body physics with ultracold dipolar gases*, Phys. Rep. **464**, 71 (2008).
- [Büc07] H. Büchler, E. Demler, M. Lukin, A. Micheli, N. Prokof'ev, G. Pupillo, and P. Zoller, *Strongly correlated 2D quantum phases with cold polar molecules: controlling the shape of the interaction potential*, Phys. Rev. Lett. **98**, 060404 (2007).
- [Ber98] K. Bergmann, H. Theuer, and B. W. Shore, *Coherent population transfer among quantum states of atoms and molecules*, Rev. Mod. Phys. **70**, 1003 (1998).

References

- [Blo99] I. Bloch, T. W. Hänsch, and T. Esslinger, *Atom laser with a cw output coupler*, Phys. Rev. Lett. **82**, 3008 (1999).
- [Blo01] I. Bloch, M. Greiner, O. Mandel, T. W. Hänsch, and T. Esslinger, *Sympathetic cooling of ^{85}Rb and ^{87}Rb* , Phys. Rev. A. **64**, 021402(R) (2001).
- [Blo05] I. Bloch, *Ultracold quantum gases in optical lattices*, Nature Phys. **1**, 23 (2005).
- [Blo08] I. Bloch, J. Dalibard, and W. Zwerger, *Many-body physics with ultracold gases*, Rev. Mod. Phys.. **80**, 885 (2008).
- [Boe96] H. M. J. M. Boesten, A. J. Moerdijk, and B. J. Verhaar, *Dipolar decay in two recent Bose-Einstein condensation experiments*, Phys. Rev. A **54**, R29 (1996).
- [Bou89] M. A. Bouchiat, J. Guena, P. Jacquier, M. Lintz, and L. Pottier, *The Cs 6S-7S-6P_{3/2} forbidden three-level system: analytical description of the inhibited fluorescence and optical rotation spectra*, J. Phys. France **50**, 157 (1989).
- [Bra95] C. C. Bradley, C. A. Sackett, J. J. Tollett, and R. G. Hulet, *Evidence of Bose-Einstein condensation in an atomic gas with attractive interactions*, Phys. Rev. Lett. **75**, 1687 (1995).
- [Bra01] E. Braaten and H.-W. Hammer, *Three-body recombination into deep bound states in a Bose gas with large scattering length*, Phys. Rev. Lett. **87**, 160407 (2001).
- [Bre31] G. Breit and I. Rabi, *Measurement of nuclear spin*, Phys. Rev. **38**, 2082 (1931).
- [Bur97] E. A. Burt, R. W. Ghrist, C. J. Myatt, M. J. Holland, E. A. Cornell, and C. E. Wieman, *Coherence, correlations, and collisions: what one learns about Bose-Einstein condensates from their decay*, Phys. Rev. Lett. **79**, 337 (1997).
- [Cat08] J. Catani, L. D. Sarlo, G. Barontini, F. Minardi, and M. Inguscio, *Degenerate Bose-Bose mixture in a three-dimensional optical lattice*, Phys. Rev. A. **77**, 011603 (2008).
- [Chi00] C. Chin, V. Vuletić, A. J. Kerman, and S. Chu, *High resolution Feshbach spectroscopy of cesium*, Phys. Rev. Lett. **85**, 2717 (2000).
- [Chi01] C. Chin, *Cooling, collisions and coherence of cold cesium atoms in a trap*, Ph.D. thesis, Stanford University (2001).

References

- [Chi04] C. Chin, V. Vuletić, A. J. Kerman, S. Chu, E. Tiesinga, P. J. Leo, and C. J. Williams, *Precision Feshbach spectroscopy of ultracold Cs₂*, Phys. Rev. A **70**, 032701 (2004).
- [Chi08] C. Chin, R. Grimm, P. Julienne, and E. Tiesinga, *Feshbach resonances in ultracold gases*, arXiv:0812.1496 (2008).
- [Cor77] A. Corney, *Atomic and laser spectroscopy*, Oxford Classic Texts in the Physical Sciences, 1977.
- [Cor02] E. A. Cornell and C. E. Wieman, *Nobel Lecture: Bose-Einstein condensation in a dilute gas, the first 70 years and some recent experiments*, Rev. Mod. Phys. **74**, 875 (2002).
- [Cor06] S. L. Cornish, S. Thompson, and C. Wieman, *Formation of bright matter-wave solitons during the collapse of attractive Bose-Einstein condensates*, Phys. Rev. Lett. **96**, 170401 (2006).
- [Cou98] P. Courteille, R. S. Freeland, D. J. Heinzen, F. A. van Abeelen, and B. J. Verhaar, *Observation of a Feshbach resonance in cold atom scattering*, Phys. Rev. Lett. **81**, 69 (1998).
- [Cub03] J. Cubizolles, T. Bourdel, S. J. J. M. F. Kokkelmans, G. V. Shlyapnikov, and C. Salomon, *Production of long-lived ultracold Li₂ molecules from a Fermi gas*, Phys. Rev. Lett. **91**, 240401 (2003).
- [Dal99] F. Dalfovo, S. Giorgini, L. P. Pitaevskii, and S. Stringari, *Theory of Bose-Einstein condensation in trapped gases*, Rev. Mod. Phys. **71**, 463 (1999).
- [Dan08] J. Danzl, E. Haller, M. Gustavsson, M. Mark, R. Hart, N. Bouloufa, O. Dulieu, H. Ritsch, and H.-C. Nägerl, *Precision molecular spectroscopy for ground state transfer of molecular quantum gases*, arXiv:0811.2374 (2008).
- [Dei08] J. Deiglmayr, A. Grochola, M. Repp, K. Mörtlbauer, C. Glück, J. Lange, O. Dulieu, R. Wester, and M. Weidemüller, *Formation of ultracold polar molecules in the rovibrational ground state*, Phys. Rev. Lett. **101**, 133004 (2008).
- [DeM99] B. DeMarco and D. S. Jin, *Onset of Fermi degeneracy in a trapped atomic gas*, Science **285**, 1703 (1999).
- [DeM02] D. DeMille, *Quantum computation with trapped polar molecules*, Phys. Rev. Lett. **88**, 067901 (2002).

- [Don01] E. A. Donley, N. R. Clausen, S. L. Cornish, J. L. Roberts, E. A. Cornell, and C. E. Wieman, *Dynamics of collapsing and exploding Bose-Einstein condensates*, *Nature* **412**, 295 (2001).
- [Eng06] B. Engeser, *A novel surface trapping apparatus for ultracold cesium atoms and the investigation of an Efimov resonance*, Ph.D. thesis, Universität Innsbruck (2006).
- [Esr99] B. D. Esry, C. H. Greene, and J. P. Burke, *Recombination of three atoms in the ultracold limit*, *Phys. Rev. Lett.* **83**, 1751 (1999).
- [Fal00] J. Faller, *Bose-Einstein condensation in a dilute atomic vapor*, NIST Special Publication **958**, 375 (2000).
- [Fer06] F. Ferlaino, C. D’Errico, G. Roati, M. Zaccanti, M. Inguscio, G. Modugno, and A. Simoni, *Feshbach spectroscopy of a K-Rb atomic mixture*, *Phys. Rev. A* **73**, 040702 (2006).
- [Fer08] F. Ferlaino, S. Knoop, and R. Grimm, *Cold Molecules: Theory, experiment, applications*, edited by R. V. Krems, B. Friedrich, and W. C. Stwalley, arXiv:0809.3920. (2008).
- [Föl03] S. Fölling, *3D Raman sideband cooling of rubidium*, Diploma thesis, University of Heidelberg (2003).
- [Fri98] D. G. Fried, T. C. Killian, L. Willmann, D. Landuis, S. C. Moss, D. Kleppner, and T. J. Greytak, *Bose-Einstein condensation of atomic hydrogen*, *Phys. Rev. Lett.* **81**, 3811 (1998).
- [Fuk07] T. Fukuhara, Y. Takasu, M. Kumakura, and Y. Takahashi, *Degenerate Fermi gases of ytterbium*, *Phys. Rev. Lett.* **98**, 030401 (2007).
- [Gün06] K. Günter, T. Stöferle, H. Moritz, M. Köhl, and T. Esslinger, *Bose-Fermi mixtures in a three-dimensional optical lattice*, *Phys. Rev. Lett.* **96**, 180402 (2006).
- [GO98a] D. Guéry-Odelin, J. Söding, P. Desbiolles, and J. Dalibard, *Is Bose-Einstein condensation of atomic cesium possible?*, *Europhys. Lett.* **44**, 26 (1998).
- [GO98b] D. Guéry-Odelin, J. Söding, P. Desbiolles, and J. Dalibard, *Strong evaporative cooling of a trapped cesium gas*, *Opt. Exp.* **2**, 323 (1998).
- [Goo08] M. Goosen, *private communication* (2008).
- [Gór02] K. Góral, L. Santos, and M. Lewenstein, *Quantum phases of dipolar Bosons in optical lattices*, *Phys. Rev. Lett.* **88**, 170406 (2002).

References

- [Gre02] M. Greiner, O. Mandel, T. Esslinger, T. W. Hänsch, and I. Bloch, *Quantum phase transition from a superfluid to a Mott insulator in a gas of ultracold atoms*, Nature **415**, 39 (2002).
- [Gre03] M. Greiner, *Ultracold quantum gases in three-dimensional optical lattice potentials*, Ph.D. thesis, Ludwig-Maximilians-Universität München (2003).
- [Gri00] R. Grimm, M. Weidemüller, and Y. B. Ovchinnikov, *Optical dipole traps for neutral atoms*, Adv. At. Mol. Opt. Phys. **42**, 95 (2000).
- [Gri05] A. Griesmaier, J. Werner, S. Hensler, J. Stuhler, and T. Pfau, *Bose-Einstein condensation of chromium*, Phys. Rev. Lett. **94**, 160401 (2005).
- [Gry93] G. Grynberg, B. Lounis, P. Verkerk, J. Courtois, and C. Salomon, *Quantized motion of cold cesium atoms in two- and three-dimensional optical potentials*, Phys. Rev. Lett. **70**, 2249 (1993).
- [Gus08] M. Gustavsson, E. Haller, M. Mark, J. Danzl, G. Rojas-Kopeinig, and H.-C. Nägerl, *Control of interaction-induced dephasing of Bloch oscillations*, Phys. Rev. Lett. **100**, 080404 (2008).
- [Haa07] M. Haas, V. Leung, D. Frese, D. Haubrich, S. John, C. Weber, A. Rauschenbeutel, and D. Meschede, *Species-selective microwave cooling of a mixture of rubidium and caesium atoms*, New J. Phys. **9**, 147 (2007).
- [Had02] Z. Hadzibabic, C. A. Stan, K. Dieckmann, S. Gupta, M. W. Zwierlein, A. Görlitz, and W. Ketterle, *Two-species mixture of quantum degenerate Bose and Fermi gases*, Phys. Rev. Lett. **88**, 160401 (2002).
- [Hal98] D. Hall, M. Matthews, J. Ensher, C. Wieman, and E. Cornell, *Dynamics of component separation in a binary mixture of Bose-Einstein condensates*, Phys. Rev. Lett. **81**, 1539 (1998).
- [Ham02a] M. Hammes, *Optical surface microtraps based on evanescent waves*, Ph.D. thesis, Universität Innsbruck (2002).
- [Ham02b] M. Hammes, D. Rychtarik, H.-C. Nägerl, and R. Grimm, *Cold-atom gas at very high densities in an optical surface microtrap*, Phys. Rev. A. **66**, 051401 (2002).
- [Ham03] M. Hammes, D. Rychtarik, B. Engeser, H.-C. Nägerl, and R. Grimm, *Evanescent-wave trapping and evaporative cooling of an atomic gas at the crossover to two dimensions*, Phys. Rev. Lett. **90**, 173001 (2003).

- [Han00] D.-J. Han, S. Wolf, S. Oliver, C. McCormick, M. DePue, and D. Weiss, *3D Raman sideband cooling of cesium atoms at high densities*, Phys. Rev. Lett. **85**, 724 (2000).
- [Han07] T. M. Hanna, T. Köhler, and K. Burnett, *Association of molecules using a resonantly modulated magnetic field*, Phys. Rev. A. **75**, 013606 (2007).
- [Har08] M. Harris, P. Tierney, and S. L. Cornish, *Magnetic trapping of a cold Rb-Cs atomic mixture*, J. Phys. B. **41**, 035303 (2008).
- [Her03] J. Herbig, T. Kraemer, M. Mark, T. Weber, C. Chin, H.-C. Nägerl, and R. Grimm, *Preparation of a pure molecular quantum gas*, Science **301**, 1510 (2003).
- [Hop00] S. A. Hopkins, S. Webster, J. Arlt, P. Bance, S. Cornish, O. Maragó, and C. Foot, *Measurement of elastic cross section for cold cesium collisions*, Phys. Rev. A. **61**, 032707 (2000).
- [Hun08] C.-L. Hung, X. Zhang, N. Gemelke, and C. Chin, *Accelerating evaporative cooling of atoms into Bose-Einstein condensation in optical traps*, Phys. Rev. A. **78**, 011604(R) (2008).
- [Ino98] S. Inouye, M. R. Andrews, J. Stenger, H.-J. Miesner, D. M. Stamper-Kurn, and W. Ketterle, *Observation of Feshbach resonances in a Bose-Einstein condensate*, Nature **392**, 151 (1998).
- [Ino04] S. Inouye, J. Goldwin, M. L. Olsen, C. Ticknor, J. L. Bohn, and D. S. Jin, *Observation of heteronuclear Feshbach resonances in a mixture of Bosons and Fermions*, Phys. Rev. Lett. **93**, 183201 (2004).
- [Jam03] M. J. Jamieson, H. Sarbazi-Azad, H. Ouerdane, G.-H. Jeung, Y. S. Lee, and W. C. Lee, *Elastic scattering of cold caesium and rubidium atoms*, J. Phys. B. **36**, 1085 (2003).
- [JD04] R. K. J. Doyle, B. Friedrich and F. Masnou-Seeuws, *Editorial: Quo vadis, cold molecules?*, Eur. Phys. J. D **31**, 149 (2004).
- [Jez02] D. Jezek and P. Capuzzi, *Interaction-driven effects on two-component Bose-Einstein condensates*, Rev. Mod. Phys. **66**, 015602 (2002).
- [Kas94] A. Kastberg, W. D. Phillips, S. L. Rolston, R. Spreuw, and P. S. Jessen, *Adiabatic cooling of cesium to 700nK in an optical lattice*, Phys. Rev. Lett. **74**, 1542 (1994).
- [Ker99] A. J. Kermann, V. Vuletic, C. Chin, and S. Chu, *Beyond optical molasses: 3D Raman sideband cooling of atomic cesium to high phase-space density*, Phys. Rev. Lett. **84**, 439(3) (1999).

References

- [Ker04a] A. J. Kerman, J. M. Sage, S. Sainis, T. Bergeman, and D. DeMille, *Production and state-selective detection of ultracold RbCs molecules*, Phys. Rev. Lett. **92**, 153001 (2004).
- [Ker04b] A. J. Kerman, J. M. Sage, S. Sainis, T. Bergeman, and D. DeMille, *Production of ultracold, polar RbCs molecules via photoassociation*, Phys. Rev. Lett. **92**, 033004 (2004).
- [Ket99] W. Ketterle, D.S.Durfee, and D.M.Stamper-Kurn, *Making, probing and understanding Bose-Einstein condensates*, cond-mat/9904034, 1999.
- [Ket02] W. Ketterle, *Nobel lecture: when atoms behave as waves: Bose-Einstein condensation and the atom laser*, Rev. Mod. Phys. **74**, 1131 (2002).
- [Kin05] T. Kinoshita, T. Wenger, and D. S. Weiss, *All-optical Bose-Einstein condensation using a compressible crossed dipole trap*, Phys. Rev. A **71** (2005).
- [Kle08] C. Klempt, T. Henninger, O. Topic, M. Scherer, L. Kattner, E. Tiemann, W. Ertmer, and J. J. Arlt, *Radio frequency association of heteronuclear Feshbach molecules*, arXiv:0809.0340 (2008).
- [Kno08] S. Knoop, M. Mark, F. Ferlaino, J. G. Danzl, T. Kraemer, H.-C. Nägerl, and R. Grimm, *Metastable Feshbach molecules in high rotational states*, Phys. Rev. Lett. **100**, 083002 (2008).
- [Köh06] T. Köhler, K. Góral, and P. S. Julienne, *Production of cold molecules via magnetically tunable Feshbach resonances*, Rev. Mod. Phys. **78**, 1311 (2006).
- [Kot06] S. Kotochigova and E. Tiesinga, *Ab initio relativistic calculation of the RbCs molecule*, J. Chem. Phys. **123**, 174304 (2006).
- [Kot08] S. Kotochigova, *private communication* (2008).
- [Kra04] T. Kraemer, J. Herbig, M. Mark, T. Weber, C. Chin, H.-C. Nägerl, and R. Grimm, *Optimized production of a cesium Bose-Einstein condensate*, Appl. Phys. B **79**, 1013 (2004).
- [Kra06] T. Kraemer, M. Mark, P. Waldburger, J. G. Danzl, C. Chin, B. Engeser, A. D. Lange, K. Pilch, A. Jaakkola, H.-C. Nägerl, and R. Grimm, *Evidence for Efimov quantum states in an ultracold gas of cesium atoms*, Nature **440**, 315 (2006).
- [Lan08a] F. Lang, K. Winkler, C. Strauss, R. Grimm, and J. H. Denschlag, *Ultracold molecules in the ro-vibrational triplet ground state*, Phys. Rev. Lett. **101**, 133005 (2008).

References

- [Lan08b] A. Lange, K. Pilch, A. Prantner, F. Ferlaino, B. Engeser, H. Nägerl, R. Grimm, and C. Chin, *Determination of atomic scattering lengths from measurements of molecular binding energies near Feshbach resonances*, arXiv:0810.5503 (2008).
- [Leo98] P. J. Leo, E. Tiesinga, P. S. Julienne, D. K. Walter, S. Kadlecsek, and T. G. Walker, *Elastic and inelastic collisions of cold spin-polarized ^{133}Cs atoms*, Phys. Rev. Lett. **81**, 1389 (1998).
- [Lew04] M. Lewenstein, L. Santos, M. A. Baranov, and H. Fehrmann, *Atomic Bose-Fermi mixtures in an optical lattice*, Phys. Rev. Lett. **92**, 050401 (2004).
- [Mad00] K. W. Madison, F. Chevy, W. Wohlleben, and J. Dalibard, *Vortex formation in a stirred Bose-Einstein condensate*, Phys. Rev. Lett. **84**, 806 (2000).
- [Mar02] A. Marte, T. Volz, J. Schuster, S. Dürr, G. Rempe, E. G. M. van Kempen, and B. J. Verhaar, *Feshbach resonances in rubidium 87: precision measurement and analysis*, Phys. Rev. Lett. **89**, 283202 (2002).
- [Mar05] M. Mark, T. Kraemer, J. Herbig, C. Chin, H.-C. Nägerl, and R. Grimm, *Efficient creation of molecules from a cesium Bose-Einstein condensate*, Europhys. Lett. **69**, 706 (2005).
- [Met99] H. J. Metcalf and P. van der Straten, *Laser cooling and trapping*, Springer, New York, 1999.
- [Mic06] P. Z. Micheli, G. K. Brennen, *A toolbox for lattice-spin models with polar molecules*, Nature Phys. **2**, 341 (2006).
- [Mie96] F. H. Mies, C. J. Williams, P. S. Julienne, and M. Krauss, *Estimating bounds on collisional relaxation rates of spin-polarized ^{87}Rb atoms at ultracold temperatures*, J. Res. Nat. Inst. Stand. Tech. **101**, 521 (1996).
- [Mie00] F. H. Mies, E. Tiesinga, and P. S. Julienne, *Manipulation of Feshbach resonances in ultracold atomic collisions using time-dependent magnetic fields*, Phys. Rev. A. **61**, 022721 (2000).
- [Mod01] G. Modugno, G. Ferrari, G. Roati, A. Simoni, and M. Inguscio, *Bose-Einstein condensation of potassium atoms by sympathetic cooling*, Science **294**, 1320 (2001).
- [Mod02a] G. Modugno, M. Modugno, F. Riboli, G. Roati, and M. Inguscio, *Two atomic species superfluid*, Phys. Rev. A **89**, 190404 (2002).
- [Mod02b] G. Modugno, G. Roati, F. Riboli, F. Ferlaino, R. Brecha, and M. Inguscio, *Collapse of a degenerate Fermi gas*, Science **297**, 2240 (2002).

References

- [Mud02] M. Mudrich, S. Kraft, K. Singer, R. Grimm, A. Mosk, and M. Weidemüller, *Sympathetic cooling with two atomic species in an optical trap*, Phys. Rev. Lett. **88**, 253001 (2002).
- [Mya96] C. Myatt, E. Burt, R. Ghrist, E. Cornell, and C. Wieman, *Production of two overlapping Bose-Einstein condensates by sympathetic cooling*, Phys. Rev. Lett. **78**, 586 (1996).
- [Ni08] K.-K. Ni, S. Ospelkaus, M. H. G. de Miranda, A. Pe'er, B. Neyenhuis, J. J. Zirbel, S. Kotochigova, P. S. Julienne, D. S. Jin, and J. Ye, *A high phase-space-density gas of polar molecules*, Science **322**, 231 (2008).
- [Osp06] C. Ospelkaus, S. Ospelkaus, K. Sengstock, and K. Bongs, *Interaction-driven dynamics of ^{40}K - ^{87}Rb Fermion-Boson gas mixtures in the large-particle-number limit*, Phys. Rev. Lett. **96**, 020401 (2006).
- [Osp08] S. Ospelkaus, A. Pe'er, K.-K. Ni, J. J. Zirbel, B. Neyenhuis, S. Kotochigova, P. S. Julienne, J. Ye, and D. S. Jin, *Efficient state transfer in an ultracold dense gas of heteronuclear molecules*, Nature Physics **4**, 622 (2008).
- [Pap08] S. Papp, J. Pino, and C. Wieman, *Studying a dual-species BEC with tunable interactions*, Phys. Rev. Lett. **101**, 040402 (2008).
- [Pet02] C. J. Pethick and H. Smith, *Bose-Einstein condensation in dilute gases*, Cambridge Univ. Pr., 2002.
- [Pil05] K. Pilch, *Weiterentwicklung eines Experiments zur Untersuchung zweidimensionaler Quantengase*, Diploma thesis, Universität Innsbruck (2005).
- [Pil08] K. Pilch, A. D. Lange, A. Prantner, G. Kerner, F. Ferlaino, H.-C. Nägerl, and R. Grimm, *Observation of interspecies Feshbach resonances in an ultracold Rb-Cs mixture*, arXiv:0812.3287 (2008).
- [Raa87] E. Raab, M. Prentiss, A. Cable, S. Chu, and D. Pritchard, *Trapping of neutral sodium atoms with radiation pressure*, Phys. Rev. Lett. **58**, 2631 (1987).
- [Reg03a] C. A. Regal, C. Ticknor, J. L. Bohn, and D. S. Jin, *Creation of ultracold molecules from a Fermi gas of atoms*, Nature **424**, 47 (2003).
- [Reg03b] C. A. Regal, C. Ticknor, J. L. Bohn, and D. S. Jin, *Tuning p -wave interactions in an ultracold Fermi gas of atoms*, Phys. Rev. Lett. **90**, 053201 (2003).
- [Rib02] F. Riboli and M. Modugno, *Topology of the ground state of two interacting Bose-Einstein condensates*, Phys. Rev. A **65**, 063614 (2002).

- [Roa02] G. Roati, F. Riboli, G. Modugno, and M. Inguscio, *Fermi-Bose quantum degenerate K-Rb mixture with attractive interaction*, Phys. Rev. Lett. **89**, 150403 (2002).
- [Roa07] G. Roati, M. Zaccanti, C. D’Errico, J. Catani, M. Modugno, A. Simoni, M. Inguscio, and G. Modugno, *^{39}K Bose-Einstein condensate with tunable interactions*, Phys. Rev. Lett. **99**, 010403 (2007).
- [Rob01] A. Robert, O. Sirjean, A. Browaeys, J. Poupard, S. Nowak, D. Boiron, C. I. Westbrook, and A. Aspect, *A Bose-Einstein condensate of metastable atoms*, Science **292**, 461 (2001).
- [Ryc04a] D. Rychtarik, *Two-dimensional Bose-Einstein condensate in an optical surface trap*, Ph.D. thesis, Universität Innsbruck (2004).
- [Ryc04b] D. Rychtarik, B. Engeser, H.-C. Nägerl, and R. Grimm, *Two-dimensional Bose-Einstein condensate in an optical surface trap*, Phys. Rev. Lett. **92**, 173003 (2004).
- [Sag05] J. M. Sage, S. Sainis, T. Bergeman, and D. DeMille, *Optical production of ultracold polar molecules*, Phys. Rev. Lett. **94**, 203001 (2005).
- [San01] F. P. D. Santos, J. Léonard, J. Wang, C. J. Barrelet, F. Perales, E. Rasel, C. S. Unnikrishnan, M. Leduc, and C. Cohen-Tannoudji, *Bose-Einstein condensation of metastable helium*, Phys. Rev. Lett. **86**, 3459 (2001).
- [Sch99] U. Schünemann, H. Engler, R. Grimm, M. Weidemüller, and M. Zielonkowski, *Simple scheme for tunable frequency offset of two lasers*, Rev. Sci. Instrum. **70**, 242 (1999).
- [SK98] D. M. Stamper-Kurn, H.-J. Miesner, A. P. Chikkatur, S. Inouye, J. Stenger, and W. Ketterle, *Reversible formation of a Bose-Einstein condensate*, Phys. Rev. Lett. **81**, 2194 (1998).
- [Söd98] J. Söding, D. Guéry-Odelin, P. Desbiolles, G. Ferrari, and J. Dalibard, *Giant spin relaxation of an ultracold cesium gas*, Phys. Rev. Lett. **80**, 1869 (1998).
- [Sta04] C. A. Stan, M. W. Zwierlein, C. H. Schunck, S. M. F. Raupach, and W. Ketterle, *Observation of Feshbach resonances between two different atomic species*, Phys. Rev. Lett. **93**, 143001 (2004).
- [Ste08] D. Steck, *Cesium D Line Data*, <http://george.ph.utexas.edu/~dsteck/alkalidata/> (2008).

References

- [Sto88] H. T. C. Stoof, J. M. V. A. Koelman, and B. J. Verhaar, *Spin-exchange and dipole relaxation rates in atomic hydrogen: rigorous and simplified calculations*, Phys. Rev. B **38**, 4688 (1988).
- [Str03] K. E. Strecker, G. B. Partridge, and R. G. Hulet, *Conversion of an atomic Fermi gas to a long-lived molecular Bose gas*, Phys. Rev. Lett. **91**, 080406 (2003).
- [Stw04] W. C. Stwalley, *Efficient conversion of ultracold Feshbach-resonance-related polar molecules into ultracold ground state $X^1\Sigma^+_{v=0, J=0}$ molecules*, Eur. Phys. J. D **31**, 221 (2004).
- [Tag08] M. Taglieber, A.-C. Voigt, T. Aoki, T. W. Hänsch, and K. Dieckmann, *Quantum degenerate two-species Fermi-Fermi mixture coexisting with a Bose-Einstein condensate*, Phys. Rev. Lett. **100**, 010401 (2008).
- [Tak03] Y. Takasu, K. Maki, K. Komori, T. Takano, K. Honda, M. Kumakura, T. Yabuzaki, and Y. Takahashi, *Spin-singlet Bose-Einstein condensation of two-electron atoms*, Phys. Rev. Lett. **91**, 040404 (2003).
- [Tha01] G. Thalhammer, *Frequenzstabilisierung von Diodenlasern bei 850, 854 und 866nm mit Linienbreiten im Kilohertz-Bereich*, Diploma thesis, Universität Innsbruck (2001).
- [Tha05] G. Thalhammer, M. Theis, K. Winkler, R. Grimm, and J. H. Denschlag, *Inducing an optical Feshbach resonance via stimulated Raman coupling*, Phys. Rev. A **71**, 033403 (2005).
- [The04] M. Theis, G. Thalhammer, K. Winkler, M. Hellwig, G. Ruff, R. Grimm, and J. H. Denschlag, *Tuning the scattering length with an optically induced Feshbach resonance*, Phys. Rev. Lett. **93**, 123001 (2004).
- [Tho05] S. T. Thompson, E. Hodby, and C. E. Wieman, *Ultracold molecule production via a resonant oscillating magnetic field*, Phys. Rev. Lett. **95**, 190404 (2005).
- [Tic04] C. Ticknor, C. A. Regal, D. S. Jin, and J. L. Bohn, *Multiplet structure of Feshbach resonances in nonzero partial waves*, Phys. Rev. A **69**, 042712 (2004).
- [Tie93] U. Tietze and C. Schenk, *Halbleiter und Schaltungstechnik*, Springer-Verlag, 1993.
- [Tie06] E. Tiesinga, M. Anderlini, and E. Arimondo, *Determination of the scattering length of the $a^3\Sigma^+$ potential of $^{87}\text{RbCs}$* , Phys. Rev. A **75**, 022707 (2006).

- [Tre01] P. Treutlein, K. Y. Chung, and S. Chu, *High-brightness atom source for atomic fountains*, Phys. Rev. A. **63**, 051401(R) (2001).
- [Unt05] P. Unterwaditzer, *Aufbau eines vollständigen Diodenlasersystems zur Laserkühlung und Detektion von gespeicherten Cäsium-Atomen*, Diploma thesis, Universität Innsbruck (2005).
- [Vul98] V. Vuletic, C. Chin, A. J. Kerman, and S. Chu, *Degenerate Raman sideband cooling of trapped cesium atoms at very high atomic densities*, Phys. Rev. Lett **81**, 5768 (1998).
- [Web03a] T. Weber, J. Herbig, M. Mark, H.-C. Nägerl, and R. Grimm, *Bose-Einstein condensation of cesium*, Science **299**, 232 (2003).
- [Web03b] T. Weber, J. Herbig, M. Mark, H.-C. Nagerl, and R. Grimm, *Three-Body recombination at large scattering lengths in an ultracold atomic gas*, Phys. Rev. Lett. **91**, 123201 (2003).
- [Web08] C. Weber, G. Barontini, J. Catani, G. Thalhammer, M. Inguscio, and F. Minardi, *Association of ultracold double-species bosonic molecules*, arXiv:0808.4077 (2008).
- [Wei99] J. Weiner, V. S. Bagnato, S. Zilio, and P. S. Julienne, *Experiments and theory in cold and ultracold collisions*, Rev. Mod. Phys. **71**, 1 (1999).
- [Wei05] M. Weidemüller, M. Reetz-Lamour, T. Amthor, J. Deiglmayer, and K. Singer, *Laser spectroscopy XVII, edited by E.A. Hinds and A. Ferguson and E. Riis*, World Scientific, 2005.
- [Wil08] E. Wille, F. Spiegelhalter, G. Kerner, D. Naik, A. Trenkwalder, G. Hendl, F. Schreck, R. Grimm, T. Tiecke, J. Walraven, S. Kokkelmans, E. Tiesinga, and P. Julienne, *Exploring an ultracold Fermi-Fermi mixture: intespecies Feshbach resonances and scattering properities of ${}^6\text{Li}$ and ${}^{40}\text{K}$* , Phys. Rev. Lett. **100**, 053201 (2008).
- [Wil09] E. Wille, *in preparation*, Ph.D. thesis, Universität Innsbruck (2009).
- [Win07] K. Winkler, F. Lang, G. Thalhammer, P. v. d. Straten, R. Grimm, and J. Hecker Denschlag, *Coherent optical transfer of Feshbach molecules to a lower vibrational state*, Phys. Rev. Lett. **98**, 043201 (2007).
- [Xu03] K. Xu, T. Mukaiyama, J. R. Abo-Shaeer, J. K. Chin, D. E. Miller, and W. Ketterle, *Formation of quantum-degenerate sodium molecules*, Phys. Rev. Lett. **91** (2003).
- [Yi07] S. Yi, T. Li, and C. Sun, *Novel quantum phases of dipolar Bose gases in optical lattices*, Phys. Rev. Lett. **88**, 170406 (2007).

Vielen Dank

Ich danke allen die zur Entstehung dieser Arbeit beigetragen und mich tatkräftig unterstützt haben. Dazu gehört natürlich vor allem Rudi Grimm, der unermüdlich trotz vielfältiger Verpflichtungen immer durch eine hervorragende Leitung der Arbeitsgruppe glänzt und durch seine Expertise Forschung auf hohem Niveau in Innsbruck ermöglicht. Ich bedanke mich auch für die unzähligen Stunden, die Rudi für die Korrektur meiner Arbeit aufgewendet hat, und für die Einbindung digitaler Audiokommentare, die mich teils recht pointiert auf die grundlegendsten Regeln zum Verfassen von wissenschaftlichen Texten hinwiesen. Weiters gebührt mein Dank Hanns-Christoph Nägerl, der bei Fragen technischer oder physikalischer Natur immer zu Diskussionen bereit war. Vielen Dank auch an Francesca für die Korrektur der ersten Version dieser Arbeit (was wohl das Schlimmste verhindert hat) und natürlich für die Mitarbeit direkt am Experiment. In italiano: Tante grazie per l' aiuto della bellissima Francesca, che ha impedita il pessimo per fare la prima correktura della mia tesi e naturalmente anche per la collaborazione nel esperimento.

Weiters danke ich den Mitstreitern im Labor: Bastian E., der mich schon während meiner Diplomarbeit unterstützt hat und auch bei der Planung dieses neuen Experiments tatkräftig zur Seite stand. Gabriel, der besonders durch seine Erfahrung in Elektronik und Programmierung wesentlich am Fortschritt beteiligt war. Andrea, die während ihrer Diplomarbeit die Arbeitslast in der Aufbauphase mitgetragen hat. Meinem langjährigen Mitstreiter Almar, dem ich viel Erfolg für die weitere Entwicklung im Experiment wünsche, und den Neuen im Labor: Markus, Bastian und David.

Bedanken möchte ich mich auch bei allen anderen in der Arbeitsgruppe. Nennen möchte ich Stefan R., der manchmal (wenn das Bier die richtige Temperatur hatte) auch noch spät abends in der WG für die Diskussion physikalischer Probleme bereit war. Besonders auch den Mitarbeitern in den Sekretariaten (Christine, Karin, Gabriel, Nicole und Patrizia), sowie in den Mechanik- und Elektronikwerkstätten (Toni, Helmut, Josef, Manuel und Arthur) möchte ich meinen Dank aussprechen.

Zuletzt noch ein herzliches Dankeschön an meine Familie, besonders meinen Eltern, die mir diese Ausbildung erst ermöglicht haben. Danke.